A FINITE ELEMENT CONTACT ALGORITHM APPLIED TO THE ANALYSIS OF EXPANDED TUBE JOINTS

by

USAMA AHMED ABDELSALAM ALI

A THESIS

Submitted to The School of Graduate Studies
in Partial Fulfilment of the Requirements
for the Degree

Doctor Of Philosophy

McMASTER UNIVERSITY

DOCTOR OF PHILOSOPHY (1995) McMASTER UNIVERSITY

(Mechanical Engineering) Hamilton, Ontario

TITLE: A Finite Element Contact Algorithm Applied to the Analysis of Expanded Tube Joints

AUTHOR: USAMA AHMED ABDELSALAM ALI,
B.Sc.(Alexandria University)
M.Sc.(Alexandria University)

SUPERVISOR: Professor M.A. Dokainish

No. OF PAGES: xiv, 190

A FINITE ELEMENT CONTACT ALGORITHM . . .

ABSTRACT

The study presented in this thesis aims at fulfilling an industrial need for solution methods suitable for the analysis of complex nonlinear engineering problems. A finite element contact algorithm is developed, implemented and verified. Furthermore, the algorithm is used for the numerical simulation of the hydraulic expansion of tube joints.

A variational formulation of the general contact problem is presented where the virtual work principle is adopted to arrive at the discretized equilibrium equations for two generic bodies coming into contact under the effect of the applied loads. The discretized contact constraint equations are derived geometrically from the kinematics of the potential contact surface nodes. A direct engineering approach is used to develop a solution algorithm which is applicable for the analysis of contact problems in general. No assumptions are made regarding the geometry of the contacting bodies, the location and extent of contact and the nature of the external loading. A non-classical bi-linear friction model is introduced where micro tangential relative displacements are allowed even under very light normal traction. The bi-linear law may be reduced to the classical Coulomb's friction law as a special case. The algorithm is made capable of handling nonlinear continuum finite elements, i.e. elements with curved sides. The equilibrium equations are solved iteratively to calculate the contact nodal forces which remove any overlap without augmenting the contact constraint equations into the original system of equilibrium equations. Instead, the contact constraint equations are solved as an inner loop in the global nonlinear iteration loop

which follows the full/modified Newton-Raphson iterative technique. The developed algorithm is implemented in the in-house general purpose non-linear finite element program INDAP[1] and verified through the solution of illustrative examples covering a wide range of contact problems of static, elastic, elasto-plastic, conformal and non-conformal contact interactions.

The developed contact algorithm is used along with two finite element models to simulate the hydraulic expansion of tube joints. A 2-D plane stress model is used to investigate the effects of the different material mechanical properties on the joint strength. A 2-D axisymmetric model is adopted to overcome the limited scope of the plane stress model. The feasibility of ignoring the geometric nonlinearity and the friction interaction are investigated. A 2^3 complete factorial numerical experiment is adopted to study the main and interaction effects of the expansion pressure, the initial radial clearance and the coefficient of friction on the residual contact pressure, representing the joint integrity, and the maximum residual tensile stress along the tube inner and outer surfaces, representing the joint quality. A new explanation to the break-off the joint strength when the joint is further expanded beyond a well-defined optimum is suggested. The adequacy of some strength measures is explored. The effects of the initial stresses and the cold-work surface layer along the tube outer surface are investigated.

---

[1] Incremental Nonlinear Dynamic Analysis Program

ACKNOWLEDGEMENT

The author would like to express his great indebtedness and thanks to all those who have supported this endeavour.

Special thanks is due to Prof. M.A. Dokainish for his invaluable guidance and unlimited support during the course of this work.

The financial support provided by the Natural Science and Engineering Research Council, NSERC operating grant #2726, and the Manufacturing Research Corporation of Ontario, MRCO 9-96244, are also acknowledged.

Last, but not the least, the author would like to express his deep gratitude towards his parents and his beloved wife for the encouragement, support and love.

TABLE OF CONTENTS

NOMENCLATURE

Roman Letters

B	B matrix
C	Constant Elasticity Tensor
E	Modulus of Elasticity
F	Normal Force Matrix
G	Contact traction transformation matrix
H	Matrix of Shape Functions
I	Identity matrix
J	Index for target surface elements
K	Stiffness matrix
N	Coefficient Matrix for Normal Constraint Equations
N_c	Number of active contactor nodes
N_d	degrees of freedom per node
N_p	Total number of nodes in the finite element model
P	Penetration Matrix
Q	Global Penetration Vector
R	Coefficient Matrix for Tangential Constraint equations
S	Boundary Surface
U	Strain Energy
W	External Work
b	Body force vector
e	Unit vector
f	Nodal force
f_c	Nodal contact force vector in the global coordinate system
f_N	Normal contact force vector
f_T	Tangential force vector
g	Elements of the transformation matrix G
h	Shape functions for displacements.
p	Penetration vector

r	External force vector
s	Label for the virtual target node
t	Traction component
t	Distributed Traction
u	Global displacement nodal vector
x,y,z	Cartesian Coordinate System

Subscripts

N	Normal Component
T	Tangential Component
k	Label for the contactor node

Superscripts

A	Label for the contactor body
B	Label for the Target body
n	Index for normal stress iterations
t	Time

Greek Letters

α	Flexibility Matrix
Γ	Boundary
Δ	Incremental operator
δ	Variational operator
ϵ	Strain Tensor
ζ	Elemental local coordinate
η	Elemental local coordinate
Θ	Tangential to Normal force ratio
θ	Tangential Coordinate
μ	Coefficient of Friction
ν	Poisson's ratio
ξ	Elemental local coordinate
Ψ	Slip Function for Friction analysis
Ω	Material Volume
σ	Stress Tensor

LIST OF TABLES

Chapter 4

LIST OF FIGURES

CHAPTER 1

INTRODUCTION

1.1 Preamble

Contact interaction is the type of phenomenon which is unavoidable in all aspects of everyday life. Simply, it is a way of communication between individual objects. In engineering applications, contact interaction is the common way of communication between different components of structural or mechanical systems. The transfer of loads is achieved through contact surfaces. Gears, cams, and clutches are common examples of a driving body which exerts forces on a driven body to transmit motion. On the other hand, in a typical rolling element bearing application, a rotating shaft is supported in a machine housing without transmitting any motion. In structural applications, bolted connections, for instance, are an obvious example of the contact problem in which loads are transmitted between static bodies. In all these examples and others, the contacting bodies are designed to perform entirely in the material elastic range of deformations. In other applications, metal forming for instance, the materials involved are deformed beyond the elastic limit to achieve permanent deformations. In engineering applications, contact interactions are usually intentional. However, there are situations where contact interactions are accidental as in vehicle crash for instance.

Contact interactions may have an outstanding effect on the behaviour of mechanical and structural systems which brings about the question of efficiency and performance. Contact interactions can be intentional or accidental; pleasant or harmful. Nevertheless, how the contact interaction would affect the efficiency and performance of a mechanical or structural system relies largely on the understanding of the contact phenomena. This understanding is crucial to enhance the beneficiary side of contact and to minimize its unpleasant consequences. Ultimately, the understanding of the contact phenomenon leads to an improved efficiency for intentional contacts and an assisted safety against accidental occasions.

Contact and friction are the two sides of the same coin. When two metallic bodies in contact are subjected to applied forces which tend to produce relative sliding motion, friction stresses develop on the interface that tend to oppose that motion. In reality, friction phenomena exist whenever contact is present. The underlying fact which brings about the friction phenomena is that all physical boundaries are rough from a microscopic point of view. The roughness of the physical boundary contributes significantly to frictional resistance. Asperities may wear down resulting in smoothing of the boundaries. At the same time, asperities may indent into the boundary resulting in new asperities. However, frictional effects may be neglected, for simplicity, in situations where frictional forces are sufficiently small. Therefore, contact problems may be classified as frictional or frictionless.

Contact problems may also be categorized into static or dynamic. The contact between two bodies is a static phenomenon if the two bodies are in static equilibrium.

Otherwise the contact is a dynamic phenomenon. In many cases, dynamic effects can be neglected and the problem can be considered quasi-static for simplicity.

If the contacting bodies are touching first at a point or along a line and under load the dimensions of the contact area are generally small compared to the dimensions of the bodies themselves, the contact is called non-conformal and the bodies are called non-conforming. In these circumstances, the contact stresses comprise a local stress concentration which can be considered independently of the stresses in the bulk of the two bodies. On the other hand, bodies whose surfaces conform to each other are likely to make contact over an area whose size is comparable with the significant dimensions of the two bodies. The contact stresses then become part of the general stress distribution throughout the bodies and cannot be separated from it. In such cases, the contacting bodies are called conforming and the contact interaction is called conformal contact.

Mathematically, the elasto-plastic material behaviour renders the problem materially nonlinear. If large displacements and/or strains are present, the problem becomes geometrically nonlinear. Contact interaction is by itself a third type of nonlinearity which is independent of either the material or the geometric nonlinearities. The contact nonlinearity arises as a result of the fact that neither the contact area nor the contact traction is known a priori. In a general contact problem, the surface area of the contact region develops as a result of the load variations and the contact traction is redistributed accordingly.

As a practical engineering application which involves contact interactions, the hydraulic expansion of tube joints is simulated using the finite element method. The expansion process is one of the complex deformation problems where the contact interaction acts along with both the geometric and material nonlinearities. The expanded joint resembles the shrink fit or rather the expansion fit, where the slightly oversize tube would be chilled, inserted in the hole and allowed to expand against the sleeve by warming up. Whereas the shrink fit or expansion fit is normally practised such that only elastic stresses are produced and the oversize of the tube is under immediate control, the expanded joint, on the other hand, necessitates plastic stresses, at least in the tube material, and the effective oversize produced is not under immediate control.

Reliable expanded tube joints are essential in a variety of industrial applications. The fastening of tubes in boiler plates, condenser tube sheets, feedwater heaters and air or oil coolers is a typical practice in which the expanded joint proved to be permanently satisfactory in operation with regard to the very important factor of manufacturing economy. One of the most critical applications of the expanded joint is the fastening of the pressure tubes of the CANDU(PHW)[1] reactors into the end fittings.

The expanded joint must not only be tight enough but also have structural integrity, to contribute to the support of the dead load and to resist the stresses and strains of temperature changes. The tightness against leakage depends upon the surface

---

[1] **CAN**adian **D**euterium-**U**ranium (**P**ressurised **H**eavy **W**ater)

conditions of the tube end and the plate hole/end-fitting, the uniformity of the expanding process and the residual contact pressure left between the tube and the plate/end fitting. The structural resistance to tension, torsion and bending depends upon the friction in the joint. This in turn depends upon the surfaces and the residual contact pressure. Beside the leak tightness and structural strength, the residual tensile stresses in the tube wall should be low enough to exclude the possibility of crack initiation and propagation. In other words, the residual tensile stresses along the tube inner and outer surfaces should be lower than the threshold of the stress corrosion cracking, SCC, stress.

In this chapter, a brief account of the role of the finite element method in the analysis of the general contact problem is introduced. Emphasis is set on the formulation, the different methods of applying the contact constraints, the searching algorithms and the friction laws. This is followed by a literature survey on the expanded tube joint where experimental, analytical and numerical studies are cited. Finally, this introductory chapter concludes with the objectives and general layout of the thesis.

1.2 Contact Problem and the Finite Element Method

In this section, the application of the finite element method in the solution of the static contact problem is dealt with. Focus is placed upon formulations which use a variational equality and the contact constraint equations are imposed on the solution. A comprehensive and more detailed review on static contact problems can be found in Zhong [1992] where more than five hundred references are grouped under the following headings:

- Mathematical aspects, fundamentals
- Contact problems with friction
- Thermal contact problems
- Material non-linear contact problems
- Geometric non-linear contact problems
- Finite element library for contact problems
- Contact problems in fracture mechanics
- Elastic foundations
- Joints: bonding, lapped, butt, dovetail, bolts, etc.
- Contact problems and geomechanics

Because of the complexity of the contact problem, both mathematicians and engineers devoted a great deal of attention to formulate and solve various types of contact problems. The progress in the contact research is divided into three stages as reported

by Zhong [1992].

In the first stage, contact bodies are restricted to rigid bodies and only global phenomena such as the total contact forces are observed and resulted in the Newton's third law and Coulomb's friction law. Coulomb's friction law divides the contact conditions into two distinctive regions; a sticking zone and a sliding zone. According to this law, the contacting bodies are in a sticking condition as long as the friction force is less than the frictional capacity defined by the coefficient of friction multiplied by the normal force. Once the friction force reaches the frictional capacity, sliding occurs. In spite of the physical and mathematical deficiencies associated with Coulomb's friction law, it is the most commonly used friction model, Oden and Piers [1983[a,b]].

The second stage of the history of the contact problem witnessed the development of the mechanical science and increasing engineering activities where local phenomena began to be observed. The second stage is marked by the monumental work of Hertz who considered the normal contact of two non-conforming bodies where under load they deform in the vicinity of their point of first contact, Johnson [1985]. Hertz developed a theory to predict the shape and size of the area of contact as it grows under increasing loads assuming that contact bodies can be regarded as elastic half-spaces with small deformation and that contact areas are small and elliptical. He also assumed that the contact boundaries are frictionless. Following Hertz, many studies have been conducted to release some of the constraints on the Hertzian contact problem, Johnson [1985]. During this stage, geometry and deformation of the

contacting bodies are assumed in such a way that available mathematical tools can be used to obtain closed-form solutions to the contact problem. Obviously, the approaches used in this stage are very restrictive and can only be applied to very special problems.

The third stage is characterized by numerical studies as a result of the advent of digital computers which opened the door for extensive numerical studies for the solution of a wide range of contact problems with arbitrary geometries, boundary conditions, and loadings. The finite element method has been the most widely used numerical technique for solving contact problems. Fortunately, the finite element method offers a systematic procedure for solving such problems with great success. The main advantage of the finite element method compared to other analysis techniques is its versatility and generality. By dividing the mathen atical model into many elements, it is possible to model any continuum with any loading and boundary conditions giving results accurate to the specified engineering tolerances. Theoretically, the finite element solution would approach the exact solution in the limit as the element size becomes infinitesimally small. This statement is true if two convergence criteria are satisfied within each individual element. However, practical limitations, including both software and hardware, usually limit the size of problems which can be handled. As the number of elements increases, the time required for input data preparation, solution and post processing increases dramatically. The cost of the overall analysis is indeed the main factor in the finite element solutions.

The finite element solutions to the contact problem may be classified into two main

formulations as described in Zhong [1993]. The contact problem may be formulated using the virtual work principal to yield a variational inequality which may be solved by minimization techniques. This formulation is referred to as the V-1 formulation. An advantage of the V-1 formulation is that all the boundary conditions are contained in the variational statement. Furthermore, with the V-1 formulation the existence and/or uniqueness of solution can be proved and error estimates can be obtained for some contact problems as discussed in detail in Kikuchi [1988]. The V-1 formulation is mathematically rigorous and is widely used in practice. However, a comprehensive mathematical background is essential to work with such a formulation. For engineering researchers, it is perhaps more convenient to deal with a straightforward formulation leading to a variational equality. The solution to the resulting variational equality has to satisfy all boundary conditions including the contact conditions. This formulation is referred to as the V-2 formulation. The main problem with the V-2 formulation is that the actual contacting boundary is, in general, unknown a priori. An incremental trial-and-error procedure may be used as shown in chapter three of this thesis. Moreover, in the V-2 formulation, the question of existence and/or uniqueness of the solution is rarely examined. However, in engineering applications, one may assume that the existence of the solution is guaranteed by the nature of the physical problems concerned.

The main ingredients of the finite element solution for contact problems may be summarized as follows:

1. Variational statement which provides a basis for the systematic finite element formulation.

2. Element formulation which represents the basis for the finite element discretization of the continuum producing a governing system of algebraic equations.
3. Material modelling which determines the stress-strain relation and plays an important role in the element formulation.
4. Contact constraint method which provides means of calculating the unknown contact forces under contact constraints.
5. Friction law which governs the frictional traction and sliding motion.
6. Searching algorithm which can detect the contacting nodes and sense any changes in the contact conditions.

In this thesis, the literature survey is restricted to the finite element solutions to the contact problem which adopt a variational equality as the basis for the discretization procedure. In other words, only the studies which use the V-2 formulation are addressed. Different methods within this category have been published and in the following discussion a brief account of some of the major articles is cited.

1.2.1 Imposing the Constraints

The variational formulation offers the basis for a systematic finite element discretization which leads to a system of linear algebraic equations. This system is referred to as the equilibrium equations and it contains as many equations as the degrees of freedom in the discretized continuum. In addition to these equilibrium

equations, a system of contact constraints has to be satisfied.

A simple way of analyzing contact problems is to model the region of anticipated contact using special interface elements. Prior to the occurrence of contact, these elements have zero stiffness. After contact, the elements have very large stiffness normal to the contact surface preventing any overlap between the contacting bodies. This approach is effective when locations of possible contact are known a priori and the extent of relative sliding between the bodies is small. Bond elements are proposed in Schafer [1975], Katona [1983] and Desai [1984] where an element stiffness matrix is derived assuming different constitutive models. In these treatments, the contact area is assumed known a priori which represents a severe constraint on the use of such elements in general engineering applications.

Another way of analyzing the contact problem is to use constraint equations to enforce the impenetrability, tension release, sticking and sliding contact conditions. This can be done either by the use of the penalty method or the Lagrange multipliers method. An interesting review is offered by Underhill [1992] where the numerical approaches for imposing the contact constraints are lumped into three main branches. These are those based on the use of Lagrange multipliers, those based on the penalty methods and the direct methods.

By using the standard finite element procedure, the discretized form of the potential energy is given by

$$\Pi(u) = \frac{1}{2}u^T K u - u^T f \qquad (1.1)$$

where,

- Π is the total potential energy for the contacting bodies,
- u is the nodal displacement vector,
- K is the stiffness matrix and
- f is the external nodal force vector.

The kinematic contact conditions may be put in the following discretized form:

$$p = Q u + {}^0p = 0 \qquad (1.2)$$

where,

- Q is a square matrix which contains a unit entry corresponding to each contactor node and the appropriate shape function corresponding to each target node as derived in the next chapter.
- ${}^0p$ is the vector of all penetrations made by contactor nodes.

Now, the contact problem may be stated as follows:

Minimize $\Pi(u)$ in equation (1.1) subject to the constraints in equation (1.2).

The Penalty Method:

In the penalty method, the constraint equations are included in the governing equations through a penalty function π_p given by:

$$\pi_p = \frac{1}{2} p^T \alpha p \tag{1.3}$$

where α is a diagonal matrix with elements α_{ii}, $i=1,L$, which are the penalty parameters. And L is the total number of the degrees of freedom of the active contactor nodes. The function to be minimized is replaced by:

$$\begin{aligned} \Pi_p &= \Pi + \pi_p \\ &= \frac{1}{2} u^T K u - u^T f + \frac{1}{2} p^T \alpha p \end{aligned} \tag{1.4}$$

Therefore, the potential Π_p is made minimum by invoking the following condition:

$$\frac{\partial \Pi_p}{\partial u} = 0 \tag{1.5}$$

Substituting eqn. (1.4) and (1.2) into eqn. (1.5), one may obtain:

$$K_p u = f_p \tag{1.6}$$

where

$$K_p = K + Q^T \alpha Q$$

$$f_p = f - Q^T \alpha {}^0p$$

The solution of eqn. (1.6) gives the displacement vector u. The contact forces are then calculated as:

$$f_c = \alpha p$$

where the penetration vector p is a function of the displacement vector u.

In eqn. (1.6), as the penalty parameter approaches infinity, the displacement constraint is exactly satisfied. As such, the solution is dependent upon a user modified parameter which might lead to an ill-conditioned matrix. However, the main advantage of the penalty method is that it does not increase the size of the governing system of equations.

As examples of finite element solutions to the contact problem using the penalty method see Chandrasekaran et al. [1987[a,b]], Pascoe and Mottersheed [1989] and Kim [1993].

Lagrange Multipliers Method:

The Lagrange multipliers method introduces the contact constraint equations by the use of extra unknowns called the Lagrange multipliers. These multipliers, upon solving the augmented system of equations, represent the reaction forces at the constrained degrees of freedom. In other words, in the Lagrange multiplier method, the contact forces are taken as primary unknowns and the impenetrability condition is enforced exactly. The function to be minimized is replaced by the following:

$$\Pi_L(u,\lambda) = \frac{1}{2}u^T K u - u^T f + \lambda^T (Q u + {}^0p) \qquad (1.7)$$

where λ is an unknown vector which contains as many elements as the number of

contact nodes and is known as Lagrange multipliers.

The potential in eqn. (1.7) may be minimized by invoking the following conditions:

$$\frac{\partial \Pi_L}{\partial u} = 0$$
$$\frac{\partial \Pi_L}{\partial \lambda} = 0 \qquad (1.8)$$

Substituting eqn. (1.7) into eqns. (1.8) yields:

$$K u - f + Q^T \lambda = 0$$
$$Q u + {}^0p = 0$$

Combining the resulting equations yields:

$$K_L u_L = f_L \qquad (1.9)$$

where,

$$K_L = \begin{bmatrix} K & Q^T \\ Q & 0 \end{bmatrix}$$
$$f_L = \begin{bmatrix} u \\ -{}^0p \end{bmatrix}$$
$$u_L = \begin{bmatrix} u \\ \lambda \end{bmatrix}$$

By solving the system of equations given by eqn.(1.9), the displacement vector and the Lagrange multipliers are obtained. The Lagrange multipliers are in fact the contact forces at the corresponding nodes.

It is obvious that in the Lagrange multipliers method the system of equations gets bigger by one row and one column for each contact node. Despite the added computational effort, the Lagrange multiplier approach is attractive considering both the generality offered and the numerical effectiveness.

As examples for the application of the Lagrange multiplier method in solving the contact problem see Okamoto and Nakazawa [1979], Bathe and Chaudhary [1984, 1985], Chudhary and Bathe [1986] and Pascoe and Mottersheed [1988, 1989].

Perturbed Lagrange Multipliers Methods:

In contact problems, the contact forces must be negative. To enforce these constraints in the Lagrange multipliers method, another set of multipliers may be used or one can use a penalty method on the set of multipliers. The perturbed Lagrange method is a modification to the Lagrange multiplier method where an extra term, a penalty term, is added to the potential function as follows:

$$\Pi_{pL} = \Pi_L + \frac{1}{2}\lambda^T \epsilon \lambda \qquad (1.10)$$

where ϵ is a diagonal matrix with elements ϵ_{ii}, i=1,L, which are referred to as the perturbing parameters.

Now the potential in eqn. (1.10) is made stationary by invoking the conditions:

$$\frac{\partial \Pi_{pL}}{\partial u} = 0$$
$$\frac{\partial \Pi_{pL}}{\partial \lambda} = 0 \qquad (1.11)$$

Substituting eqn. (1.10) into eqns. (1.11), yields:

$$K_{pL}\, u_L = f_L \tag{1.12}$$

where the augmented stiffness matrix is given by:

$$K_{pL} = \begin{bmatrix} K & Q^T \\ Q & \epsilon \end{bmatrix}$$

Examples of the application of the perturbed Lagrange multiplier method are found in Herrmann [1978], Simo [1985], Shyu et al. [1985], Gallego and Anza [1989], Simo and Laursen [1992], Laursen and Simo [1993] and Oldenburg [1994].

Direct Methods:

In categorizing the different methods for solving contact problems, direct methods are mentioned with completely different meanings. On one hand, direct methods are meant to be related to the way of imposing the contact constraints using either the penalty or the Lagrange multiplier methods to arrive at the governing system of equations, Zhong [1993]. This classification does not add much to the solution methods since it only addresses the derivation of the system of equations which may be obtained differently. On the other hand, Underhill [1992] described the direct methods as a whole class of methods which solve for the increments in the contact forces which will give correction to the displacement and reach the minimum potential energy. Among these are the work presented by Francavilla and Zienkiewiez [1975] where they considered the elastic frictionless contact problems. They used the flexibility matrix

obtained by inverting the condensed stiffness matrix formed by eliminating all the nodes except those where contact is likely to take place and those with external forces. Node-to-node contact was assumed and the algorithm is applicable for problems where only kinematic boundary conditions are present. Sachdeva et al.[1981] extended the algorithm developed by Francavilla and Zienkiewiez [1975] to handle problems with force boundary conditions as well. Sachdeva and Ramakrishnan [1981] extended the algorithm further to include frictional effects. Node-to-node contact is assumed and the compatibility of displacements for both the normal and tangential directions is applied to those nodes which do not slip. However, for sliding nodes, compatibility of displacements is applied for normal direction only and the slip condition is applied in the tangential direction. Rather than the flexibility matrix approach, Wanxie and Suming [1988] derived a stiffness matrix approach by means of a penalty function expression for the contact normal pressure and the frictional force. This treatment would allow a small penetration and a small tangential slip at very low normal pressures. Again the algorithm developed relies on node-to-node contacts.

Mahmoud et al. [1982] developed a fairly simple algorithm for frictionless contact problems. The algorithm consolidates the newly joined degrees of freedom associated with each contact node-pair, consequently; it only applies to problems which exhibit no relative tangential motion. Another severe restriction to this algorithm is that it only applies to contact problems which are purely advancing or receding and the occurrence of both events is not allowed.

Berkan [1988] introduced an incremental approach for solving general frictional contact

problems where node to segment contacts are allowed. The augmented system of the equilibrium equations and the contact constraint equations, resulting from a Lagrange multiplier method, are solved on a matrix level for the normal and tangential frictional forces. These forces are added to the global force vector and the resulting displacements are estimated and checked against any compatibility violation. In the algorithm developed by Berkan [1988], linear elements are considered and the classical laws of friction are adopted. Moreover, the solution algorithm solves for the nodal contact traction which is introduced to the finite element discretized analysis using a transformation matrix made of interpolation functions. As such, the choice of these interpolation functions would affect the resulting contact traction field.

In Sandeep [1991], the contact stresses and deformations are determined using a combination of the finite element method and a surface integral. In Underhill [1992], the equilibrium and compatibility errors are corrected separately. The correction forces from both estimates are added to the global force vector. Other examples of the finite element solutions of the contact problem which can be related to the direct methods can be found in Sun [1993] and Lee [1994].

1.2.2 Searching Algorithms

The contact constraint equations are defined at the contact nodes. One constraint equation per contactor node is needed in case of frictionless contact while two equations are needed for frictional contacts. As the load is successively applied on the

contacting bodies, nodes may lose contact and others may come into contact. In addition, sticking nodes may slide or sliding nodes may stick. In all these situations, a reliable algorithm is essential to detect any changes in the contact condition.

Node-to-node Contact:

In early studies, contacting bodies were often assumed to undergo only small displacements and rotations. Contact boundaries were discretized such that only node-to-node contacts will occur when the two boundaries come into contact, Francavilla and Zienkiewicz [1975], Sachdeva and Ramakrishanan [1981], Mahmoud et al. [1982], Wanxie and Suming [1988] and Okamoto [1979]. Such a node-to-node contact model can only be applied to problems in which relative sliding displacements of the two contacting boundaries are sufficiently small. In addition, the node-to-node contact model restricts the mesh shape at the contact boundaries to be of the same size which would lead to unnecessary mesh refinement of one of the contacting boundaries. For the node-to-node contact no search need to be done.

Node-to-segment Contact:

For more general applications, node-to-segment contacts should be used. Contacts between general contact boundaries can then be represented by contacts between contact nodes and contact segments. Most of the contact searching algorithms for the node-to-segment contacts rely on the definition of master and slave contact surfaces. A master or slave surface consists of master or slave segments, respectively. In addition, the nodes on the master or slave segments are called master or slave nodes, respectively. Node to straight segment contact can be found in Chaudhary and Bathe

[1986] and Berkan [1988] while node to curved segment contact can be found in Pascoe and Mottershead [1988].

Master-Slave Algorithm:

In contact searching, slave nodes are tested against master segments for any overlap to determine all overlapping slave nodes and declare them active. The active slave nodes define the contact area in the current iteration. The searching procedure consists of three main steps. First, a master node which is nearest to a given slave node is determined. Then, a master segment which has that master node is found. Finally, in the third step, the location of the touching point on the master surface is calculated. No slave node is allowed to overlap any master segment and this is called a one-path treatment. In a two-path treatment, the search is performed once more for the overlap of master nodes in slave segments.

The master-slave algorithm is conceptually simple. One has to define, a priori, the potential master and slave surface combinations. Therefore, it can be inefficient and unreliable for large contact systems with arbitrary potential contact nodes.

Single Surface Algorithm:

In the single surface searching algorithm, there is no need to specify contact pairs, a priori. Thus, arbitrary contacts can be handled. It also consists of three main steps as in the master-slave algorithm. However, in the single surface algorithm every contact node is both a slave node and a master node. The so called "bucket sort" is used to find a master node which is nearest to a given slave node.

Hierarchy-territory Algorithm:

In the hierarchy-territory algorithm, Zhong [1990], a contact system is decomposed into contact hierarchies, namely, the contact body, the contact surface, the contact segment, the contact edge and the contact node. Two distinctive contact searching schemes are used. A pre-contact searching is based on the definition of a territory for the contact hierarchy. The post-contact searching is based on the contact history. In the pre-contact searching, hierarchy territories are compared. If the territories of two hierarchies do not intersect with each other, no contact between the two hierarchies is possible and contact searching is then not to be performed between them. Otherwise contact searching is performed between the lower level hierarchies of those two hierarchies. On the other hand, in the post-contact searching a contact node is tested with its target segment and, if necessary, also the neighbouring segments of its target segment. For a detailed description of the hierarchy-territory contact-searching algorithm and others see chapter 10, Zhong [1993].

1.2.3 Friction Laws and the Finite Element Method

Friction laws have received a great deal of attention in the finite element implementations of different contact algorithms. Whenever frictional contact is mentioned, Coulomb's law of friction is invited. Sometimes Coulomb's law is praised and in other occasions it is criticized. Simplicity is the source of the wide application of the Coulomb's law of friction in the finite element analysis of general contact problems. However, it has physical and mathematical deficiencies which bring about

the critic.

In the following discussion, two mathematical models for the quasi-static dry friction are considered; a classical model which adopts the Coulomb's friction law and a non-classical model which is suggested to cure some of the physical and mathematical deficiencies in the Coulomb friction law. By quasi-static friction it is meant that the frictional mechanisms present when two metallic surfaces are pressed slowly together and are in static equilibrium or are slowly displaced relative to one another. It should be mentioned that the simplest friction model is the model of no friction. This means no restriction is imposed on the tangential displacements or forces and only the impenetrability condition is to be satisfied. See for instance Parisch [1989] who used both the penalty and Lagrange multipliers methods, Huh and Kwak [1991] who used Lagrange multipliers and Ayari and Saouma [1991] who used a direct method.

Classical Laws of Friction:

The classical laws for quasi-static dry friction as given by Oden and Martins [1985] may be summarized as follows:

1. If the two bodies are at rest or moving together without relative motion, the tangential force f_t must reach a critical value f_c before any relative motion of the two bodies can occur. That critical value is proportional to the normal contact force f_n, i.e.

$$f_c = \mu_s f_n$$

The coefficient of proportionality, μ_s, is known as the static coefficient of friction.

2. The static coefficient of friction is independent of the apparent area of contact.
3. During relative sliding of the two bodies, the frictional force is proportional to the normal contact force and acts in the opposite direction to the relative sliding velocity v_t, i.e.

$$f_t = -\mu_d f_n \frac{v_t}{|v_t|}$$

where μ_d is known as the dynamic coefficient of friction.

4. The dynamic coefficient of friction is smaller than the static one, but both are independent of the apparent area of contact and the relative sliding velocity.

These classical friction laws have been implemented in several finite element procedures for solving the frictional contact problem as in Chandrasekaran et al. [1987[a,b]], Bathe and Mijailovich [1988], Chaudhary and Bathe [1986], Bathe and Chaudhary [1985], Pascoe and Mottershead [1988, 1989], Mottershead and Pascoe [1992] and Lee [1994]. Kwak [1991] implemented an orthotropic extension of the Coulomb's friction law where two distinctive coefficients of friction are used in the two orthogonal directions.

Non-classical Laws of Friction:

While the classical laws can be used to describe the global behaviour of the two points in contact, they do have physical and mathematical deficiencies. For instance, it has

been proved experimentally that a small relative motion of the two contacting bodies is possible even if the tangential force, f_t, is smaller than the frictional capacity, f_c. On mathematical grounds, if the Coulomb's law of friction is applied point wise in contact problems involving linearly elastic bodies, the fundamental question of existence is open. In order to account for the micro-tangential displacements and the non-local character of the frictional contact, non-linear non-local friction laws are suggested by Oden and Pires [1983[a]]. In the nonlinear laws a frictional stiffness is used to account for the micro tangential displacements and the Coulomb friction law can be obtained as a special case by setting this frictional stiffness to a very large value. In the non-local friction law, the impending motion at a point of contact between two deformable bodies will occur when the shear stress at that point reaches a value proportional to a weighted measure of the normal stresses in a neighbourhood of the point. The non-linear non-local friction laws are examined in Oden and Pires [1983[b]]. In another way of departure from the classical laws, Klarbring et al. [1988] used Coulomb's friction law and a power law normal compliance while Ibrahimbegovic and Wilson [1992] presented a computational model for friction based on a regularized form of the Coulomb friction law. A power law is also used in the normal direction to relate the approach and the normal contact force. The regularized Coulomb friction law is also implemented in Saran and Wagoner [1991]. In Anand and Tong [1993], an adhering-slipping constitutive model for the frictional contact is presented.

1.3 Expanded Tube-to-tubesheet Joints

Reliable tube-to-tubesheet joints are essential in a variety of industrial applications. Fitting tubes into steam generator plates and condenser end shields are among the most common practices where the expanded joints were proven to be satisfactory. The expanded joint is the most repeatable process in the manufacturing of tube and shell heat exchangers. As such the expanding process has to be reliable in producing joints with specific requirements. The basic requirements of an expanded joint are structural integrity and quality. The structural integrity is required to contribute to the support of the dead load and to resist stresses and strains of temperature changes during operation. The structural strength can be broken down into three types, namely, axial pull-out, torsion and bending strength. On the other hand, quality means that the joint has to be leak tight and the residual stresses in the tube transition zone has to be low in order to avoid stress corrosion cracking.

Three main techniques are used to manufacture the joint, namely, roller, hydraulic and explosive. The roller expander is the most common method of expansion because of its easiness and effectiveness. A typical roller expander consists of three or five tapered rollers travelling along a tapered steel mandrel. The rollers are held in place around the mandrel by a cylindrical cage. The tube is inserted into the hole and the mandrel inside the tube is rotated either manually or using a hydraulic motor. As the rollers rotate and travel along the mandrel, the tube is forced to expand. The axial travel of the expander is limited by a thrust collar which can be adjusted by a locking

nut. Hydraulic expansion is gaining a great deal of attention mainly because of its reliability. A typical hydraulic expander consists of a cylindrical probe through which the pressurized fluid is discharged between two seals. As such, hydraulic expansion uses direct pressurization of the tube. Explosive forming can be defined as a solid state welding operation where an explosive charge is placed in a polymeric sleeve inside the tube. The explosion of this charge creates a collision front travelling along the tube axis forming the joint.

The expanded joints have been in use for almost 150 years. Being deceivingly simple, the joint did not receive enough analyzing effort from the academic point of view. As the industrial applications advance, the need for high operating pressures and temperatures requires re-evaluation of the manufacturing techniques and procedures. Several experimental, analytical and numerical analyses have been published displaying the experience gained over the years. A detailed account of a variety of these studies is presented in a review paper by Abdelsalam and Dokainish [1993a]. In what follows, a literature survey is presented in three subsections dealing with the experimental, analytical and numerical techniques employed to study the expanded tube-to-tubesheet joints.

1.3.1 Experimental Studies

The first English literature dealing with the analysis of the rolled joint is published by Oppenheimer [1927] despite being in practical use for a long time before. In this original presentation, Oppenheimer realized the fact that the holding strength of the

expanded joint is made of two contributing forces, namely, the pure holding force and the projecting resistance. The pure holding force depends upon the friction between the tube outer surface and the hole, the contact surface area and the contact pressure. The resisting force of the projecting tube against being drawn into the smaller diameter tubesheet hole depends upon the cone angle of the tube end for plain joints or the groove geometry for grooved ones. Several experimental studies have been devoted to the determination of the joint strength. The methods employed fall into two main categories; direct pull and push-out tests and contact pressure measurements. Obviously, the direct pull or push-out tests, on a tension or compression machine, gives the total joint strength whereas the contact stresses can only be related to the pure holding force. It has been reported, Fender [1985], that the pull-out strength is 6 to 8 % higher than the push-out strength and this is attributed to the lack of what is called the ideal parallel expansion.

It has been experimentally observed that the expanded joint strength has a well-defined peak-value corresponding to a certain degree of expansion beyond which the strength breaks-off suddenly upon further expansion, Fisher and Cope [1935] and Grimison and Lee [1943]. The break-off the joint strength is attributed to the smoothing of the contacting surfaces upon relative axial sliding, Fisher and Cope [1943].

A reliable indicator of the degree of expansion has been a question without a definite answer. Several studies have been published suggesting different indicators. The partial extrusion, Fisher and Cope [1935] and Fisher and Brown [1954], the input power, Fisher and Cope [1943], total extrusion, Grimison and Lee [1943], the increase

in the tube inner diameter, Grimison and Lee [1943], mandrel travel, Maxwell [1943], torque, Alexander and Ford [1956], reduction in tube-wall-thickness, Gaffoglio and Thiele [1981], and the expansion pressure, Krips and Podhorsky [1976], are among the most commonly proposed indicators. There is still a bit of confusion over whether any of these indicators is satisfactory from the consistency and practicality points of view. The size effect has been exposed once where the results showed that it is not significant, Alexander and Ford [1956]. Comparisons between the plain and grooved joint strengths led to the conclusion that the grooved joints are about 30% stronger, Haslinger and Fisher [1985].

More recently, the question of residual tensile stress determination is addressed as a result of leaks resulting from the stress corrosion cracking mechanism, SCC. Studies have been initiated in order to detect and measure these residual stresses using strain gauge measurements, Toba [1966], Bazergui and Lemarquis [1976], Hamerski [1978], Urgami et al. [1982], stress corrosion cracking tests Toba [1966] and chemical etching, Druez [1983] and Druez et al. [1985]. It is found that large tensile stresses remain on the inner tube surface in the vicinity of the expanded region. Heat treatment reduces the residual stresses significantly, however, it also reduces the interference pressure, Bazergui and Lemarquis [1976]. The initial clearance has been reported as the most significant factor affecting the residual stress level, Toba [1966].

1.3.2 Analytical Studies

Analytically, two models are introduced to calculate the residual contact pressure or

the residual stresses in the tube transition zone. The 2-D plane stress model was first proposed by Goodier and Schoessow [1943]. This model applies the thick-cylinder theory and satisfies the classical elasticity equilibrium and compatibility equations along with von-Mises yield criterion assuming perfect plasticity. This model assumes an infinite uniform plate and no clearance. A uniform pressure is applied inside the hole which leads the problem to be simplified further and becomes one-dimensional. The residual contact pressure is shown to be proportional to the extent of the plastic zone in the plate. As the pressure increases the plastic zone spreads outwards until it reaches a maximum value of 1.75 r_i, where r_i is the hole radius and the corresponding expansion pressure is 1.155 S_y, where S_y is the material yield strength. Any further increase in the expansion pressure is defeated, in the idealized model, by axial extrusion. Unlike the graphical method for obtaining the residual contact pressure presented by Goodier & Schoessow, Nadai [1943,1950] developed a general method to calculate the residual contact pressure analytically. Sachs [1947] and Krips and Podhorsky [1976] presented two different versions of the 2-D plane stress model, with finite dimensions, leading to different results.

The 2-D plane stress model has received a further development by introducing the 2-D annulus model by Soler and Hong [1984]. The annulus model consists of concentric thin elements with the inner most element being the tube. Equilibrium and compatibility are satisfied along the boundaries. The 2-D annulus model has been refined further in order to introduce strain hardening and initial clearance, Wienstock and Soler [1985]. A detailed account of the 2-D annulus model along with the developed FORTRAN code is presented in Singh and Soler [1984].

A two-dimensional axisymmetric model was introduced by Updike et al. [1988,1989] to calculate the residual stresses in the tube transition zone. This model divides the tube into three sections, expanded, transition and the rest of the tube. Compatibility and equilibrium are invoked at the adjacent boundaries of these sections. Full contact is assumed and the contact pressure is assumed uniform. This model was refined in Updike et al. [1990] to account for grooves by adding a continuous distribution of annular disks surrounding the tube. Radial clearance is represented by a step function of the axial coordinate.

1.3.3 Finite Element Studies

The first finite element analysis for the expansion process was presented by Wilson [1978]. The main objective was to determine the magnitude and location of the maximum residual tensile stresses in the tube. A mesh of axisymmetric quadrilateral finite elements is presented to model the tube and the tubesheet with special gap elements to fill the clearance between them. The load is simulated by a uniform pressure distribution which bears more resemblance to the hydraulic expansion technique.

In a trial to model the rollers action, Ramu et al. [1987], the internal pressure is applied over the rolling length in 100 cycles of loading and unloading to simulate 20 revolutions of a five roller expander. Another way of representing the rollers action is suggested, Aufaur [1987], where a radial displacement with exactly the same profile as the roller is prescribed on the tube inner surface.

Since the single tube model does not take into consideration the effect of the adjacent tubes, the seven-tube plane stress model was proposed, Podhorsky and Krips [1979] and Scott et al. [1981]. It has been reported that the single tube model seems to adequately predict the residual contact pressure corresponding to the case of simultaneous expansion while giving an overestimation when the sequential expansion is used, Chaaban et al. [1989]. Due to the many parameters involved, a fractional factorial design was proposed by Ma et al. [1990]. A primary statistical analysis using a single-tube model showed that the yield strength of the tube seems to be the most significant parameter followed by the expansion pressure level. A new explanation to the break-off the joint strength, if it is expanded beyond a certain optimum pressure, is introduced by Abdelsalam and Dokainish [1993^{b}]. Gracie et al. [1993] introduced six finite element models used to simulate the results obtained for the roller expanding of a pressure tube into an end-fitting. These six models are useful only for cases where the maximum and residual experimental profiles of the tube are known. In Hwang et al. [1993], the effect of the hole pitch on the residual contact pressure was investigated using a 2-D plane stress model. In addition, a 2-D axisymmetric model was used to study the effects of the expansion pressure, the radial gap and the extent of the pressurized zone on the residual contact pressure. Chaaban et al. [1993] suggested an empirical equation using the orthogonal design method combined with the finite element method. The proposed equation gives the residual contact pressure as a function of some material and geometric design parameters.

1.4 Objectives & Layout of the Thesis

1.4.1 Objectives

The main objectives of the study presented in this thesis are:

1. To develop a reliable and quantitatively accurate contact algorithm which is capable of solving general frictional contact problems with the following main features:

   Versatility: meaning that the algorithm is suitable for conformal/non-conformal, static/quasi-static and linear/nonlinear frictional contact problems in general engineering applications.

   Modularity: which means the algorithm is programmed in a separate module and is then connected to the main program.

   Generality: being general, the contact algorithm is able to handle contact between more than one pair of contacting surfaces without any extra effort.

2. To investigate the hydraulic expansion of tube-to-tubesheet joints using the developed algorithm.

It should be mentioned that the contact algorithm developed in Berkan [1988] is used as a starting point for the new proposed contact algorithm. The formulation of the general contact problem is re-examined to be able to arrive at the governing equations systematically in a straight forward fashion. The contact algorithm is extended to handle nonlinear continuum elements and to adopt a more general friction law. The way the contact traction is calculated is modified in order to minimize the effect of the interpolation functions on the results. Finally the algorithm is verified qualitatively and quantitatively through the solution of some contact examples which have known closed form solutions.

1.4.2 Layout of the Thesis

The thesis consists of five chapters beginning with an introductory chapter which includes four major sections. The first section illustrates the definition and importance of the finite element solution to the general contact problem in general terms. In addition, the definition of the expanded tube joint and its application is provided. In the second section, the different finite element solutions to the contact problem are reviewed. In the Third section, the expansion of tube-to-tubesheet joints is reviewed. Finally, the first chapter concludes with a brief summary of the objectives and layout of the thesis.

In chapter two, the formulation of the general contact problem is demonstrated. The basic theory of contact is discussed. The formal statement of the general contact problem is stated. The V-2 formulation is adopted to arrive at the equilibrium equations governing the general contact problem. The finite element discretization of the contact problem is developed. The discretized contact constraint equations are derived from the physical kinematic considerations. These constraints are imposed upon the equilibrium equations to arrive at the augmented system of equations governing the general contact problem. Finally, the bi-linear friction law is stated. Although other non-classical friction laws are available, the bi-linear friction law seems to be most suitable for engineering applications. This is mainly because its physical background is well understood.

The development, implementation and verification of the contact algorithm are

introduced in chapter three. First, the system of equations is solved on a sub-matrix level. This is followed by a normal and tangential iteration loops. The computer implementation of the developed solution strategy is discussed with a brief account of the main subroutines. Chapter three concludes with three illustrative examples to demonstrate the applicability of the developed algorithm.

Chapter four introduces two finite element models for the hydraulic expansion of the expanded tube joints where the contact problem plays an important role in its integrity and quality. A 2-D plane stress model is adopted to study the effects of the material mechanical properties on the joint strength. A 2-D axisymmetric model is presented to explore the distribution of the residual contact traction and the residual axial and hoop stresses along the tube inner and outer surfaces. The 2-D axisymmetric model is also used to study the effect of ignoring the geometric nonlinearity and the frictional interaction. A 2^3 factorial design matrix is adopted to study the effect of the expansion pressure, the initial radial clearance and the coefficient of friction on the residual contact traction and the maximum tensile stress along the tube. The effects of the expansion pressure and the initial radial clearance are further investigated with relation to the residual contact pressure, the residual tensile stress peak, the axial extrusion, the increase in the inner and outer tube radii and the wall-thickness- reduction ratio. Chapter four concludes with the study of the effect of the initial stresses and the cold-work layer along the as-fabricated tube outer surface on the residual tensile stresses in the expanded tube.

Finally, chapter five summarizes the main conclusions of the thesis along with suggested recommendations for future research work.

CHAPTER 2

CONTACT PROBLEM FORMULATION

2.1 Introduction

In this chapter, the mathematical formulation of the general contact problem is developed. By the general contact problem it is meant that no restriction is to be imposed on the type of analysis, material models or geometries of the contacting bodies. In other words, the formulation is suitable for linear and nonlinear kinematic motions, linear and nonlinear material behaviours for bodies having arbitrary shapes and configurations.

The contact problem may be formulated in a strong or a weak form. The strong form is made of differential equations associated with boundary conditions expressed in a continuous fashion. The strong form leads to exact solutions but those solutions are not possible except for problems with simple geometries, loadings and boundary conditions. On the other hand, the weak forms adopted by the finite element method lead to approximate solutions which are suitable for engineering practices. In addition, the use of the weak forms in the finite element formulation leads to solutions being obtained in a systematic manner irrespective of the geometries, materials, loads or boundary conditions.

To start with, a basic description of the general contact problem between two generic bodies coming into contact under the action of external loads is presented. However, it should be noted that the developed equations are equally applicable to problems with more than one pair of contacting surfaces without any conceptual difficulty. The basic description includes the notation, the governing equations and the physical contact constraints all expressed in a continuous fashion. This detailed description is followed by the formal statement or the strong form of the general contact problem. Then the principle of virtual work is utilized to obtain an appropriate variational statement, suitable for the finite element discretization. Using the developed variational statement, the weak form, the discretized finite element equations are derived systematically following the standard finite element procedure as given by Bathe [1986]. Furthermore, the discretized contact constraint equations are derived from the kinematics of deformation and enforced on the standard system of equations using a direct engineering approach.

2.2 Basic Theory of Contact

A general contact system is defined as being a mechanical or structural system which involves two or more components interacting with each other. It is also possible that two surfaces which belong to one component interact producing a contact pair. As the configuration of the system changes, sticking, sliding, and tension release contact conditions may occur between any combination of pre-defined pairs of potential contacting surfaces. However, as a study model, a two body contact system can be used without losing any generality. Moreover, the location of the potential contact interactions is explicitly defined, a priori. This restriction limits the application of the algorithm to intentional contact problems where the potential contacting surfaces are known, a priori.

Consider the two bodies, A and B, occupying domains ${}^0\Omega^A$ and ${}^0\Omega^B$, respectively, at some reference configuration defined by the time instance $t=0$ in a fixed global coordinate system $[x, y, z]$ as shown in Figure 2.1. The two bodies are brought into contact by a combination of prescribed traction and displacements applied on the surfaces, ${}^0\Gamma_F$ and ${}^0\Gamma_D$, respectively. Consequently, contact forces develop in the region of contact where neither the contact traction nor the contact boundary, ${}^t\Gamma_c$, is known a priori which results in two sets of additional unknowns but with no additional equations yet.

At the time instant t, the two bodies, A and B, occupy the domains ${}^t\Omega^A$ and ${}^t\Omega^B$,

respectively. The two bodies are assumed simply connected so that there is no interior boundary in any of the bodies and the boundaries are denoted by ${}^t\Gamma^A$ and ${}^t\Gamma^B$, respectively. The interior volumes are denoted by ${}^tV^A$ and ${}^tV^B$, respectively. Thus, one can write

$$ {}^t\Omega^A = {}^tV^A \bigcup {}^t\Gamma^A $$
$$ {}^t\Omega^B = {}^tV^B \bigcup {}^t\Gamma^B $$

where U is the union operator.

At any time instant t, the boundary of each contact body can be defined as

$$ {}^t\Gamma^A = {}^t\Gamma^A_D \bigcup {}^t\Gamma^A_F \bigcup {}^t\Gamma^A_O $$
$$ {}^t\Gamma^B = {}^t\Gamma^B_D \bigcup {}^t\Gamma^B_F \bigcup {}^t\Gamma^B_O $$

where,

- ${}^t\Gamma_D$ denotes the parts of the boundary where displacements are prescribed,
- ${}^t\Gamma_F$ denotes the parts of the boundary where loads are prescribed,
- ${}^t\Gamma_o$ denotes the potential contact boundary.

In the study of contact problems, it is required to predict the behaviour of the contact system from time $t=0$ to time $t = T > 0$, i.e. within the time domain $[0,T]$. The behaviour of the contact system is governed by four main groups of equations, namely, the equilibrium equations, the strain-displacement relations, the constitutive equations, and the equations representing the boundary conditions.

Equilibrium Equations:

For a body occupying the domain ${}^t\Omega$ and having ${}^t\Gamma$ as its surface boundary, applying Newton's second law of motion on an infinitesimal material volume, the following equilibrium equations may be obtained:

$$\frac{\partial {}^t\sigma_{ji}}{\partial {}^tx_j} + {}^tb_i = 0$$

where i and j runs as x, y and z and summation over repeated indices is implied.

These are three equations in the three cartesian coordinates *x, y* and *z*. The left subscript denotes the configuration at which the quantity is measured. As such, the following definitions apply:

- ${}^t\sigma_{ij}$ is the symmetric stress tensor.
- ${}^tx_i$ is the spatial coordinates, x, y and z.
- ${}^tb_i$ is the i^{th} component of the body forces.

Strain-Displacement Relations:

According to the infinitesimal strain theory the strain tensor is given by:

$${}^t\epsilon_{ij} = \frac{1}{2}\left({}^tu_{i,j} + {}^tu_{j,i}\right)$$

where ${}^tu_{i,j}$ is the partial derivative of ${}^tu_i$ with respect to ${}^tx_j$..

Constitutive Equations:

Constitutive equations relate the stresses to the strains in a deformable body. These

relations are mainly material dependent. However, extra care should be directed to these situations where geometric and/or material non-linearities are present. This concern is discussed in deep details in Bathe [1986], chapter 6. It suffice, for this presentation, to consider only linear-elastic materials along with the infinitesimal theory of deformation. For such materials, the relation between the stresses and strains is given by the generalized Hooke's law, i.e.

$$^{t}\sigma_{ij} = C_{ijkl}\ ^{t}\epsilon_{kl}$$

where

C_{ijkl} is the constant elasticity tensor

$= \lambda\, \delta_{ij}\delta_{kl} + \mu\, (\delta_{ik}\delta_{jl} + \delta_{il}\delta_{jk})$

λ, μ are the Lame constants

$\lambda = Ev/(1+v)(1-2v)$

$\mu = E/2(1+v)$

$\delta_{ij} = 0$ for $i \neq j$

$= 1$ for $i = j$

E is the modulus of elasticity

v Poisson's ratio

Boundary Conditions:

Two types of boundary conditions are present in a general contact problem. These are the prescribed loads, traction and displacement, and the unknown contact conditions. Assuming that the boundary Γ is smooth everywhere, a set of unit vectors $[e_1, e_2, e_3]$ may be defined at each point x_k on the boundary, where e_1 denotes the normal

outward unit vector, and e_2 & e_3 are two orthogonal tangential unit vectors at the same point x_k such that

$$ {}^{t}e_1 = {}^{t}e_2 \times {}^{t}e_3 $$

where the x in the above expression denotes a vector product.

Therefore, the force boundary conditions can be expressed as:

$$ {}^{t}\sigma_{ij}\ {}^{t}e_j = {}^{t}\bar{t}_i \qquad , i,j=x,y,z $$

where t_i is the $i^{th.}$ component of the prescribed boundary traction.

The displacement boundary conditions can be expressed as:

$$ {}^{t}u_i(x,t) = {}^{t}\bar{u}_i \qquad , i=x,y,z $$

where u_i is the $i^{th.}$ component of the prescribed displacement.

Contact Conditions:

Let the two boundary points x^A and x^B be in contact with each other at time t and that the unit boundary vectors at the two points are such that

$$ {}^{t}e_i^{A} = -\,{}^{t}e_i^{B} \qquad (2.2.1) $$

The two boundary points and their associated normal and tangential vectors are shown in figure(2-2). If the contact traction at x^A and x^B are denoted by ${}^{t}t^{A}$ and ${}^{t}t^{B}$, respectively, then by Newton's third law one may write,

$$ {}^{t}\mathbf{t}^{A} = -{}^{t}\mathbf{t}^{B} \qquad (2.2.2) $$

where ${}^{t}\mathbf{t}$ can be expressed in the following tensorial form:

$$ {}^{t}\mathbf{t} = {}^{t}t_i \, {}^{t}e_i \qquad (2.2.3) $$

In this form, t_i is the component of $\mathbf{t}$ in the direction of e_i , i.e.

$$ {}^{t}t_i = {}^{t}\mathbf{t} \cdot {}^{t}e_i \qquad (2.2.4) $$

From equations (2.2.1)-(2.2.4), the following result may be deduced:

$$ {}^{t}t_i^{A} = {}^{t}t_i^{B} $$

As such, the right superscripts A and B will be suppressed in what follows, i.e. we will have only ${}^{t}t_1$, ${}^{t}t_2$ and ${}^{t}t_3$ corresponding to the three local coordinates ${}^{t}e_1$, ${}^{t}e_2$ and ${}^{t}e_3$, respectively.

Assuming that the two contacting boundaries are not to be welded together, i.e. tensile normal traction is not allowed on the contacting boundaries, we can write the following constraint in the normal direction:

$$ {}^{t}t_1 \leq 0 $$

It is to be noted that the above constraint contributes to the complexities of the contact problem since it is in an inequality form rather than the regular equality form

experienced in regular boundary value problems. This condition is referred to as the *mechanical contact condition*.

From a purely physical reasoning, the following mathematical constraint can be established:

$$^tV^A \bigcap {}^tV^B = \phi$$

where ϕ denotes a null space. And this is called the *impenetrability* condition which means that no penetration should ever occur during the course of all admissible deformations.

The above form of the impenetrability condition cannot be used directly in the solution procedure and a usable form is developed as follows.

If a penetration function, p, is defined as:

$$^tp(x) = {}^tx^A - {}^tx^B$$

therefore, the impenetrability condition may be stated as follows:

$$^tp(x) \cdot {}^te_1 = 0$$

When oblique contact occurs, the penetration of the contactor body into the target body can be broken down into normal and tangential penetrations. As the impenetrability condition in the normal direction indicates no normal penetration is allowed, the friction law controls the tangential penetration. As such, the following

constraint may be imposed on the tangential penetrations:

$$^{t}\mathrm{p}(x) \,.\, {}^{t}e_2 = {}^{t}u_{T2}$$

$$^{t}\mathrm{p}(x) \,.\, {}^{t}e_3 = {}^{t}u_{T3}$$

where u_{T2} and u_{T3} are the prescribed relative tangential displacements according to the friction law adopted.

Moreover, the frictional traction always act in an opposite direction to the relative tangential displacement. This condition may be expressed in the following form:

$$^{t}t_2 \,.\, {}^{t}p_2 \leq 0 \qquad \forall \quad {}^{t}x \in {}^{t}\Gamma_c$$

$$^{t}t_3 \,.\, {}^{t}p_3 \leq 0 \qquad \forall \quad {}^{t}x \in {}^{t}\Gamma_c$$

A friction law relates the normal traction, the tangential traction and the tangential displacement. Since the form of friction laws does not interfere with the formulation presented in this thesis, it is presented at the end of this chapter.

2.3 Formal Statement of the General Contact Problem

Summarizing the description outlined in the previous section, the contact problem may be formally stated as follows:

Given ${}^t\mathbf{t}$ on ${}^t\Gamma_F$ and ${}^t\mathbf{b}$ on ${}^t\Omega$, $t \in [0,T]$, find $\mathbf{u}(x,t)$ for all $t \in [0,T]$ such that all the following conditions are satisfied:

1. Equations of Equilibrium:

$$ {}^t\sigma_{ji,j} + {}^t b_i = 0 $$

2. Strain-Displacement Relations:

$$ {}^t\epsilon_{ij} = \frac{1}{2}\left({}^t u_{i,j} + {}^t u_{j,i}\right) $$

3. Constitutive Relations:

$$ {}^t\sigma_{ij} = C_{ijkl}\ {}^t\epsilon_{kl} $$

4. Prescribed Displacements:

$$ {}^t u_i(x,t) = {}^t\bar{u}_i $$

5. Prescribed Traction:

$$ {}^t\sigma_{ij}\ {}^t e_j = {}^t\bar{t}_i $$

6. Contact Conditions:

$$
\begin{aligned}
{}^{t}\mathrm{p}(x) \,.\, {}^{t}e_1 &= 0 && \forall \quad {}^{t}x \in {}^{t}\Gamma_C^A \\
{}^{t}t_1 &\leq 0 && \forall \quad {}^{t}x \in \Gamma_C^A \bigcup {}^{t}\Gamma_C^B \\
{}^{t}t_1 \,.\, {}^{t}p_1 &= 0 && \forall \quad {}^{t}x \in {}^{t}\Gamma_o
\end{aligned}
$$

7 Friction Laws:

$$
\begin{aligned}
{}^{t}\mathrm{p}(x) \,.\, {}^{t}e_2 &= {}^{t}u_{T2} && \forall \quad {}^{t}x \in {}^{t}\Gamma_C^A \\
{}^{t}\mathrm{p}(x) \,.\, {}^{t}e_3 &= {}^{t}u_{T3} && \forall \quad {}^{t}x \in {}^{t}\Gamma_C^A \\
{}^{t}t_2 \,.\, {}^{t}p_2 &\leq 0 && \forall \quad {}^{t}x \in {}^{t}\Gamma_C \\
{}^{t}t_3 \,.\, {}^{t}p_3 &\leq 0 && \forall \quad {}^{t}x \in {}^{t}\Gamma_C
\end{aligned}
$$

2.4 Variational Formulation

The formal statement of the contact problem presented in the previous section is called the strong form. Based on this strong form, only a few special case contact problems have been analytically solved resulting in closed-form solutions as provided in Johnson [1985]. Numerical techniques are necessary for solving contact problems with complex geometry, material behaviour and loading.

The finite element method has proven to be one of the most powerful tools in solving such problems. In order to provide a basis for the finite element discretization, energy methods are used to obtain an appropriate variational principle. In this presentation, the principle of virtual work is adopted. In words, the principle of virtual displacements states that:

The total virtual work of the external forces on any kinematically admissible virtual displacement field equals the total virtual work of the internal stress field on the virtual strain field corresponding to that virtual displacement field.

Accordingly, one can write

$$\delta W_i = \delta W_b + \delta W_s + \delta W_p + \delta W_c \qquad (2.4.1)$$

where, the left hand side of this equation is the internal virtual work which is given by:

$$\delta W_I = \int_V \delta \epsilon_i \sigma_i \, dV$$

and the right hand side is the external work made of the following components:

$$\delta W_b = \int_V \delta u_i f_i^b \, dV$$

$$\delta W_s = \int_S \delta u_i^S t_i^s \, dS$$

$$\delta W_p = \sum_P \delta u_i^P f_i^P$$

$$\delta W_c = \int_{\Gamma_c} \delta u_i^c t_i^c \, dS$$

where f^b, t^S, f^P and t^c are the body force, the surface traction, the concentrated force acting on point p and the contact traction, respectively. The quantities δu, δu^s, δu^P, δu^c are the virtual displacement of the body, the virtual displacement of the surface s, the virtual displacement of the material point p and the virtual relative displacement of the contact surface, respectively.

Equation (2.4.1) is the mathematical representation of the virtual work principal which is to be adopted to develop the discretized finite element equations in the next section.

2.5 Finite Element Discretization

In this section, the finite element method is adopted to develop the discretized version of the governing system of equations for a general contact problem. In the standard finite element procedure, the continuum Ω of the problem is divided into sub-domains $\Omega^{(E)}$ called the finite elements. According to the geometry of the mathematical model, the finite elements take different types including solid, shell, beam, ... etc. Different element types are introduced to represent different mathematical models adopting different geometric and/or load assumptions. In general, a 3-D solid element suffice to cover all engineering applications. However, there exist such cases where using the 3-D solid element would lead to extremely large number of degrees of freedom which expands the size of the system of equations leading to an expanded solution time. For example, a dam structure has a very large longitudinal dimension relative to its width and height. Such a very long structure can be mathematically represented by a plane strain model. In contrast, a very short flat ring subjected to in-plane forces can be simulated by a plane stress model. Also, slender structures are modeled by beam elements and shell structures by shell elements.

In what follows, we consider three-dimensional bodies which may be approximated by collections of finite solid elements inter-connected at a specified number of points called nodes. The continuous distribution of a field variable, which is the displacement u(x,y,z) in our case, is approximated by rather piece-wise continuous functions called the shape or interpolation functions, $h_i^{(E)}(\xi,\eta,\zeta)$, as follows:

$$\mathbf{u}^{(E)} = H^{(E)}\, u^{(E)} \qquad (2.5.1)$$

where,

$\mathbf{u}^{(E)}$ is the elemental distributed displacement vector,

$H^{(E)}$ is a matrix of shape functions,

$u^{(E)}$ is the elemental nodal displacement vector and

ξ, η, ζ are the local coordinates within an element.

Substituting eqn. (2.5.1) into the strain-displacement relations given in section 2.4, the elemental strains, $\epsilon^{(E)}$, corresponding to the elemental displacement field, $\mathbf{u}^{(E)}$, can be expressed as

$$\epsilon^{(E)} = B^{(E)}\, \mathbf{u} \qquad (2.5.2)$$

where, $B^{(E)}$ is the strain displacement matrix where the rows of this matrix are obtained by appropriately differentiating and combining rows of the matrix H.

Substituting equations (2.5.1 and 2.5.2) into the statement of the virtual work principle, eqn. (2.4.1), the discretized finite element equations may be stated as follows:

$$k\, u = r$$

where,

K is the stiffness matrix which is given by,

$$K = \sum_{E} \int_{V^{(E)}} B^{(E)T} C^{(E)} B^{(E)} \, dV^{(E)}$$

u is the global nodal displacement vector,

r is the global nodal force vector which can be written in the following form:

$$r = r_b + r_s + r_p + r_c$$

where, r_b, r_s, r_p and r_c are the equivalent nodal force vectors corresponding to the body force, the surface traction, the concentrated force and the contact traction, respectively, and are given by:

$$r_b = \sum_{E} \int_{V^{(E)}} H f^b \, dV^{(E)}$$

$$r_s = \sum_{E} \int_{S^{(E)}} H^s t^s \, dS^{(E)}$$

$$r_p = f^p$$

$$r_c = \sum_{E} \int_{\Gamma_c^{(E)}} H^s t^c \, dS^{(E)}$$

Up to this point, the effect of the contact interactions has been included in the equilibrium equations through the equivalent contact nodal force vector, r_c. The inclusion of these contact forces requires a prior knowledge of the contact area which is not generally guaranteed. Therefore, an iterative procedure is essential and the equilibrium equations takes the following incremental form:

$$K^{(i)} \Delta u^{(i+1)} = \Delta r^{(i)} + r_c^{(i+1)} \qquad (2.5.3)$$

and the force vector is modified as follows:

$$\Delta r^{(i)} = r - f_e^{(i)}$$

where,

f_e is the force vector equivalent to the internal stresses.

The iterations are terminated upon convergence which is characterized by $\Delta u^{(i+1)}$ approaches zero or a very small preset tolerance for practical calculations. It can be concluded that at convergence the contact forces are equal to the out of balance force vector.

In the following section, the discretized form of the contact constraint equations is derived and later on it is imposed on the system of equilibrium equations as illustrated in section 2.7.

2.6 Discretized Constraint Equations

In section 2.2, the contact constraint equations are stated in a general continuous fashion which is not suitable for the finite element analysis. As such, a discretized form is derived. Figure 2.3 shows the contactor and target discretized contact surfaces. The contact constraint equations are derived for a single contactor node, k, penetrating a target surface segment, J, and then the equation(s) is(are) extended to include all penetrating contactor nodes. Two conditions are dealt with in this section; the impenetrability condition and the Newton's third law of action and reaction.

Impenetrability Condition:

The impenetrability condition states that no overlap should ever be allowed between any of the contacting bodies. In other words, the vector of penetration at all contacting nodes has to equal zero. Figure 2.4, shows a schematic diagram for the contactor node k as it penetrates the target surface segment, J, at the end of the $i^{th.}$ iteration within the time step from t to $t+\Delta t$. First we define a virtual node s on the target surface segment J. The position vector for the target node can be expressed as follows:

$$x_s^{(i)} = x_k^{(i)} - p_k^{(i)} \qquad (2.6.1)$$

where p_k is the vector of penetration (overlap) after the $i^{th.}$ iteration.

At the end of the $(i+1)^{th.}$ iteration, the contactor node assumes a new surface position marked by $k^{(i+1)}$ and the virtual target node moves to the position marked by $s^{(i+1)}$ as shown in figure 2.4.

From the kinematics of motion, as shown in Figure 2.4, one may write:

$$x_s^{(i+1)} + \Delta u_{rk}^{(i+1)} = x_k^{(i+1)} \tag{2.6.2}$$

Subtracting eqn. (2.6.1) from eqn. (2.6.2) yields

$$\Delta u_s^{(i+1)} + \Delta u_{rk}^{(i+1)} = \Delta u_k^{(i+1)} + p_k^{(i)} \tag{2.6.3}$$

In other words, the corrective displacement increments, $\Delta u_s^{(i+1)}$ and $\Delta u_k^{(i+1)}$ bring the contactor node, k, back on the target surface away from the virtual surface node, s, in general.

The displacement of the virtual node, s, can be obtained from the nodal values of the target nodal displacements using the shape functions,

$$\Delta u_s^{(i+1)} = h_j^{(e)}(\xi_s^{(i)}, \eta_s^{(i)}, \zeta_s^{(i)})\, \Delta u_j^{(e)(i+1)} \tag{2.6.4}$$

where the index j runs over the surface nodes of the target segment.

Substituting eqn. (2.6.4) into eqn. (2.6.3) the constraint equation takes the following form:

$$p_k^{(i)} + \Delta u_k^{(i+1)} - h_j^{(e)}(\xi_s^{(i)}, \eta_s^{(i)}, \zeta_s^{(i)})\, \Delta u_i^{(e)(i+1)} = \Delta u_{rk}^{(i+1)}$$

Furthermore, this equation can be written in the following form:

$$p_k^{(i)} + Q_k^{(i)} \Delta u^{(i+1)} = \Delta u_{rk}^{(i+1)} \qquad (2.6.5)$$

where,

$\Delta u^{(i+1)}$ is the global displacement vector, and

$Q_k^{(i)}$ is a vector of the same length as the global nodal displacement vector with all entries being zero except the location corresponding to the contactor node, k, and the corresponding target surface nodes.

At this stage it would be useful to show in some detail the structure of the constraint equation. In a two dimensional problem, for a single contactor node k penetrating the target surface segment defined by nodes a, b and c, eqn. (2.6.5) can be written in the following form:

$$\begin{bmatrix} 1 & 0 & -h_a & 0 & -h_b & 0 & -h_c & 0 \\ 0 & 1 & 0 & -h_a & 0 & -h_b & 0 & -h_c \end{bmatrix}^{(i)} \begin{bmatrix} \Delta u_{kx} \\ \Delta u_{ky} \\ \Delta u_{ax} \\ \Delta u_{ay} \\ \Delta u_{bx} \\ \Delta u_{by} \\ \Delta u_{cx} \\ \Delta u_{cy} \end{bmatrix}^{(i+1)} + \begin{bmatrix} p_{kx} \\ p_{ky} \end{bmatrix}^{(i)} = \begin{bmatrix} \Delta u_{rkx} \\ \Delta u_{rky} \end{bmatrix}^{(i+1)}$$

Resolving the contact constraint in the normal, (n_x , n_y), and tangential, (t_x , t_y), local directions, results in the following set of constraint equations for a single penetrating contactor node in the normal and tangential local directions:

$$N_k^{(i)} \Delta u^{(i+1)} + p_{kN}^{(i)} = \Delta u_{rkN}^{(i+1)}$$
$$R_k^{(i)} \Delta u^{(i+1)} + p_{kT}^{(i)} = \Delta u_{rkT}^{(i+1)}$$

where,

$$N_k^{(i)} = \left[n_x \;\; n_y \;\; -n_x h_a \;\; -n_y h_a \;\; -n_x h_b \;\; -n_y h_b \;\; -n_x h_c \;\; -n_y h_c\right]^{(i)}$$
$$R_k^{(i)} = \left[t_x \;\; t_y \;\; -t_x h_a \;\; -t_y h_a \;\; -t_x h_b \;\; -t_y h_b \;\; -t_x h_c \;\; -t_y h_c\right]^{(i)}$$

In general with more than one contactor node coming into contact at the same time, the contact constraint equations may be written in the following form:

$$N^{(i)} \Delta u^{(i+1)} + p_N^{(i)} = \Delta u_{rN}^{(i+1)}$$
$$R^{(i)} \Delta u^{(i+1)} + p_T^{(i)} = \Delta u_{rT}^{(i+1)} \qquad (2.6.6)$$

In the above equations, $p_N^{(i)}$ and $p_T^{(i)}$ are two vectors containing all the values of the normal and tangential overlaps, respectively, for all contactor nodes in action. $N^{(i)}$ and $R^{(i)}$ are rectangular matrices with one row corresponding to each individual contactor node.

In general frictional contact problems, two constraint equations per contactor node are needed. One equation constraints the motion in the normal direction and the other in the tangential direction.

In case of sticking contact condition the relative sliding vector is put to zero and one

may obtain:

$$N^{(i)} \Delta u^{(i+1)} + p_N^{(i)} = 0$$
$$R^{(i)} \Delta u^{(i+1)} + p_T^{(i)} = 0 \qquad (2.6.7)$$

where p_N and p_T are the normal and tangential overlaps which have to be removed.

On the other hand, in case of sliding contact condition, only the normal displacement is constrained and the tangential sliding displacement can take any value. Therefore, only the first equation in the set of equations (2.6.7) is to be considered.

Newton's Third Law:

First, the contact nodal force vector may be written as the vector sum of the normal and tangential nodal force vectors as follows:

$$r_c^{(i+1)} = f_N^{(i+1)} + f_T^{(i+1)} \qquad (2.6.8)$$

Now, the Newton's 3rd. law applied on the contact forces amounts to the contact force at the contactor node k being equal to the contact force at the corresponding virtual target node s and in the opposite direction. Consequently, for the contactor node k, one may write

$$r_{cs}^{(i+1)} = - r_{ck}^{(i+1)} \qquad (2.6.9)$$

where r_{cs} and r_{ck} are the contact forces at the virtual node s and the contactor node k, respectively.

Applying the principle of virtual work, the equivalent nodal forces acting on the target surface segment are given by:

$$r_{cJ}^{(i+1)} = r_{cs}^{(i+1)} h_J^{(i+1)} \qquad (2.6.10)$$

where r_{cJ}, J=a,b and c, is the equivalent target nodal contact force vector.

Combining eqns. (2.6.8), (2.6.9), and (2.6.10) yields,

$$r_c^{(i+1)} = N^T f_N^{(i+1)} + R^T f_T^{(i+1)} \qquad (2.6.11)$$

where, the italic f_N *and* f_T are the scalar normal and tangential forces, respectively.

As such, the expression of the contact force vector given by eqn.(2.6.11) implicitly satisfies the Newton's third law of action and reaction.

2.7 Imposing Contact Constraints

It has already been established that the contact problem is a non-linear problem which requires an iterative solution procedure in order to solve for the unknown contact area and contact traction satisfying the contact conditions.

Using eqns (2.5.3) and (2.6.11), the incremental form of the equilibrium equations of the discretized contact system is given by:

$$K^{(i)} \Delta u^{(i+1)} = \Delta r^{(i)} + N^{(i)T} f_N^{(i+1)} + R^{(i)T} f_T^{(i+1)} \qquad (2.7.1)$$

Rearranging the equilibrium equations with respect to the three sets of unknowns, the following matrix form is obtained:

$$\begin{bmatrix} K & -N^T & -R^T \\ 0 & 0 & 0 \\ 0 & 0 & 0 \end{bmatrix}^{(i)} \begin{bmatrix} \Delta u \\ f_N \\ f_T \end{bmatrix}^{(i+1)} = \begin{bmatrix} \Delta r \\ 0 \\ 0 \end{bmatrix}^{(i)} \qquad (2.7.2)$$

For the sticking contact condition, the contact constraint equations can be expressed in the following matrix form:

$$\begin{bmatrix} 0 & 0 & 0 \\ -N & 0 & 0 \\ -R & 0 & 0 \end{bmatrix}^{(i)} \begin{bmatrix} \Delta u \\ f_N \\ f_T \end{bmatrix}^{(i+1)} = \begin{bmatrix} 0 \\ p_N \\ p_T \end{bmatrix}^{(i)} \qquad (2.7.3)$$

Combining eqns. (2.7.2)&(2.7.3), the augmented system of equations may be written

in the following matrix form:

$$\begin{bmatrix} K & -N^T & -R^T \\ -N & 0 & 0 \\ -R & 0 & 0 \end{bmatrix}^{(i)} \begin{bmatrix} \Delta u \\ f_N \\ f_T \end{bmatrix}^{(i+1)} = \begin{bmatrix} \Delta r \\ p_N \\ p_T \end{bmatrix}^{(i)} \qquad (2.7.4)$$

The augmented system of equations, given by eqn. (2.7.4), contains zeros along the main diagonal which is not desirable in solution techniques utilizing Gauss elimination method or any of its variants. This difficulty will be dealt with in the next chapter where we present the computer implementation of the contact algorithm.

It should be noted that in this thesis, the contact constraint equations are never augmented with the equilibrium equations as given by eqn. (2.7.4). Instead, the solution is performed on a matrix level to obtain corrective normal and tangential contact force vectors that remove all the overlaps and satisfy the friction law.

2.9 Friction Law

In this section the non-classical nonlinear friction law, proposed by Oden and Pires [1983], is considered. This law allows for the micro relative tangential displacements of the contacting bodies before the bulk sliding motion commences. It is worth noting that Coulomb friction law can be deduced as a special case of the non-linear law. The bi-linear friction law may take the form:

$$t_T \leq \mu t_N \quad : \quad t_T = -E_f u_T$$

$$t_T > \mu t_N \quad : \quad t_T = -\mu t_N \frac{u_T}{|u_T|}$$

where,

E_f is referred to as the friction modulus,

μ is the coefficient of friction, and

u_T is the tangential relative sliding displacement.

If the friction modulus, E_f, approaches infinity, we may write the friction law in the following form:

$$t_T \leq \mu t_N \quad : \quad u_T = 0$$

$$t_T > \mu t_N \quad : \quad t_T = -\mu t_N \frac{u_T}{|u_T|}$$

which is the classical Coulomb's law of friction.

Figures 2.5 and 2.6 show schematic representation of the nonlinear law and Coulomb's law, respectively.

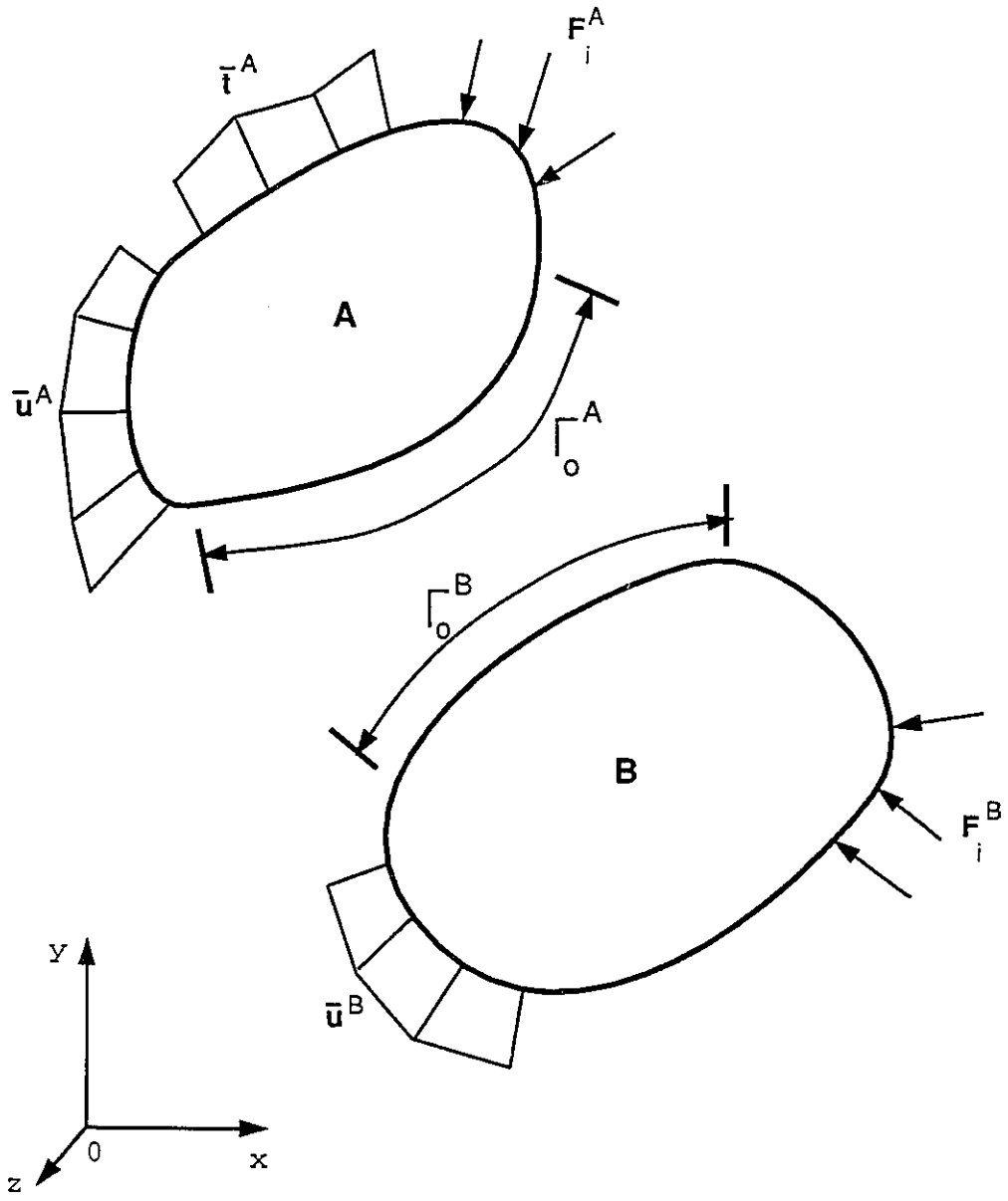

Figure 2.1: Two Generic Bodies Coming into Contact

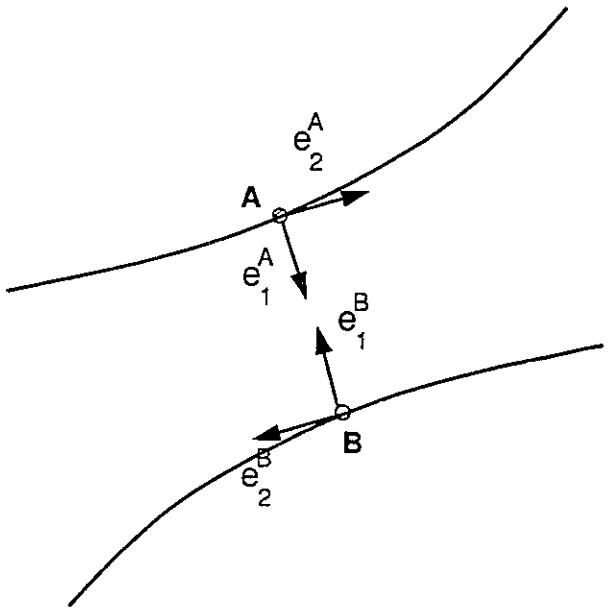

Figure 2.2: Local Coordinate System

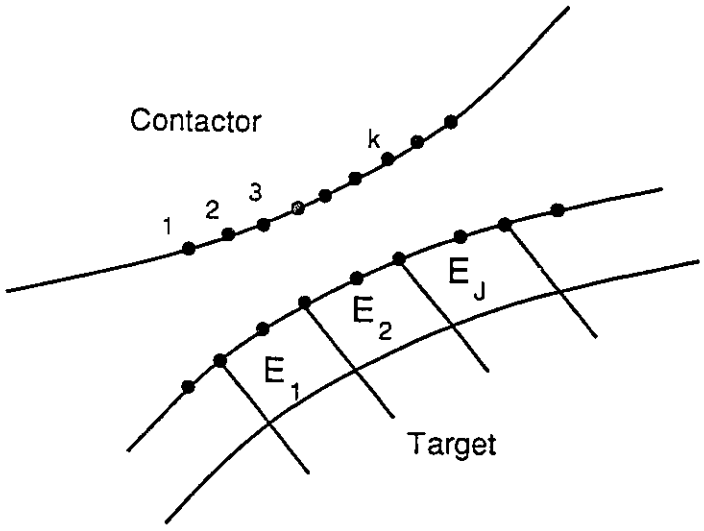

Figure 2.3: Discretized Contact Surfaces

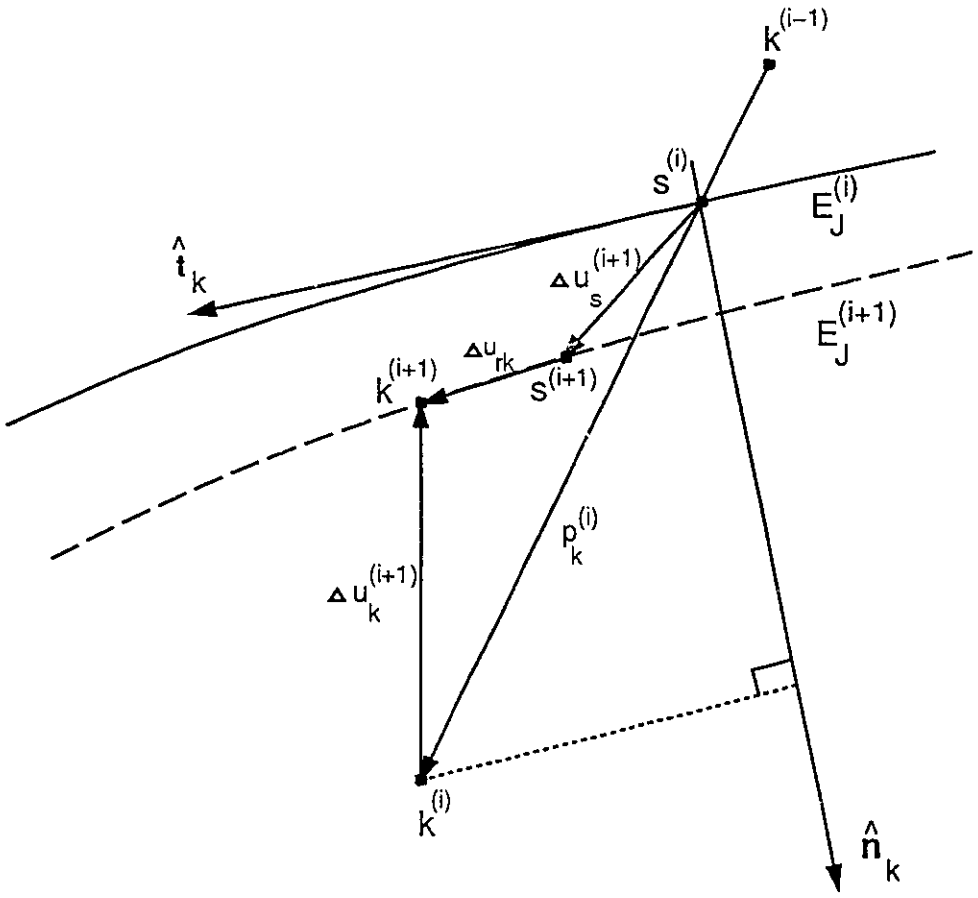

Figure 2.4: Kinematics of a Penetrating Contactor Node k.

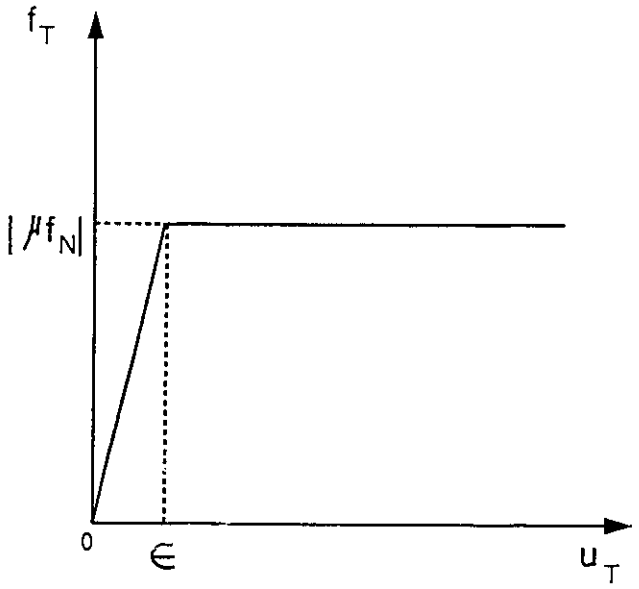

Figure 2.5: Non–Linear Friction Law

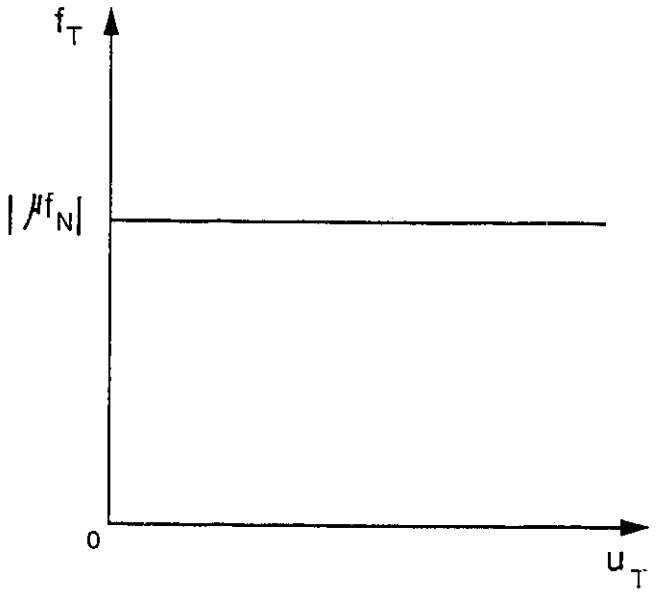

Figure 2.6: Coulomb's Friction Law

CHAPTER 3

CONTACT ALGORITHM

3.1 Introduction

In this chapter, the solution strategy of the general contact problem, formulated in chapter two, is presented. The solution strategy includes the development and the computer implementation of the contact algorithm. The developed contact algorithm presented in this chapter belongs to the direct methods in solving general contact problems where the contact constraint equations are satisfied iteratively by the use of corrective contact nodal forces.

Three main features make the presented algorithm novel. Firstly, a bi-linear non-classical friction law is adopted in the analysis of frictional contact using a direct method and the classical Coulomb's law is deduced as a special case. The bi-linear friction law allows for micro relative tangential displacements under very small normal traction. Secondly, the algorithm is made capable of handling nonlinear finite elements, i.e., elements with curved sides. These elements are essential for a close geometric representation of practical engineering problems with curved boundaries. Thirdly, the contact equations are solved for the nodal values of the contact forces that satisfy the contact constraint equations. Consequently, the contact traction is calculated using the

principle of virtual displacements after convergence is achieved. This treatment makes the solution insensitive to the choice of the shape functions interpolating the contact traction. This sensitivity is a result of including these interpolation functions in the iterative procedure. Moreover, solving for the contact nodal forces is consistent with the overall finite element solution strategy where all distributed quantities are discretized.

The presentation of the contact algorithm begins with the solution of the system of equations on matrix level. This solution step results in three sets of equations that give the global nodal displacement vector and the normal and tangential contact nodal force vectors. Then the solution strategy is broken down into a normal iteration loop and a tangential iteration loop. In the normal iteration loop, we solve for the unknown contact area. The contact area is defined by surface nodes having negative contact normal forces. This is followed by the satisfaction of the friction law on the estimated contact area. Upon convergence of both the normal and tangential iteration loops, the resulting contact nodal forces are distributed over the contact surface to get the equivalent contact traction. This is done using linear shape functions and the transformation matrix is lumped using the row sum method. The computer implementation of the solution strategy is demonstrated with schematic flow charts. Since the developed algorithm is added to the Incremental Nonlinear Dynamic Analysis Program, INDAP, as a separate module, a short note on INDAP is presented. This is followed by a presentation of the contact routines where special attention is directed towards the searching algorithm, the scaling procedure and the estimation of the matrix that transforms the contact forces to contact traction. Finally, illustrative

examples are solved to demonstrate the applicability of the algorithm in a variety of contact problems which ranges form elastic non-conformal contacts to elasto-plastic conformal contact situations. The problem of an elastic sphere pressed between two rigid blocks is invoked to demonstrate the ability of the developed algorithm to solve non-conformal elasto-static unilateral contact problems without friction. The finite element solution obtained using the developed algorithm is compared with the closed-form solution known as the Hertzian solution and is summarized in Appendix A. Then friction is included in the analysis and the role of both the coefficient of friction and the friction modulus is interpreted. To address the problem of conformal elasto-static contact, the problem of a cylinder pressed between two rigid blocks is solved for fictional and frictionless contacts. Finally, the thick cylinder theory is invoked to check the developed algorithm against conformal elasto-plastic contact problems. The finite element solution is compared with the closed-form solution presented in Appendix A.

3.2 Solution of the System of Equations

In the previous chapter, the system of equations governing the contact problem is derived. Two sets of extra unknowns are present because of contact; these are the normal and tangential contact nodal force vectors. The system of equations as given by eqn. (2.7.4) has zeroes in its diagonal which is not desirable in the standard solution techniques based on Gauss elimination method where a zero pivot would lead to immature termination of the solution procedure. In order to get around this difficulty without disturbing the equation solver, the equations are solved first on a matrix level by successive elimination of the different sets of unknowns. Consequently, an iterative procedure is suggested to solve for the normal and the tangential contact nodal force vectors which are required to satisfy the contact conditions.

Applying simple algebraic manipulations on matrix level on the set of equilibrium equations given by eqn. (2.7.1), the incremental displacement vector may be written in the following form:

$$\Delta u^{(i+1)} = K^{(i)^{-1}} \left[\Delta r^{(i)} + N^T f_N^{(i+1)} + R^T f_T^{(i+1)} \right] \tag{3.2.1}$$

Substituting the displacement vector given by eqn. (3.2.1) into the first set of contact constraint equations given by eqn. (2.6.7), one may write the normal contact nodal force vector in the following form:

$$[NN]^{(i)} f_N^{(i+1)} = -(p_N^0 + p_N^{(i)}) - [NR]^{(i)} f_T^{(i+1)} \tag{3.2.2}$$

The square matrices $[NN]^{(i)}$ and $[NR]^{(i)}$ are given by:

$$[NN]^{(i)} = N^{(i)} K^{-1(i)} N^{T(i)}$$
$$[NR]^{(i)} = N^{(i)} K^{-1(i)} R^{T(i)}$$

The penetration vector p_N^0 is given by:

$$p_N^0 = N K^{-1} \Delta r^{(i)}$$

From now on, the iteration index will be dropped from all quantities except when confusion is inevitable and it is understood that all quantities without the superscript denoting the iteration number belongs to the $i^{th.}$ iteration.

The two matrices [NN] and [NR] may be interpreted as being direct and cross flexibility matrices, respectively. Direct flexibility is defined as the displacement in the normal/tangential direction due to a unit force in the same direction. On the other hand, a cross flexibility is the displacement in the normal/tangential direction due to a unit force in the other direction. As such, the $(i,j)^{th.}$ element in [NN] is the normal displacement at the contactor node i due to a unit normal contact force at the contactor node j. Similarly, the $(i,j)^{th}$ element in [NR] is the normal displacement of the contactor node i due to a unit tangential contact force at node j.

For a contact system with N_p total number of nodes and N_c active contactor nodes, both N and R are N_c x (N_p*N_d) rectangular matrices and K is (N_p*N_d) x (N_p*N_d) square matrix where N_d is the total number of degrees of freedom per node. As such, the two

matrices [NN] and [NR] become $N_c x N_c$ square matrices. The inverse of [NN] and [NR] would be the direct and cross contact stiffness matrices, respectively.

Now, we have equation (3.2.2) stating that a normal force vector f_N is needed to compensate for the normal overlap from the previous iteration plus the overlap introduced by the increment in the out of balance force vector and any normal overlap caused by the tangential forces. A geometric interpretation of eqn. (3.2.2) is given in Figure 3.1 for a simple case depicting normal contact where no tangential components are present.

Substituting the displacement vector, Δu, from eqn. (3.2.1) into the second contact constraint equation given by eqn. (2.6.7), the tangential nodal force vector may be expressed as follows:

$$[RR]^{(i)} f_T^{(i+1)} = -(p_T^0 + p_T^{(i)}) - [RN]^{(i)} f_N^{(i+1)} \qquad (3.2.3)$$

where [RR] is a direct flexibility matrix similar to [NN] but in the tangential direction and is given by:

$$[RR] = R K^{-1} R^T$$

and the tangential penetration vector p_T^0 is given by:

$$p_T^0 = R K^{-1} \Delta r^{(i)}$$

Obviously, eqn. (3.2.3) representing the tangential direction, is similar to eqn. (3.2.2) in the normal direction. It may be interpreted similarly as shown in Figure 3.2 for a

case of pure tangential motion.

Now, if both normal and tangential penetrations are present, it might occur that the normal contact forces introduce tangential overlap and vice versa as depicted in Figure 3.3 where a general case of overlap is depicted.

Substituting the normal nodal contact force vector, f_N, from eqn. (3.2.2) into eqn. (3.2.3) yields:

$$[a_T] f_T^{(i+1)} = - (p_T^{(i)} + p_T^0) - [RN] [NN]^{-1} (p_N^0 + p_N^{(i)}) \qquad (3.2.4)$$

where $[a_T]$ is given by:

$$[a_T] = [RR] - [RN] [NN]^{-1} [NR] \qquad (3.2.5)$$

In eqn. (3.2.4) a tangential force vector f_t acts upon the flexibility matrix $[a_T]$ producing corrective displacements to compensate for the tangential overlaps $p_T^{(i)}$, p_T^0 and the tangential overlap due to the normal overlaps.

The question now is how to compensate for the vector of normal overlap in order to satisfy the impenetrability constraint and the vector of tangential overlap to satisfy the friction law. This is achieved through the application of normal and tangential nodal contact forces on both the contactor and the target surfaces.

From the first sight, the solution procedure might seems obvious. One might think of solving eqn. (3.2.4) for the tangential forces then substitute these forces into eqn.

(3.2.2) to get the normal forces. Having obtained the normal and tangential forces it would be trivial to calculate the displacement vector in eqn. (3.2.1). The problem with this line of thought is that the contact area is not known and it has to be determined before solving for the tangential forces. The solution for these nodal contact forces is obtained in two nested iteration loops for the normal and tangential overlaps. In the normal iteration loop, the nodal contact normal forces that remove the normal overlap are estimated. Having obtained an estimation for the nodal contact normal forces, the contact area can be defined. Over the defined contact area, the nodal contact tangential forces are estimated according to the friction laws.

3.3 Solution Strategy

The procedure begins by assuming sticking contact conditions and we proceed incrementally towards the normal contact forces that remove all the compatibility violations. This starting assumption will give an estimate for the contact area decided upon using the normal nodal forces. Then the tangential forces are estimated and checked against the friction law. In other words, we solve for the contact area first then we fulfil the friction law on the estimated area. Having updated the frictional forces according to the friction law adopted, a new estimate for the normal forces is obtained and checked for any tensile forces which would suggest the release of the corresponding nodes from the active contact set. The contact iterations are continued as illustrated in what follows until convergence is achieved.

3.3.1 Normal Iteration Loop

Since the contact area is not known a priori, a normal iteration loop is introduced to define that contact area or more precisely to define the active contactor nodes. By the active contactor nodes it is meant the contactor nodes experiencing compressive normal contact forces. All nodes experiencing tensile normal force are released from the active set and the contact force is set to zero.

Let us suppose that (n) normal iterations have been completed. At the end of the $(n)^{th}$ normal iteration the normal contact nodal force vector may be expressed, using eqn.

(3.2.2), in the following form:

$$[NN]^{(i)} f_N^{(n)} = - (p_N^0 + p_N^{(n)}) - [NR]^{(i)} f_T^{(n)} \qquad (3.3.1)$$

The system in eqn. (3.3.1) is made of N_c algebraic equations containing $2*N_c$ unknown normal and tangential contact nodal forces. An assumption has to be made to reduce the number of unknowns to the number of equation so that the system would be solvable. This can be done by introducing the tangential to normal force ratio at each contactor node defined as:

$$[\theta_{ii}] = f_{Ti}/f_{Ni}$$

where it is assumed that the above mentioned ratio is known and kept constant during the normal iterations. As such, eqn. (3.3.1) may be expressed in the form:

$$[a_N] f_N^{(n)-} = - (p_N^0 + p_N^{(n)}) \qquad (3.3.2)$$

where $[a_N]$ is an N_c*N_c normal flexibility matrix given by:

$$[a_N] = [NN] + [NR][\theta]_{ii} \qquad (3.3.3)$$

Moreover, the condition of compressive surface traction is expressed as follows:

$$\begin{aligned} f_{Ni}^{(n)-} &= f_{Ni}^{(n)} \qquad \text{for} \quad f_{Ni}^{(n)} \leq 0 \\ f_{Ni}^{(n)-} &= 0 \qquad\quad \text{for} \quad f_{Ni}^{(n)} > 0 \end{aligned} \qquad (3.3.4)$$

where the second line in eqn. (3.3.4) indicates tension release of contactor nodes with tensile normal force.

In incremental form, the normal overlap vector and the normal contact force vectors may be written as follows:

$$\begin{aligned} p_N^{(n+1)} &= p_N^{(n)} + \Delta p_N \\ f_N^{(n+1)} &= f_N^{(n)} + \Delta f_N \end{aligned} \tag{3.3.5}$$

which upon using eqn. (3.3.2) yields,

$$\Delta p_N = -[\alpha_N]\, \Delta f_N \tag{3.3.6}$$

This is a system of N_c linear algebraic equations which is constrained by two conditions corresponding to weather the previous iteration led to a gap or an overlap as indicated in eqn. (3.3.4).

Now, in the $(n+1)^{th.}$ iteration, the following conditions are enforced:

$$\begin{aligned} p_N^{(n+1)} &= 0 \qquad \text{for} \quad p_N^{(n)} \geq 0 \\ f_N^{(n+1)} \cdot p_N^{(n+1)} &= 0 \qquad \text{for} \quad p_N^{(n)} < 0 \end{aligned} \tag{3.3.7}$$

The condition in the first line in eqn. (3.3.7) is satisfied by nodes penetrating the target surface in the $(n)^{th.}$ normal iteration and in the next iteration the overlap should be eliminated. Furthermore, the condition in the second line is satisfied if the contactor node is outside the target body at the end of the $(n)^{th.}$ iteration and in the next iteration either it comes to contact and the overlap should be zero or remains off contact and the normal force is zero.

Substituting eqns. (3.3.5) and (3.3.6) into eqn. (3.3.7) and neglecting the second order terms we obtain the following set of algebraic equations:

$$[a_N]\Delta f_N = p_N^{(n)} \qquad \text{for } p_N^{(n)} \geq 0$$
$$\left([a_N] f_N^{(n)} - p_N^{(n)}\right)\Delta f_N = f_N^{(n)} p_N^{(n)} \qquad \text{for } p_N^{(n)} < 0$$

Finally, the above two sets of equations for penetrating and non penetrating contact nodes can be expressed in the following uniform set:

$$\left([a_N][F] - [P]\right)\Delta f_N = [F]\, p_N^{(n)} \tag{3.3.8}$$

where the normal penetration vector, p_N, at the $(n)^{th.}$ iteration is estimated from:

$$p_N^{(n)} = - p_N^0 - [NN] f_N^{(n)} - [NR] f_T^{(n)} \tag{3.3.9}$$

and the elements of the diagonal matrices, [F] and [P], are given by:

$$f_{ii} = 1 \quad , \quad p_{ii} = 0 \qquad \text{for } p_N^{(n)} \geq 0$$
$$f_{ii} = f_{Ni}^{(n)} \quad , \quad p_{ii} = p_{Ni}^{(n)} \qquad \text{for } p_N^{(n)} < 0$$

Now, the system in eqn. (3.3.8) consists of N_c linear equations in the incremental contact nodal force vector, Δf_N.

Having obtained an estimate for Δf_N, the increment in the normal penetration vector Δp_N can be estimated form eqn. (3.3.5). Consequently, eqn.(3.3.5) can be used to update the normal contact force and penetration vectors. The normal iterations continues until convergence is reached which is indicated by a vanishing overlap.

3.3.2 Tangential Iteration Loop

In the normal iteration loop, the ratio between the tangential to normal forces is kept constant in order to arrive at an estimate for the contact area and a first estimate for the tangential forces. Having obtained that estimate, for the contact area, friction iteration loop is started to check the tangential forces against the friction law. Similar to the basic idea of removing all normal overlaps, the tangential overlaps have to be removed in case of sticking contact using coulomb's friction law if the frictional forces are below the frictional capacity. If using a non-classical friction law as suggested in this study, the tangential displacements are not removed but controlled according to the nonlinear friction law.

Let it be assumed that (r) friction iterations have been completed. At the end of the $(r)^{th.}$ friction iteration, the tangential displacements can be obtained, using eqn. (3.2.3), as follows:

$$p_T^{(r)} = - p_T^0 - [RN] f_N^{(r)} - [RR] f_T^{(r)} \qquad (3.4.3)$$

In the $(r+1)^{th.}$ friction iteration, either we have a micro or macro sliding. This uncertainty in deciding upon the friction state can be dealt with by combining both constraints in one unified mathematical form as follows:

$$\left(f_{Ti}^{(r+1)} + E_f p_{Ti}^{(r+1)}\right)\left(f_{Ti}^{(r+1)} + \phi_i^{(r)} f_{Ni}^{(r+1)}\right) = 0 \qquad (3.4.3)$$

where the diagonal matrix ϕ is given by:

$$\phi_i^{(n)} = \frac{p_{Ti}^{(n)}}{|p_{Ti}^{(n)}|}\mu_i \qquad (3.4.4)$$

The constraint equation given in eqn. (3.4.3) states that either there exist a micro slip and the tangential force is equal to the friction modulus times the tangential displacement. Otherwise, the tangential force is equal to the frictional capacity determined by the normal force multiplied by the coefficient of friction which corresponds to a condition of macro slip.

Eqn. (3.4.3) contains the three sets of unknowns; these are the normal forces, tangential forces and the relative tangential displacements. The whole idea now is to express the increment in the normal traction and the tangential overlap in terms of the increment of the tangential traction keeping only one independent variable in eqn. (3.4.3).

In incremental form, we have,

$$\begin{aligned} f_{Ti}^{(r+1)} &= f_{Ti}^{(n)} + \Delta f_{Ti} \\ f_{Ni}^{(r+1)} &= f_{Ni}^{(n)} + \Delta f_{Ni} \\ p_{Ti}^{(r+1)} &= p_{Ti}^{(n)} + \Delta p_{Ti} \end{aligned} \qquad (3.4.5)$$

Using eqns. (3.2.4) and (3.4.5), we may write,

$$\Delta p_T = [\alpha_T]\Delta f_T \qquad (3.4.6)$$

Furthermore, using eqns. (3.2.2) and (3.4.5),

$$\Delta f_N = [TN]\,\Delta f_T \tag{3.4.7}$$

where,

$$[TN] = -[NN]^{-1}\,[NR]$$

Substituting eqns. (3.4.6) and (3.4.7) into the frictional constraint in eqn. (3.4.3) yields:

$$\left(f_{Ti}^{(r)} + \Delta f_{Ti} + E_f(p_{Ti}^{(r)} + \Delta p_{Ti})\right]\left[f_{Ti}^{(r)} + \Delta f_{Ti} + \phi_i^{(r)}\,(f_{Ni}^{(r)} + \Delta f_{Ni})\right] = 0$$

Expanding, rearranging and neglecting the second order terms, the following set of N_c linear equations in the incremental tangential forces is obtained,

$$\left([\psi_1] + [\psi_2] + E_f[\alpha_T][\psi_2] + [\phi][TN][\psi_1]\right)\Delta f_T = -\text{Diag.}\left([\psi_1][\psi_2]\right) \tag{3.4.8}$$

where, $[\Psi_1]$ and $[\Psi_2]$ are diagonal matrices with components given by

$$\begin{aligned} \psi_{1ii} &= f_{Ti}^{(r)} + E_f p_{Ti}^{(r)} \\ \psi_{2ii} &= f_{Ti}^{(r)} + \frac{p_{Ti}^{(r)}}{|p_{Ti}^{(r)}|}\mu_i f_{Ni}^{(r)} \end{aligned} \tag{3.4.9}$$

Solving for the incremental tangential force vector, the normal force vector for the $(r+1)^{th}$ friction iteration can be obtained from:

$$f_N^{(r+1)} = f_N^{(r)} + [TN]\Delta f_T \qquad (3.4.10)$$

and the magnitudes of the frictional forces are checked so that they do not exceed the frictional capacity where,

$$f_{Ti}^{(r+1)} = \left| f_{Ti}^{(r)} + \Delta f_{Ti} \right| \leq \left| \mu_i f_{Ni}^{(r+1)} \right|$$

If this is not the case, the friction iterations are continued with the tangential traction taken as equal to the frictional capacity. Knowing both the normal and tangential forces, the tangential displacement can be calculated from eqn. (3.4.3) and the tangential iterations continue until convergence is achieved.

At the end of the friction iteration, new values for the contact forces are obtained. Using these forces as initial values, the normal iteration loop is repeated and followed by another friction iteration. The iteration procedure is continued until the changes in the forces are small when compared to a specified norm.

3.3.3 Contact Traction

In the finite element solution to the contact problem, we solve for the nodal contact force vectors in the normal and tangential directions. These contact nodal forces are equivalent to the distributed contact traction in a virtual work sense. In other words, the work done by the nodal contact forces in going through an admissible displacement

field is equal to the work done by the equivalent distributed contact traction in going through the same virtual displacement field. The equivalent force vector to a distributed traction obtained using the virtual work principle is called the consistent load vector if the same shape functions are used for interpolating both the displacements and stresses.

Applying the principle of virtual work on a three dimensional 9-node surface segment where a distributed traction t(x,y,z) is prescribed, the following equation holds:

$$\int_A \mathbf{t}(x,y,z)\, \delta\mathbf{u}(x,y,z)\, dA = f_i \delta u_i \qquad , i=1,2,\ldots,9 \tag{3.5.1}$$

where summation over the repeated index i is implied.

The distributed virtual displacement can be expressed in terms of the nodal values as:

$$\delta\mathbf{u}(x,y,z) = \delta u_i h_i(\xi,\eta,\zeta) \qquad , i=1,2,\ldots,9 \tag{3.5.2}$$

Similarly, the distributed traction can be expressed in terms of its nodal values as follows,

$$\mathbf{t}(x,y,z) = t_j \phi_j(\xi,\eta,\zeta) \qquad , j=1,2,\ldots,9 \tag{3.5.3}$$

where ϕ represents the shape functions for the stress interpolation which in general could be different from the displacement shape functions.

Substituting eqns. (3.5.2 and 3.5.3) into the virtual work expression given by eqn.

(3.5.1), one may write

$$\int_A t_j \phi_j \, \delta u_i h_i \, dA = f_i \delta u_i$$

Therefore, one may rearrange in the homogeneous form:

$$\left[t_j \left(\int_A \phi_j h_i dA \right) - f_i \right] \delta u_i = 0$$

For an arbitrary virtual displacement $\delta u_i \neq 0$, $i = 1,2,\ldots,9$ we arrive at:

$$f_i = G_{ij} t_j \qquad (3.5.4)$$

where the elements of the transformation matrix [G] are given by:

$$G_{ij} = \int_A h_i \phi_j \, dA \qquad (3.5.5)$$

If the shape functions for interpolating the traction are chosen to be the same displacement shape functions, the transformation matrix G is a 9x9 square matrix similar to the consistent mass matrix used in dynamic analyses as described in Bathe [1986].

In general, the integral in eqn. (3.5.5) to evaluate the elements of the transformation matrix [G] is not straightforward. As such, numerical integration is invoked as will be illustrated in the next section where the computer implementation of the contact algorithm is discussed in details.

Now, the normal and tangential distributed traction are obtained from the normal and tangential nodal contact force vectors as follows:

$$t_N = [G]^{-1} f_N$$
$$t_T = [G]^{-1} f_T \qquad (3.5.6)$$

Since the inverse of the transformation matrix [G] is required to calculate the normal and tangential nodal values of the distributed contact traction, a lumped equivalent would be of great significance.

3.4 Computer Implementation

The contact algorithm in its first version is implemented in INDAP as a separate module interacting with the other modules organized by the master routine. INDAP is a general purpose displacement-based nonlinear finite element program which is capable of solving a wide variety of structural linear and non-linear problems. In order to achieve maximum versatility and to make it open for further development, INDAP has been organized in a modular form. Furthermore, each module is divided into a number of sub-modules. This modular form makes it possible to an experienced user to modify the program according to the needs demanded by the specific problem at hand. Owing to its open architecture, it is also possible to upgrade the program by simply inserting new modules. Special purpose programs can be created by putting together a number of modules and/or sub-modules of INDAP and some additional modules if necessary.

In its most recent structure, INDAP consists of the following seven main modules:

1. *Pre-processor:* processes the user's input data.
2. *Master Organizer*: controls the global communication between the main modules.
3. *Element Librarian:* calculates the stiffness, mass and damping matrices for different elements.
4. *Material module:* determines the state of stress and the current stress-strain relationship.
5. *Equation solver:* puts together the discretized structure and carry out the

numerical solution of the assembled structure.

6. *Contact Algorithm:* detects and removes any compatibility violation between contacting bodies.
7. *Post-processor:* displays the input and output data for visual inspection.

A schematic diagram for INDAP main modules is shown in Figure 3.4. A detailed account of the different finite elements, material models, and kinematic formulations implemented in INDAP can be found in the user's, theoretical, and verification manuals Dokainish [1988[a,b,c]].

3.4.1 INDAP Master Routine

The master routine, MASTER, in INDAP is the main processor which controls the flow of data throughout the whole program. The master routine organizes the flow of data between the three main modules; the librarian, the material and the solver. Figure 3.5 shows a brief flow chart for MASTER where two main loops can be recognized. The outer most loop is the loop over the load time steps. The inner loop is the nonlinear iteration loop where the full or the modified Newton-Raphson iterative schemes are adopted.

In the nonlinear iteration loop using Newton-Raphson technique, the out of balance load vector is applied on the original or updated stiffness matrix and the corresponding incremental displacement vector is calculated. Iteration continues until equilibrium is achieved. A new load step is applied and so on. If during the global nonlinear iteration

loop contact is detected, the contact main routine CONTCT is invoked to asses the compatibility violation and calculate the contact forces that remove any overlap and satisfy the friction law. Since the contact area is not known a priori, an iteration procedure is developed. Upon convergence of the contact iterations, the contact forces are added to the out of balance force vector and the nonlinear iterations continue. Within the master routine the contact module is treated as a solid box as shown in Figure 3.5 which will be exploited in the following subsections.

3.4.2 Contact Routines

In this section the box representing the contact module in the master routine is exploited in Figure 3.6 where a simplified flow chart representing the contact algorithm is shown. The contact iterations begin by initializing the contact arrays in subroutine CNTINT. This is followed by the overlap detection by the searching algorithm in subroutine SEARCH. If overlap is detected, the contact constraint equations are formed for all penetrating nodes in subroutine CNCSTR. The normal and tangential contact forces are estimated in subroutine CNTSLV and the displacement vector corresponding to these contact forces is obtained and the configurations of the contacting bodies are updated. The new configurations have to be checked for overlap and the loop continues until all overlaps are removed. The contact force vector in the global coordinate system is estimated in subroutine CNEQLB and we are back to the master routine.

3.4.2.1 Initialization Routine, CNTINT

CNTINT is a subroutine which is responsible for initializing the contact arrays at the beginning of each contact iteration step. This routine has two branches. One branch for the first contact iteration while the second branch is for all subsequent iterations. In the first iteration:

The contact information are read from the contact tape,

The increment in the tangential displacement is calculated and

The position vector is updated

On the other hand, for all subsequent iterations:

The local coordinates of the virtual target node s are updated and

The contactor nodes sliding over a new target mate are identified

3.4.2.2 Searching Algorithm, SEARCH

The contact constraint equations are derived in the previous chapter for one contactor node penetrating a target segment and then generalized to account for more contactor nodes penetrating different target surface segments. However, nothing has been mentioned about how can we decide upon which node penetrates which segment. In other words, we need a mechanism by which it would be possible to identify all active contact pairs accurately and efficiently. By a contact pair it is meant the contactor or hitting node and the target surface segment. This identification process can be done by using what is called searching algorithms. A searching algorithm should be capable of detecting all penetrating nodes and their corresponding target segments and sense any change in the contact conditions of sticking, sliding and tension release. It should

also be capable of determining and updating the local coordinates of the contactor nodes with respect to the local coordinate system of the corresponding target segment.

The searching algorithm adopted in this study is one of the commonly used algorithms in the literature, Zhong [1993]. It is a one-path treatment often called master-slave algorithm. For two generic bodies coming into contact, one body is called the contactor, slave or hitting body while the other is called the target or master. Moreover, the nodes and surface segments on a master/slave body are called master/slave nodes and segments, respectively. In a one-path treatment of contact interface, only the contactor nodes are checked against penetration into the target body. In other words, the target nodes can penetrate the contactor body. Therefore, it is recommended to choose the contactor body to be the one having the finer mesh.

The only user input information for the master-slave algorithm is two separate node lists for the potential contactor and target nodes.

The algorithm runs as follows:

1. For each potential contactor node, find the closest target node.
2. Find the surface segment/segments which shares this target node.
3. check if the contactor node is close enough to the target body. If not, go to step 8.
4. If the closest target node is a mid-side node in a 2D problem or a centre face node in a 3D problem, then the element which contains that node is definitely

the one to be paired with the contactor node. Go to 7.

5. Find the local coordinates of the contactor node in the candidate target segments.
6. From the local coordinates it can be decided which target segment is the one to be paired with the current contactor node.
7. Store the contactor node and the corresponding target segment as a contact pair. Also, store the local coordinates of the contactor node in the corresponding target segment.
8. Loop over all potential contactor nodes.

Before going into the tedious work of calculating the local coordinates of every single contactor node in its corresponding target surface segment, it would be wiser if we check first if the node is inside the target body or even close. This is because the calculation of the local coordinates of the contactor node in the target element, in a general contact problem, requires the solution of a system of non-linear equations which is a costly procedure as illustrated later.

This check can be done in 3D contacts by evaluating the volume of the prism made up by joining the contactor node with three corner nodes of its companion target surface segment as shown in Figure 3.7.a. Using a convenient sign convention it becomes possible to decide on a node that penetrating the target body by just watching the sign of the measured volume. From the figure, it can be stated that the contactor node, k, has penetrated the target segment, J, iff

$$V = x_{12} \times x_{14} \cdot x_{1k} < 0$$

where,

$$x_{1k} = x_k - x_1 , \qquad x_{12} = x_2 - x_1 \qquad \text{and} \qquad x_{14} = x_4 - x_1$$

Similarly, in 2D problems, we estimate the area of a triangle made up by joining the contactor node with the corner nodes of its corresponding target edge as shown in Figure 3.7.b. And penetration occurs iff

$$A = v_{1k} \times v_{12} < 0$$

Now, let us discuss how can we determine the coordinates of the contactor or hitting node k in the local coordinate system of the corresponding target segment J. In the isoparametric finite element formulation, both the displacement field and the position vector are expressed in terms of the same shape functions and the corresponding nodal values of displacement and position, respectively. Therefore, in a general 3D solid element in a cartesian coordinate system, we have the following equations:

$$\begin{bmatrix} x_k \\ y_k \\ z_k \end{bmatrix} = \begin{bmatrix} x_1 & x_2 & \cdots & x_N \\ y_1 & y_2 & \cdots & y_N \\ z_1 & z_2 & \cdots & z_N \end{bmatrix} \begin{bmatrix} h_1 \\ h_2 \\ \cdot \\ \cdot \\ \cdot \\ h_N \end{bmatrix}$$

where,

N is the total number of nodes per element, and

h_i is the shape function corresponding to node i.

The shape functions are expressed in terms of the local coordinates ξ, η, and ζ evaluated at the contactor node k, i.e.

$$h_i = h_i(\xi_k, \eta_k, \zeta_k), \qquad i=1,N$$

As such we have three equations which are to be solved for the three unknown local coordinates. In the case of 2D linear elements, the above system of equations can be written in the form,

$$\begin{bmatrix} x_k \\ y_k \end{bmatrix} = \frac{1}{4} \begin{bmatrix} x_1 & x_2 & x_3 & x_4 \\ y_1 & y_2 & y_3 & y_4 \end{bmatrix} \begin{bmatrix} +1 & +1 & +1 & +1 \\ +1 & -1 & +1 & -1 \\ +1 & -1 & -1 & +1 \\ +1 & +1 & -1 & -1 \end{bmatrix} \begin{bmatrix} 1 \\ \xi \\ \eta \\ \xi\eta \end{bmatrix}$$

These two equations can be easily reduced to a single quadratic equation in only one variable. However if nonlinear elements are to be considered, the problem becomes nonlinear and we need an iterative solution technique.

On the other hand, with the 3D linear elements, i.e. elements with straight edges, we do not have the luxury of simple equations as demonstrated for the linear 2D elements. Instead we have the following set:

$$\begin{bmatrix} x_k \\ y_k \\ z_k \end{bmatrix} = \frac{1}{8} \begin{bmatrix} x_1 & x_2 & \cdots & x_8 \\ y_1 & y_2 & \cdots & y_8 \\ z_1 & z_2 & \cdots & z_8 \end{bmatrix} \begin{bmatrix} +1 & +1 & +1 & +1 & +1 & +1 & +1 & +1 \\ +1 & -1 & +1 & +1 & -1 & +1 & -1 & -1 \\ +1 & -1 & -1 & +1 & +1 & -1 & -1 & +1 \\ +1 & +1 & -1 & +1 & -1 & -1 & +1 & -1 \\ +1 & +1 & +1 & -1 & +1 & -1 & -1 & -1 \\ +1 & -1 & +1 & -1 & -1 & -1 & +1 & +1 \\ +1 & -1 & -1 & -1 & +1 & +1 & +1 & -1 \\ +1 & +1 & -1 & -1 & -1 & +1 & -1 & +1 \end{bmatrix} \begin{bmatrix} 1 \\ \xi \\ \eta \\ \zeta \\ \xi\eta \\ \eta\zeta \\ \zeta\xi \\ \xi\eta\zeta \end{bmatrix}$$

It is obvious that these equations require an iterative solution procedure. Moreover, in case of 3D nonlinear elements the problem becomes even worse. Having established the fact that we need an iterative procedure in order to be able to tackle general contact problems, we proceed as follows.

In a general nonlinear problem represented by the equation $y = f(x)$, linearizing in the neighbourhood of a prior estimate, x_0, a new estimate can be found and is given by

$$y^{(i+1)} = y^{(i)} + \Delta y$$

where, the increment in the dependent variable y is given by

$$\Delta y = \frac{\partial f(x)}{\partial x} \Delta x$$

In a similar fashion, the increment in the global coordinates of the contactor node k can be determined from the system of equations given by

$$\begin{bmatrix} \Delta\xi \\ \Delta\eta \\ \Delta\zeta \end{bmatrix} = \left[J^{(i)}\right]^{-1} \begin{bmatrix} x_k - x^{(i)} \\ y_k - y^{(i)} \\ z_k - z^{(i)} \end{bmatrix}$$

where, [J] is the Jacobian matrix and is given by

$$[J] = \begin{bmatrix} \frac{\partial h_i}{\partial\xi} x_i & \frac{\partial h_i}{\partial\eta} x_i & \frac{\partial h_i}{\partial\zeta} x_i \\ \frac{\partial h_i}{\partial\xi} y_i & \frac{\partial h_i}{\partial\eta} y_i & \frac{\partial h_i}{\partial\zeta} y_i \\ \frac{\partial h_i}{\partial\xi} z_i & \frac{\partial h_i}{\partial\eta} z_i & \frac{\partial h_i}{\partial\zeta} z_i \end{bmatrix}$$

The new estimates are determined from

$$(\xi, \eta, \zeta)^{(i+1)} = (\xi^{(i)} + \Delta\xi^{(i+1)}, \eta^{(i)} + \Delta\eta^{(i+1)}, \zeta^{(i)} + \Delta\zeta^{(i+1)})$$

Iterations continue until the incremental values of the local coordinates become smaller than a pre set tolerance.

3.4.2.3 Constraint Routine, CNCSTR

Subroutine CNCSTR is responsible for calculating the normal and tangential contact matrices [N] and [R] for all active contactor nodes as determined by SEARCH. Moreover, CNCSTR estimates the normal and tangential penetration vectors p_N^0 and p_T^0. Subroutine CNCSTR invokes the utility routine SHP2D which gives the shape functions for the 2-D isoparametric finite elements. It also gives the normal and tangential vectors to the target surface. In case of frictionless contacts, only [N] and p_N^0 are evaluated.

3.4.2.4 Contact Solver, CNTSLV

In subroutine CNTSLV, the normal forces that remove the overlap in the normal iteration loop and the tangential forces that satisfy the friction law in the friction loop are estimated. Having obtained the converged contact force vectors, the corresponding contact displacement vector is obtained.

Normal Iteration Loop:

The normal iteration loop is performed in subroutine SIGITR which is schematically

represented by the flow chart in Figure 3.8. The normal stress iterations are summarized in the following steps:

1. Calculate the normal overlap vector $p_N^{(n)}$ from eqn. (3.3.9)
2. Calculate the increment in the normal forces which removes the overlap by solving eqn. (3.3.8).
3. Check convergence and update the normal forces using eqn. (3.3.5).

During the normal contact iterations, a scaling procedure is devised to speed up the convergence. In the $(n+1)^{th}$ normal contact iteration, either the contact traction or the normal penetration vector is zero, this translates to the following contact constraint:

$$f_{Ni}^{(n+1)} \cdot p_{Ni}^{(n+1)} = 0$$

Let us assume that the normal traction and the normal penetration vectors are equal to their respective values at the $(n)^{th}$ iteration plus the incremental change multiplied by a scale factor which brings the contactor node on the target surface, i.e.

$$f_{Ni}^{(n+1)} = f_{Ni}^{(n)} + s\,\Delta f_{Ni}$$
$$p_{Ni}^{(n+1)} = p_{Ni}^{(n)} + s\,\Delta p_{Ni}$$

Therefore, the scale factor can be determined form the following quadratic form:

$$A\,s^2 + B\,s + C = 0$$

where the three constants of the quadratic form are given by:

$$A = \sum_{i=1}^{N_c} \Delta f_{Ni} \Delta u_{Ni}$$

$$B = \sum_{i=1}^{N_c} \Delta f_{Ni} u_{Ni}^{(n)} + f_{Ni}^{(n)} \Delta u_{Ni}$$

$$C = \sum_{i=1}^{N_c} f_{Ni}^{(n)} u_{Ni}^{(n)}$$

The solution to this quadratic equation gives the value of the scale factor s. If it is negative it should be ignored.

Tangential Iteration Loop:

In case of frictional contacts, the tangential traction is obtained iteratively in order to satisfy the friction law along with the normal contact constraints. In the friction iterations, the normal iterations are performed as an inner loop lest it should occur that the normal constraints are violated during the friction iterations. Figure 3.9 shows a simplified flow chart for the friction iteration loop. The friction iterations go as follows:

1. Calculate [NN], [RR] and [NR]
2. Calculate θ_{ii} for each contactor node.
3. Calculate $[\alpha_N]$ from eqn. (3.3.3)
4. Call SIGITR to obtain the normal forces and the contact area. If converged ICHEK is set to 0
5. If both the normal and tangential forces are converged, exit the friction iteration loop. If not, continue.
6. Calculate $[\alpha_T]$ from eqn. (3.2.5).
7. Calculate friction forces corresponding to the new normal forces using the

estimated ratio θ_{ii} .

8. Calculate the tangential displacement from eqn. (3.4.3).

9. Calculate Ψ_1 and Ψ_2 from eqn. (3.4.9).

10. Solve the system in eqn. (3.4.8) for the incremental tangential forces.

11. Update the normal forces using eqn. (3.4.10).

12. Check the convergence in the tangential contact forces. If converged, set IFCHK flag to 1. Go to 2.

3.4.2.6 Contact Force Vector, CNEQLB

At the end of each contact iteration, the contact forces are obtained in the local normal and tangential coordinates at each individual contactor node. In order to add the contact forces to the global force vector, a transformation of the contact normal and tangential forces to the global coordinate system has to be carried out. This is done in subroutine CNTFRC and the transformation is given by eqn. (2.6.11).

3.4.2.5 Contact Traction, CNTRAC

As discussed in section 3.3.3, the normal and tangential contact nodal force vectors are distributed over the contact surface using the inverse of the transformation matrix [G]. It is also noted that for the evaluation of the transformation matrix [G], numerical integration is necessary. For a 3-D surface, the ijth element in [G] is given by:

$$G_{ij} = \int_{-1}^{+1}\int_{-1}^{+1} h_i(\xi)\,\phi_j(\eta)\,|J(\xi,\eta)|\,d\xi\,d\eta$$

where $|J(\xi,\eta)|$ is the determinant of the 2x2 Jacobian matrix.

Using Gauss quadrature for evaluating the above integral gives:

$$G_{ij} = \sum_{k=1}^{n_\xi} \sum_{l=1}^{n_\eta} h_i(\xi_{kl}, \eta_{kl})\, \phi_j(\xi_{kl}, \eta_{kl})\, w_k$$

where n_ξ, n_η are the numbers of the sampling points in the local coordinate system represented by ξ and η and the surface is given by $\zeta = 1$.

If both shape functions used for interpolating the contact traction are the same as those used for interpolating the displacement field, the above Gauss formula would suffice. However, for nonlinear finite elements having parabolic shape functions interpolating the displacement field, the shape functions interpolating contact traction are chosen to be linear. This is consistent with the stresses everywhere in the continuum. The linear interpolation of the contact stress field over three node 2-D surface, for instance, leads to a discontinuity at the mid-side node and the integration over the whole segment can not be performed using the above formula.

Let us consider the case of a 2-D element side with three surface nodes where the contact surface is represented by the $\eta = 1$ parametric curve. The displacement field is interpolated using the standard quadratic shape functions $h_i(\xi)$, $i = 1,2,3$ shown in Figure 3.10.a and the surface traction is interpolated by the linear shape functions $\phi_j(\xi)$, $j = 1,2,3$ shown in Figure 3.10.b. Obviously, the ϕ_j's are discontinuous over the full element surface. As such, the integral for estimating the transformation matrix [G] has to be broken into two integrals as follows:

$$G_{ij} = \int_{-1}^{0} h_i(\xi)\,\phi_j(s)\,x(\xi)\,|J(\xi)|\,d\xi + \int_{0}^{+1} h_i(\xi)\,\phi_j(s)\,x(\xi)\,|J(\xi)|\,d\xi$$

In order to use the standard Gauss quadrature formula where the integral runs from -1 to +1, a change of parameters is necessary. Let

$\xi=(s_2 - 1)/2$ for $\xi=[-1,0] \Rightarrow s_2=[-1,+1]$

and $\xi=(s_1 + 1)/2$ for $\xi=[0,+1] \Rightarrow s_1=[-1,+1]$

Therefore, in both regions, $d\xi = ds_2/2 = ds_1/2$

The algorithm for estimating the contact nodal traction from the contact nodal forces become more efficient if the matrix [G] can be diagonalized or lumped. The diagonalization of the matrix makes the inversion operation trivial. In this study the row sum method is used. In the row sum method, the diagonal matrix is computed from;

$$\bar{G}_{ij} = \begin{cases} \sum_k G_{ik} & i = j \\ 0 & i \neq j \end{cases}$$

where k=1,2,3.

Using the above mentioned parameter transformation and the matrix diagonalization, the first diagonal element in the lumped transformation matrix [G] is given by:

$$\bar{G}_{11} = \frac{1}{2}\int_{-1}^{+1} h_1(s_2)\left[\phi_2(s_2) + \phi_{32}(s_2)\right]x(s_2)\,|J(s_2)|\,ds_2 + \frac{1}{2}\int_{-1}^{+1} h_1(s_1)\left[\phi_1(s_1) + \phi_{31}(s_1)\right]x(s_1)\,|J(s_1)|\,ds_1$$

Similar expressions can be obtained for the other two diagonals and the Gauss quadrature may be used to evaluate the integral numerically.

Different combinations of the shape functions are investigated. It is found that using linear shape functions for both the contact traction and the displacement field results in oscillations in the contact traction distribution where the average profile underestimates the contact traction field. On the other hand, if parabolic shape functions are used for both, stress oscillations remain with an over-estimated average if three integration points are used in the numerical integration. The oscillations could be suppressed and the average is corrected by using the reduced integration technique.

In conclusion, two options are available for the estimation of the transformation matrix G. Either use parabolic interpolation for the displacements and linear interpolation for the contact traction or use parabolic interpolation for both with reduced integration scheme.

3.5 Illustrative Examples

In this section, the developed contact algorithm is examined qualitatively and quantitatively, when possible, against a wide range of contact problems. These include frictionless, frictional, elastic, elasto-plastic, linear, non-linear, conformal and non-conformal contact problems. A Hertzian contact example is solved using the developed algorithm where a sphere is pressed against a rigid foundation without friction. Hertz contact is an elastic non-conformal contact problem which has a closed form solution given in Appendix A. This problem is also solved with the presence of friction. Unfortunately, no closed form solution is available for the frictional case. As an example of elastic *conformal* contact problems, an elastic cylinder is pressed axially between two rigid blocks. Again, no closed form solution is available for such a problem. Finally, the algorithm is checked against an *elasto-plastic* conformal contact problem; that is the internal pressurization of a composite cylinder. The results obtained numerically using the developed algorithm are compared with the closed form solution summarized in Appendix A.

For convenience, the presentation of the various examples follows a strict sequence; a mathematical model, material data, finite element mesh, boundary conditions, and finally results and discussion. When available, the analytical solutions for the problems depicted in this section are summarized in Appendix A as will be pointed out in each example.

3.5.1 Example #1: An Elastic Sphere between two Rigid Blocks

This is an example of elasto-static non-conformal contact between an elastic body with a rigid foundation. A 50 mm radius elastic sphere is pressed between two rigid blocks as shown in Figure 3.11a and it is required to calculate the resulting contact traction. If friction is ignored, this becomes the classic Hertzian contact problem where a closed form solution is available in Johnson [1985] and is given in Appendix A.

Mathematical Model:

Owing to the double symmetry, only one quarter of the sphere is considered. The rigid block is fixed in space while the horizontal surface of the sphere is given a uniform prescribed down-ward displacement as shown in Figure 3.11b.

Mechanical Properties:

The material mechanical properties for the elastic sphere are as follows:

Young's Modulus, E = 200 GPa

Poisson's Ratio, v = 0.3

Finite Element Mesh:

The mathematical model in Figure 3.11b is discretized using the finite element mesh shown in Figure 3.12 where it can be noticed that the mesh is refined close to the potential contact area for more accurate results. A total of 207 axisymmetric 9-node isoparametric quadrilateral finite elements are used for the sphere and only one 4-node element is used for the rigid block.

Boundary Conditions:

To load the model, the prescribed uniform displacements are applied on the nodes along the horizontal edge of the sphere mesh. On the other hand, the nodes along the vertical edge are constrained in the x-direction only. All nodes on the element representing the rigid block are completely fixed in both x and y-directions.

Results & Discussion:

All the modelling details are fed into INDAP through a user's input file with the proper format as explained in INDAP User's Manual, Dokainish [1988]. The input file for this primary case is reported in Appendix A as a sample input file.

The deformed configuration of the model is shown in Figure 3.13 where an exaggerated view of the vicinity of the contact area is depicted. It can be observed that the contact area terminates at a mid-side node with an extended radius of 8.0143 mm as compared to the 8.0 mm radius obtained from the closed form solution corresponding to 1.28 mm down-ward prescribed displacement. The normalized contact pressure distributions obtained from the finite element analysis for different prescribed downward displacements of 0.256, 0.768 and 1.28 mm are shown in Figure 3.14 along with the analytical solution represented by the solid lines.

It should be pointed out that the agreement of the finite element solution with the Hertzian solution is different at different load levels. They agree well when the load level is such that the contacting area terminates at a finite element node. In addition, a deviation from the Hertzian solution would not be a surprise as the contact area gets

bigger. This is b ·ause the Hertzian theory assumes that the contact area is negligible with respect to the dimension of the contacting bodies.

Frictional Contact:

The problem of a sphere compressed between two rigid blocks is solved with the introduction of friction between the contacting surfaces. The prescribed displacement is 1.28 mm. Friction coefficients of 0.0, 0.3, 0.6 and 0.9 are used with a friction modulus of 10^{12}. This value for the friction modulus reduces the friction model to the Coulomb's friction law.

The finite element solutions are shown in Figure 3.15 represented by symbols while the analytical solution for frictionless contact is represented by the solid line. The involvement of friction into the analysis offers a tangential resistance against relative sliding. This resistance is responsible for the increase in the normal contact pressure as shown in Figure 3.15. As can be seen from the distribution of the tangential contact traction, the contact area is divided into two distinctive zones. An inner sticking zone where the friction forces are less than the frictional capacity and an outer sliding zone where the frictional forces are equal to the frictional capacity. As the coefficient of friction increases, the sticking zone expands radially on the expense of the sliding zone. The effect of the friction modulus on both the normal and tangential traction is shown in Figure 3.16. As the friction modulus decreases, the contacting surfaces are allowed a higher relative tangential displacement which leads to lower normal and tangential traction.

3.5.2 Example #2: Rigid Block & Elastic Cylinder

As an example of elasto-static *conformal* contact problems an elastic cylinder is pressed axially between two rigid blocks as shown in Figure 3.17a.

Mathematical Model:

Due to the double symmetry, only one quarter of the continuum is modelled as shown in Figure 3.17b. The rigid block is given a downward vertical prescribed displacement of 1 mm. The left side of the cylinder is fixed in the radial direction while the bottom surface is fixed in the vertical direction.

Mechanical Properties:

The material mechanical properties of both the cylinder and the blocks are as follows:

Young's Modulus, E = 200 GPa

Poisson's Ratio, v = 0.3

Finite Element Mesh:

The mathematical model is discretized using a total of 400 axisymmetric 9-node isoparametric quadrilateral finite elements for the cylinder and only one 4-node element for the rigid block as shown in Figure 3.18.

Boundary Conditions:

All nodes along the bottom surface of the cylinder are fixed in the y-direction while all nodes along the left side are fixed in the x-direction. The four nodes of the block

element are given a prescribed displacement of -1 in the y-direction.

Results & Discussion:

Figure 3.19 shows the distribution of the normal and tangential traction, respectively, for different friction coefficients assuming Coulomb's law of friction. Including friction into the analysis deviates the uniform pattern of the normal contact traction showing a very large value at the boundary of the contact area. However, the value of the coefficient of friction does not have much of an effect on the normal contact traction. On the other hand, as the coefficient of friction increases the extent of the sticking zone enlarges. This is logical since as the friction coefficient increases, the frictional capacity increases which results in more nodes being unable to slide.

3.5.3 Example #3: Internally Pressurized Composite Cylinder

As an example of *elastic-plastic* conformal contact problems with both contacting bodies being deformable, the thick-cylinder theory is invoked to demonstrate the applicability of the developed finite element contact algorithm. A composite cylinder with two rigid end supports internally pressurized to a maximum pressure value and then the pressure is removed completely. This problem also demonstrates the ability of the algorithm to handle loading and unloading scenarios.

Mathematical Model:

The composite cylinder considered has an inner cylinder with 1.0 and 1.1 in inner and outer radii, respectively, while the outer radius of the outer cylinder is 2.0 in. The

geometry, loading and boundary conditions are all axisymmetric. As such, an axisymmetric model is adopted as shown in Figure 3.20a.

Mechanical Properties:

An elastic perfectly plastic material model, given in Figure 3.20b, is adopted with the material mechanical properties for both cylinders given by:

Young's Modulus, E = $30*10^6$ psi

Poisson's Ratio, v = 0.3

Yield Strength, S_y = $30*10^3$ psi

Finite Element Mesh:

The mathematical model is discretized using 4 and 18 isoparametric 9-node quadrilateral 2-D axisymmetric finite elements for the inner and outer tubes, respectively. The finite element mesh is shown in Figure 3.21.

Boundary Conditions:

The two end supports prevent any axial deformation and this is translated in the finite element model by fixing all the nodes in the mesh in the axial direction. A uniform pressure is applied on the inner surface of the inner cylinder to a maximum of 18.0 ksi and then it is reduced to zero. Contact interaction is expected between the outer and inner surfaces of the inner and outer cylinders, respectively.

Results & Discussion:

The radial and hoop stress distributions, at maximum loading, along the radial distance

are compared with the analytical solution as shown in Figure 3.22. The finite element solution is represented by symbols while the closed-form solution is represented by the solid line. Obviously, an excellent agreement between the two solutions is evident. This indicates that the contact algorithm works for materially non-linear contact problems.

Assuming elastic unloading, the residual stresses may be obtained by subtracting from the elastic-plastic stress distribution a stress distribution which would have occurred at the same pressure if the material had remain elastic. Figure 3.22 shows the residual radial and tangential stress distributions obtained using the finite element method after the pressure load is removed completely compared with the closed-form solution. The excellent agreement suggests the adequacy of the developed algorithm for handling unloading situations as well.

Plane Strain Model:

The internal pressurization of the composite cylinder with two end supports may also be mathematically represented by a plane strain model. Only one quarter of the composite cylinder is used due to the double symmetry with regard to any two perpendicular axes in the cross-section plane.

The finite element discretization of the plane strain model is shown in Figure 3.23. A total of 465 nodes and 105 isoparametric 9-node quadrilateral 2-D plane strain elements are used. In Figure 3.23, the first inner layer of elements represents the inner tube.

All nodes along the x-axis are fixed in the y-direction while all nodes along the y-axis are fixed in the x-direction. Different values of the internal pressure are applied along the inner surface of the inner tube.

The normalized contact pressure is plotted against the angular position as shown in Figure 3.24 for the different pressure values of 12.0, 15.0 and 18.0 ksi. The solid lines represent the analytical solution as estimated form the closed form solution provided by the thick-cylinder theory. Figure 3.25 shows the equivalent stress fringe plot corresponding to the pressure value of 18.0 ksi. It is obvious from the figure that the plastic zone has extended beyond the contact boundary. As such, it can be concluded that the developed contact algorithm works for materially non-linear conformal contact problems involving deformable bodies.

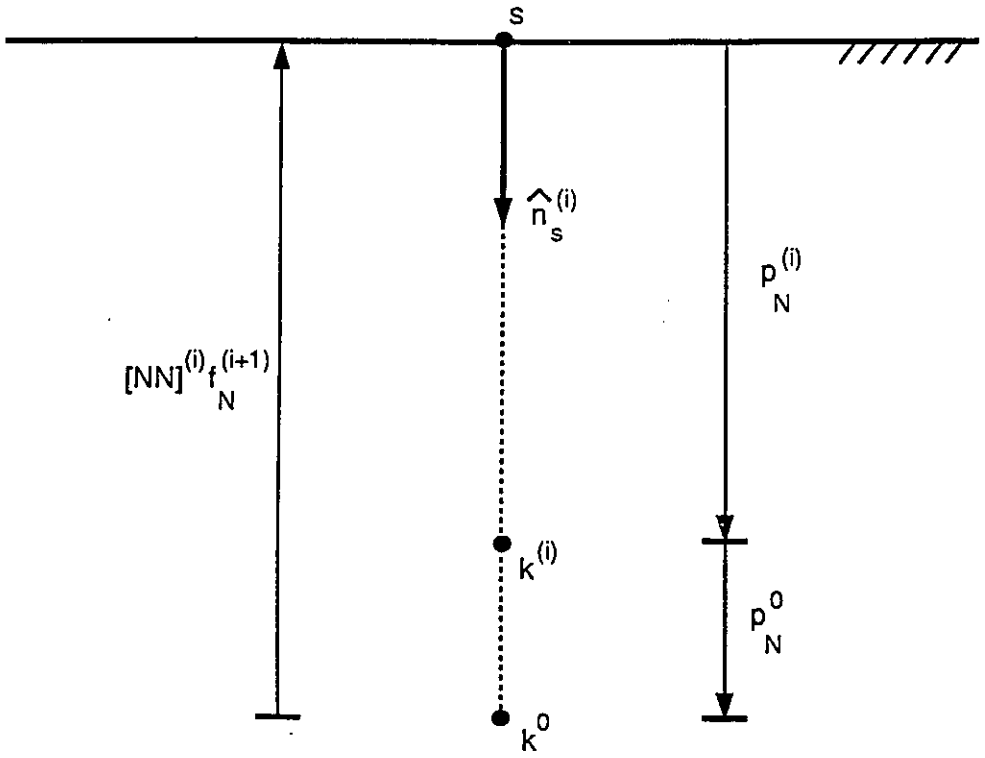

FIGURE 3.1: Geometric Representation of Eqn. (3.2.2)

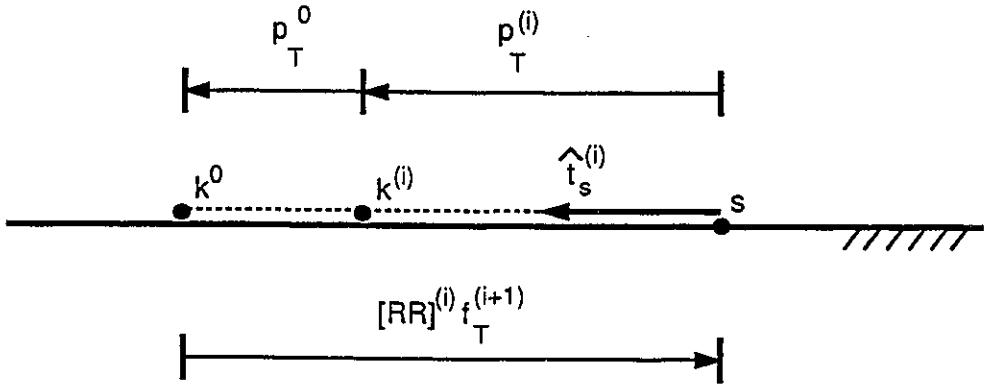

FIGURE 3.2: Geometric Representation of Eqn. (3.2.3)

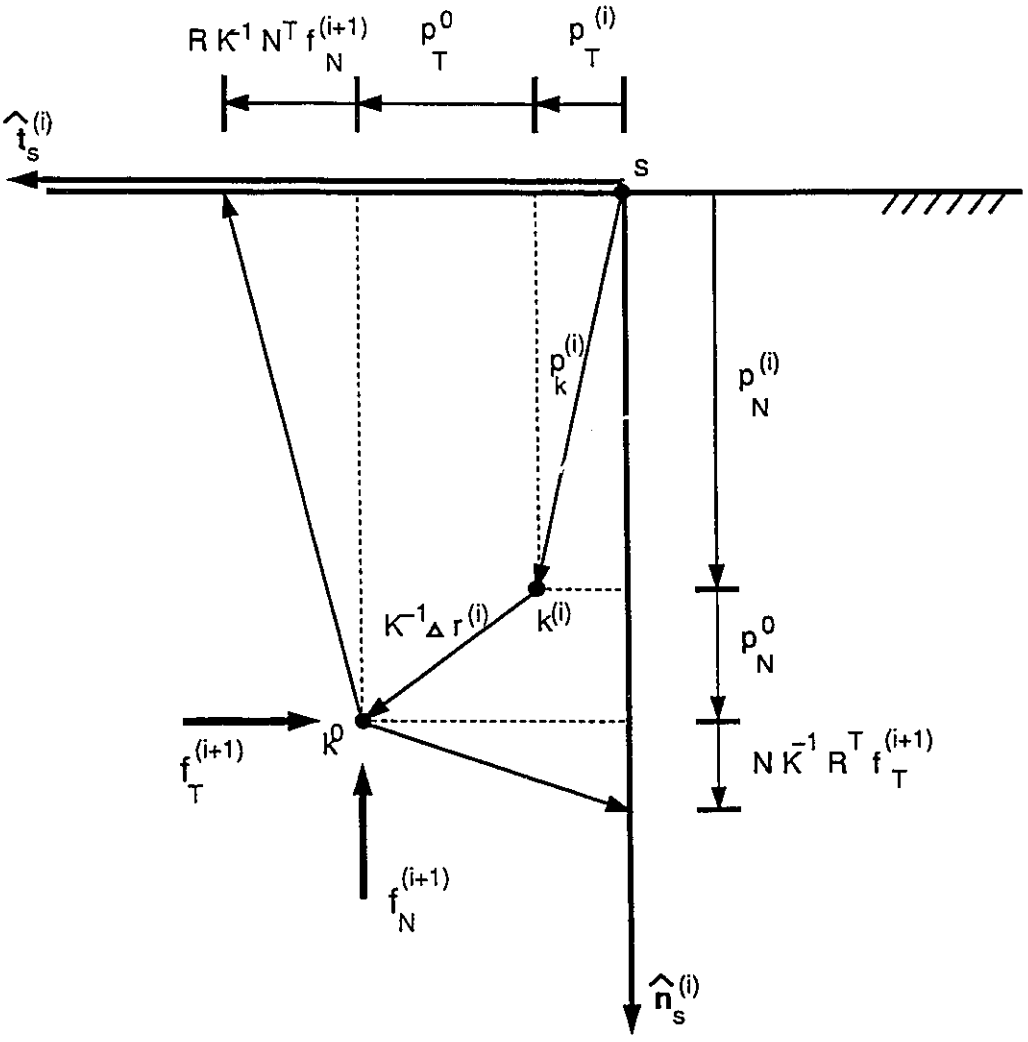

FIGURE 3.3: Combined Normal and Tangential Penetration

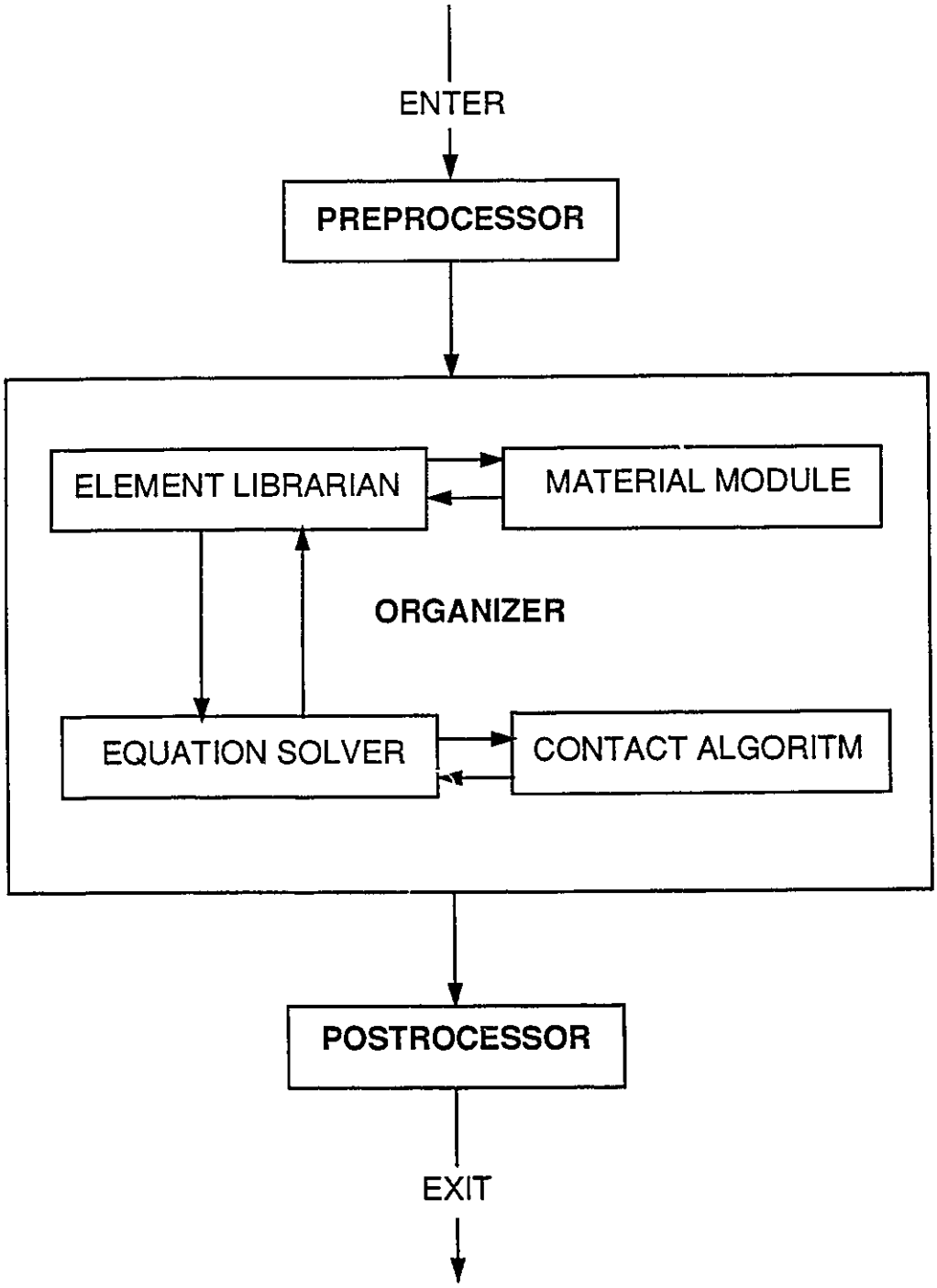

FIGURE 3.4: General Layout for INDAP

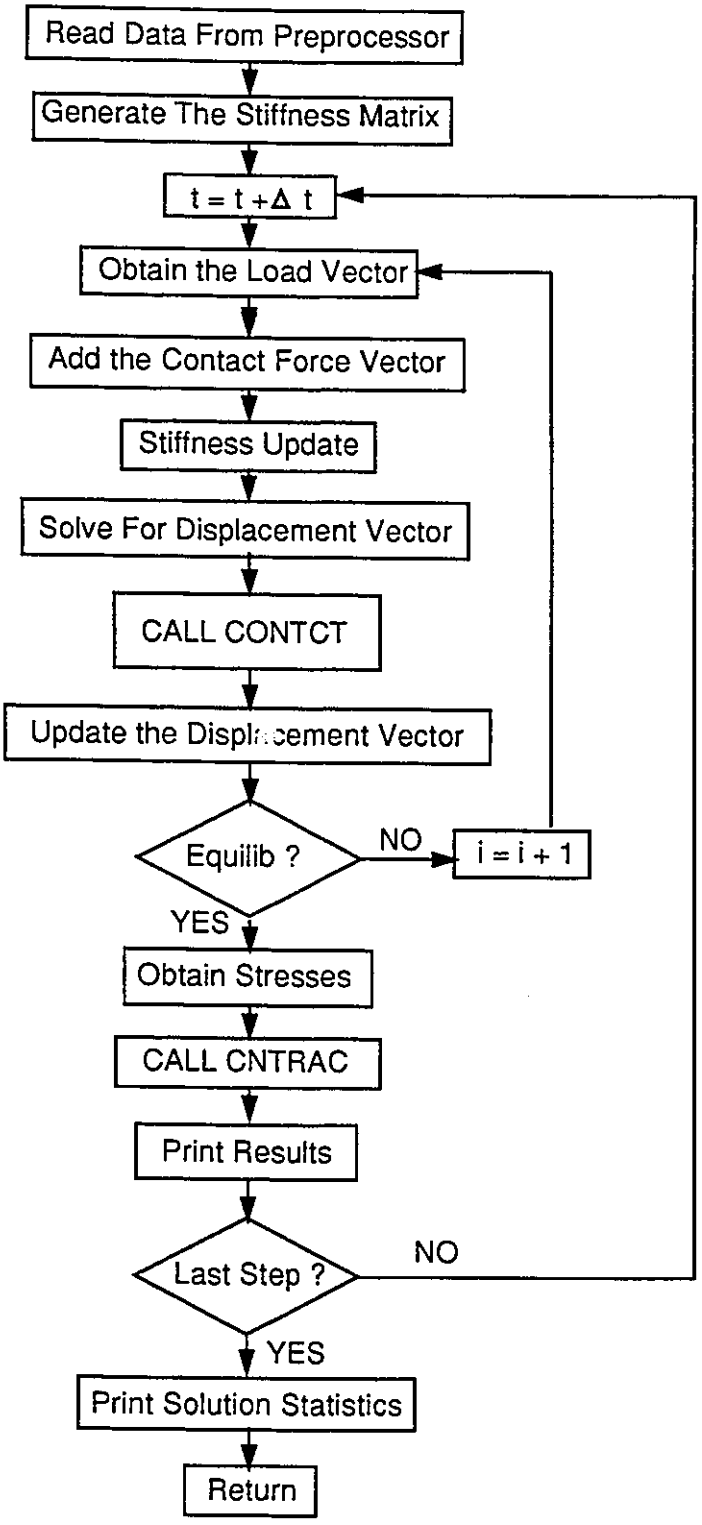

Figure 3.5: Flow Chart for the Master Routine

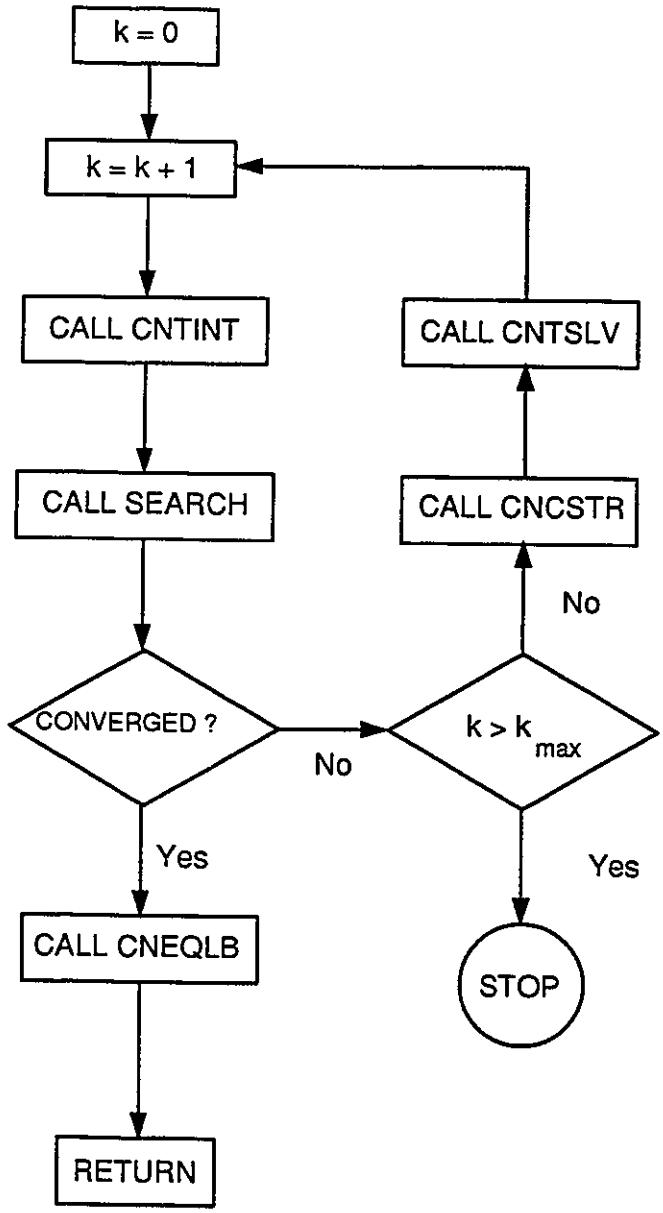

Figure 3.6: Smplified Flow Chart for the Contact ALgorithm CONTCT

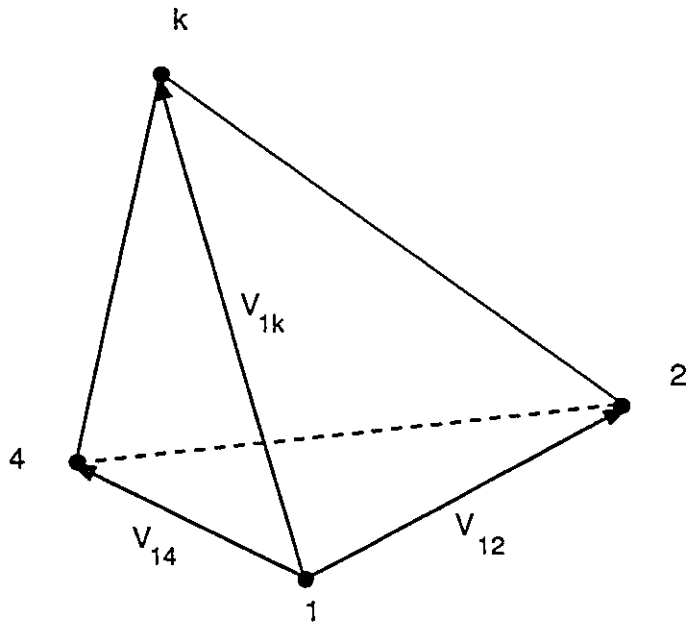

Figure 3.7a: 3–D Volume made by a Contactor node k.

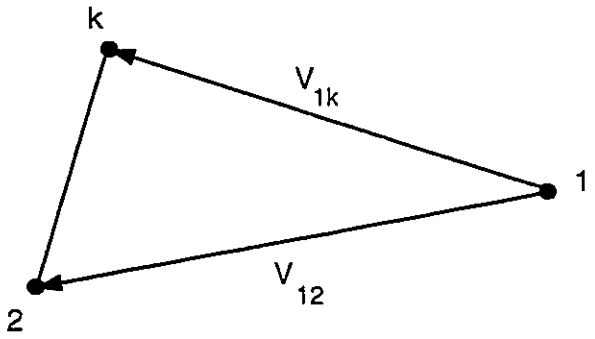

Figure 3.7b: 2–D Area made by a Contactor node k.

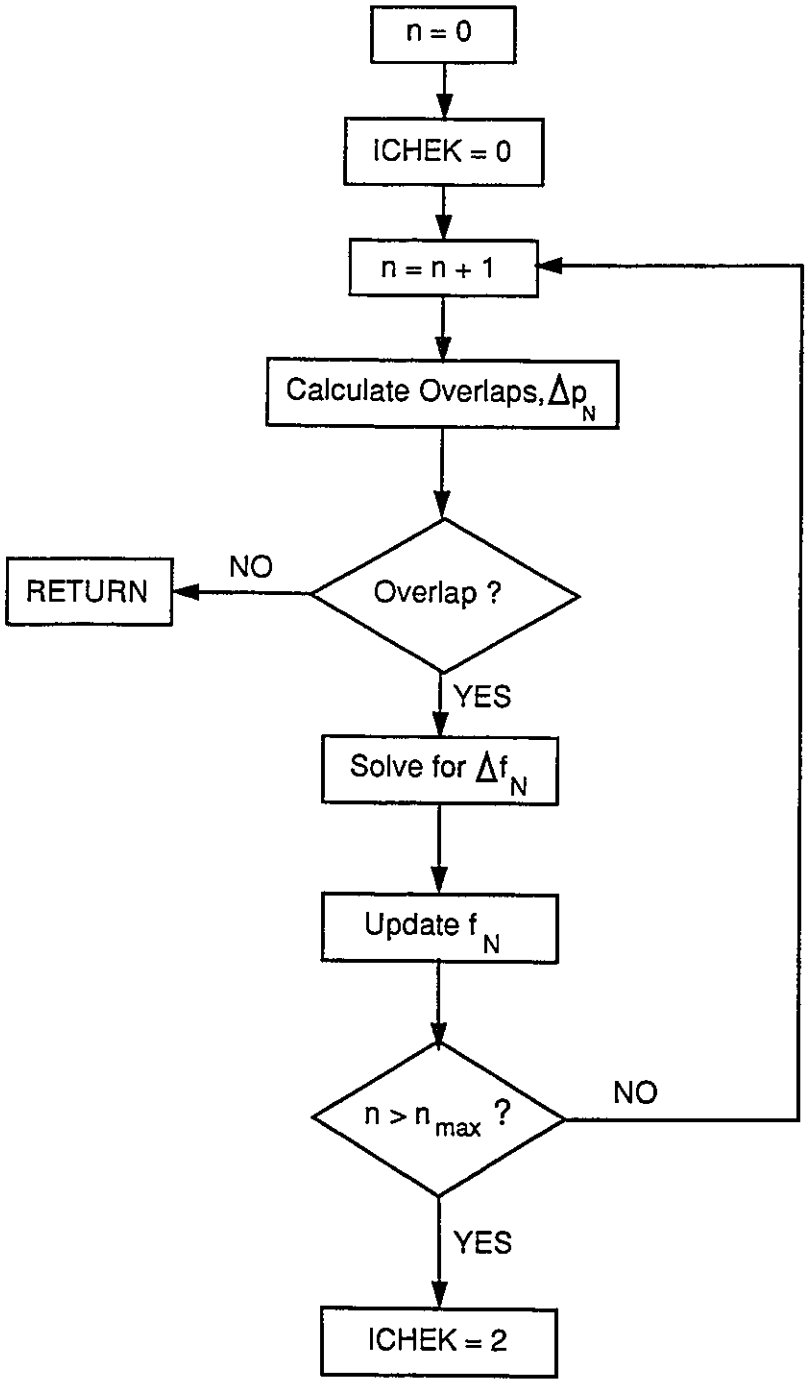

Figure 3.8: Flow Chart for the Normal Iteration Loop

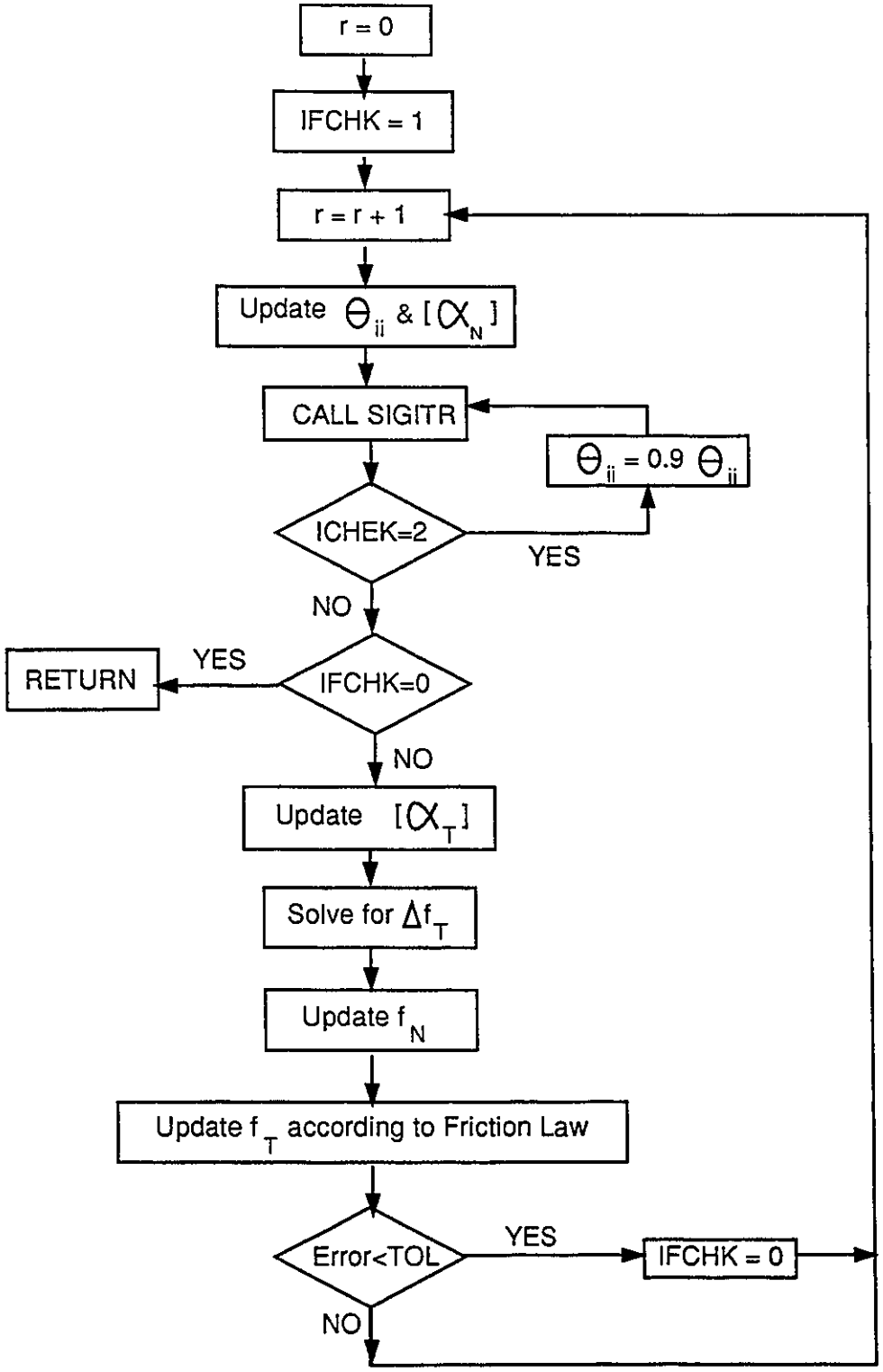

Figure 3.9: Flow Chart for the Friction Iteration Loop

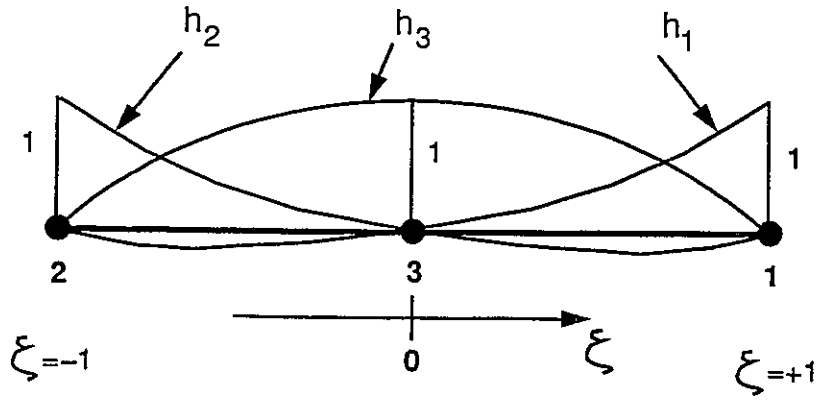

a. Quadratic Interpolation

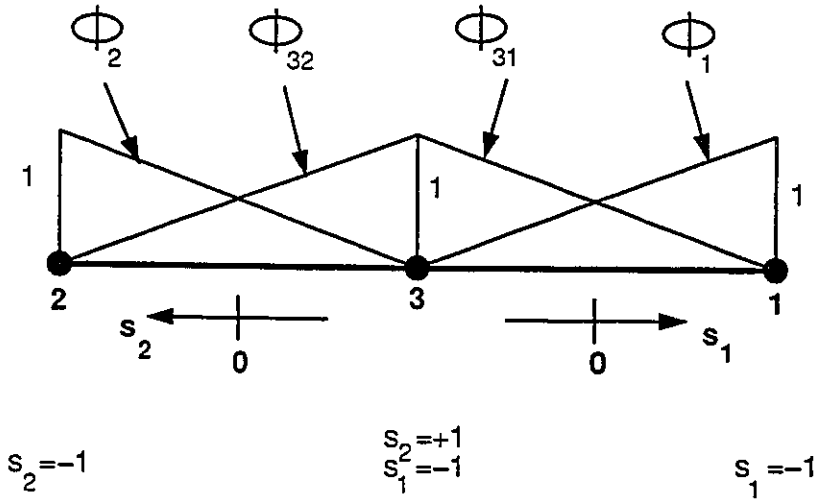

b. Linear Interpolation

Figure 3.10: Displacement and Contact Stress Shape Functions

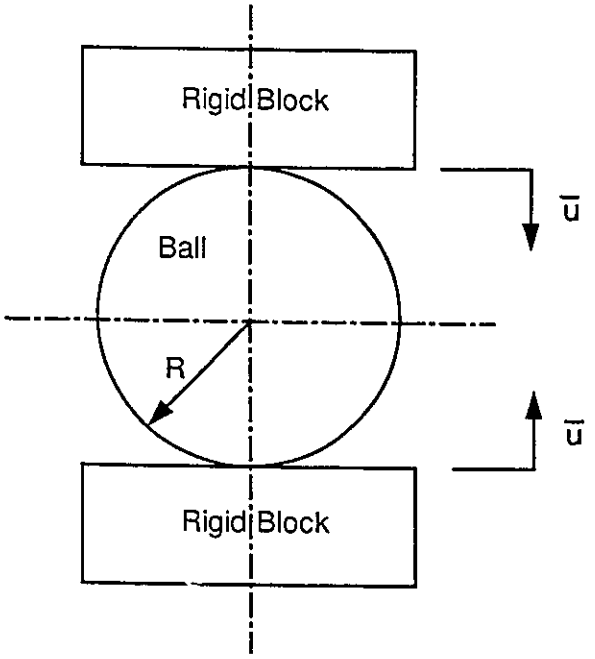

Figure 3.11a: A Ball Compressed between Two Rigid Blocks, Example 1

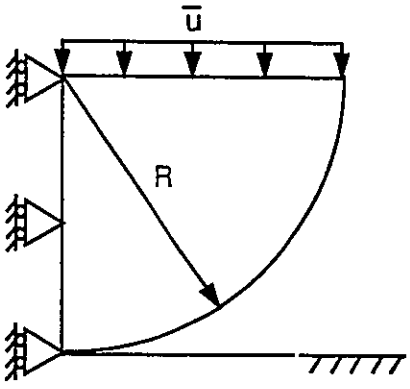

Figure 3.11b: Mathemetical Model for Example 1

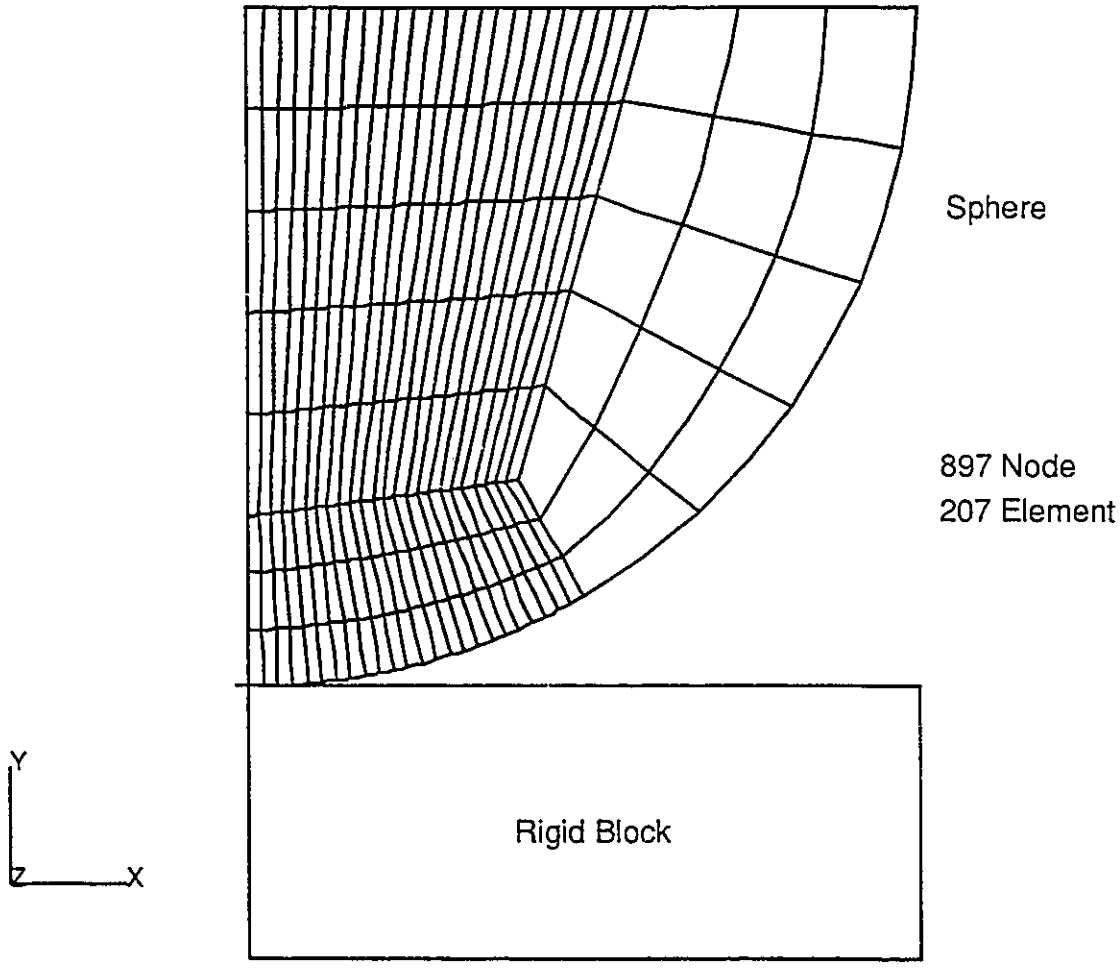

Figure 3.12: Finite Element Mesh for Hertz Contact Problem

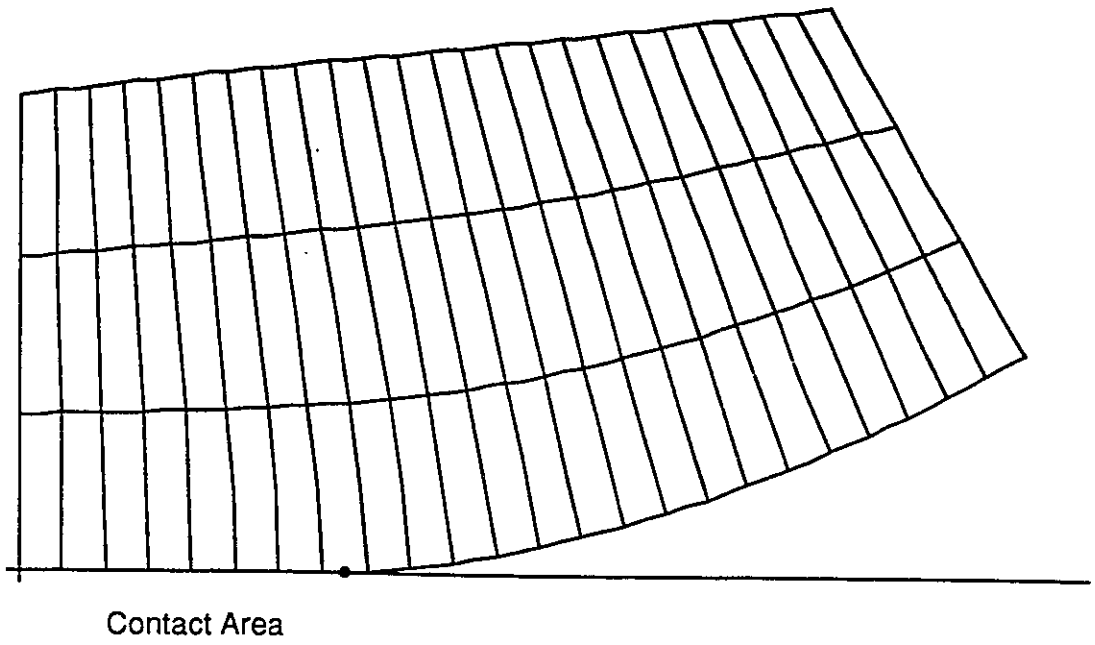

Figure 3.13: Deformed Configuration for Hertz Problem.

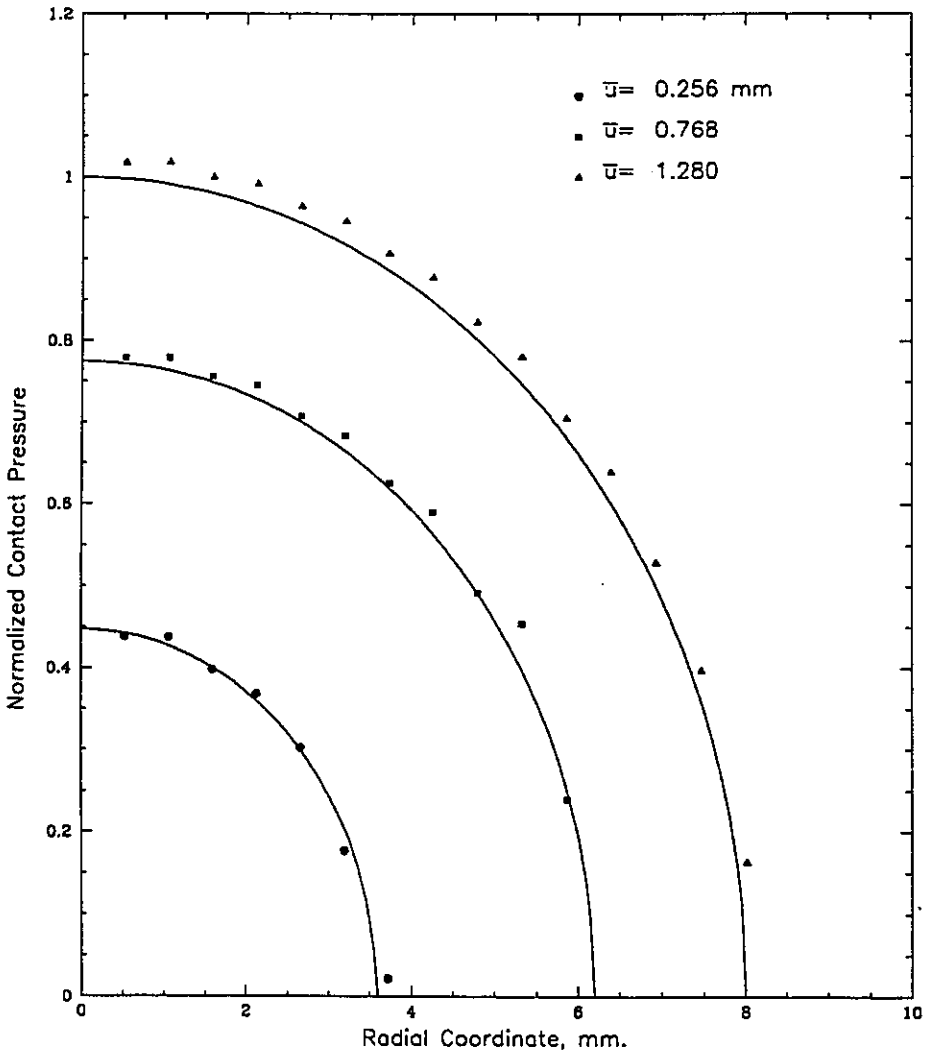

Figure 3.14: Normal Contact Pressure Distribution for Hertz Example at Different Load Values
(Solid Lines indicate closed-form Hertz solution)

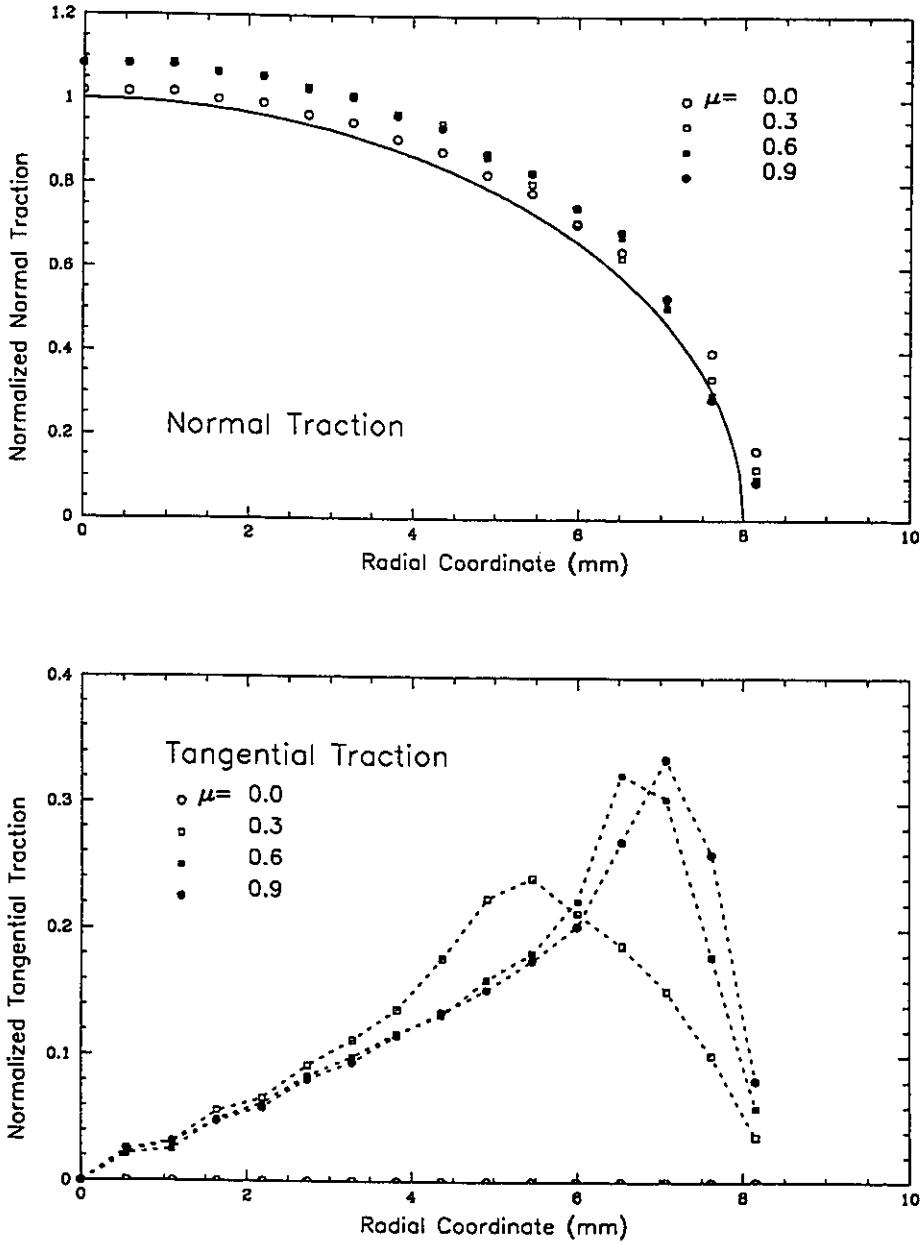

Figure 3.15: Normal & Tangential Contact Traction for Different Friction Coefficients, μ

$E_f = 10^{12}$

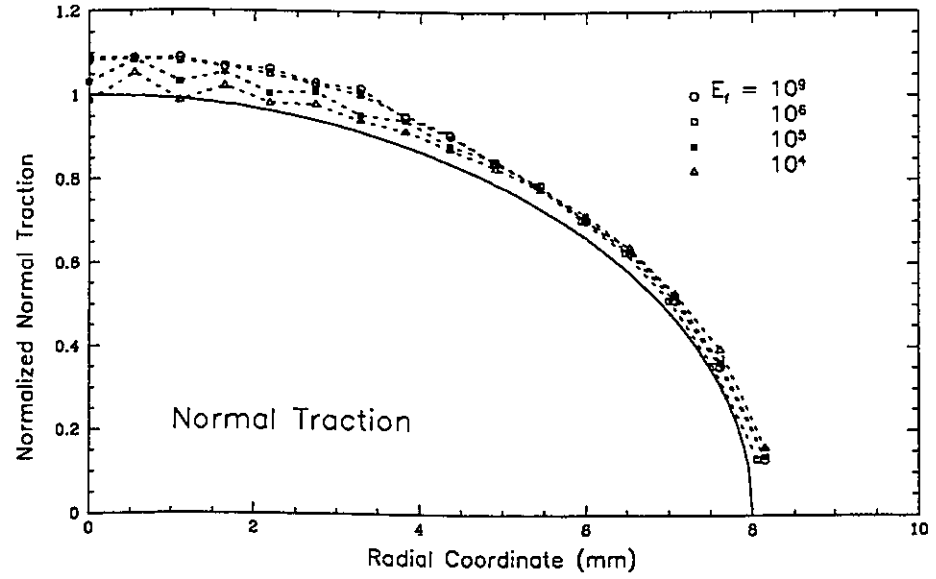

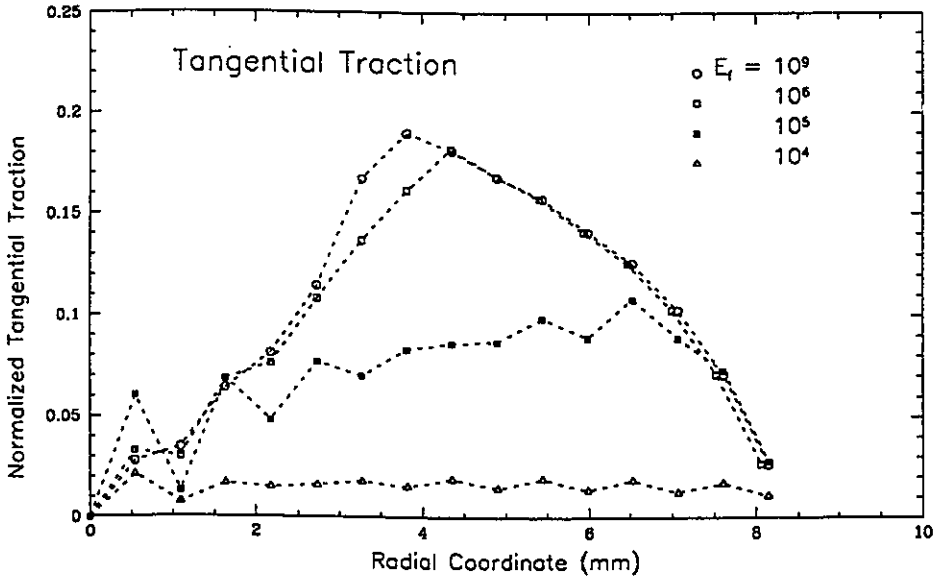

Figure 3.16: Normal & Tangential Contact Traction for Different Friction Modulii, E_f

$\mu = 0.2$

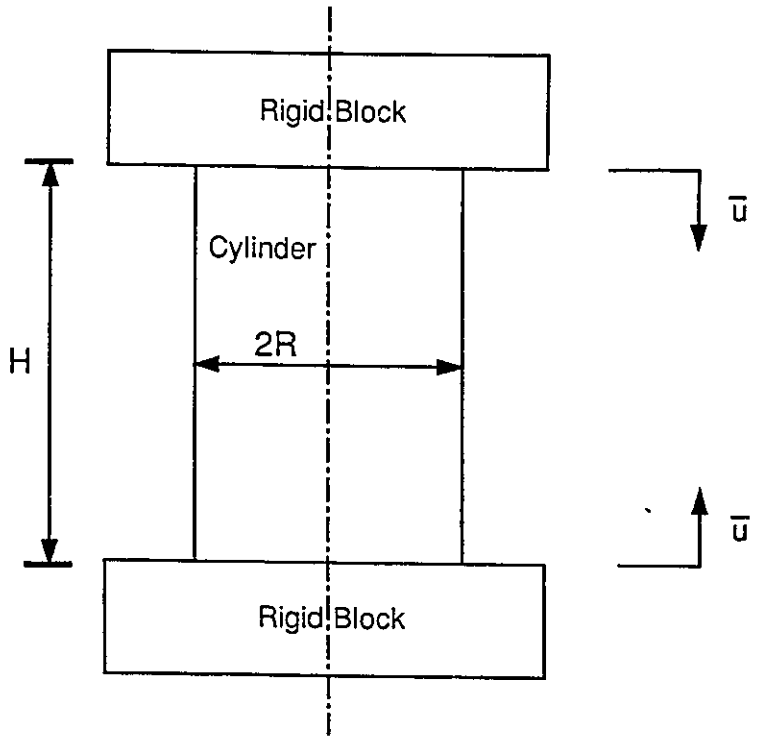

Figure 3.17a: A Cylinder Pressed Between Two Rigid Blocks, Example 2

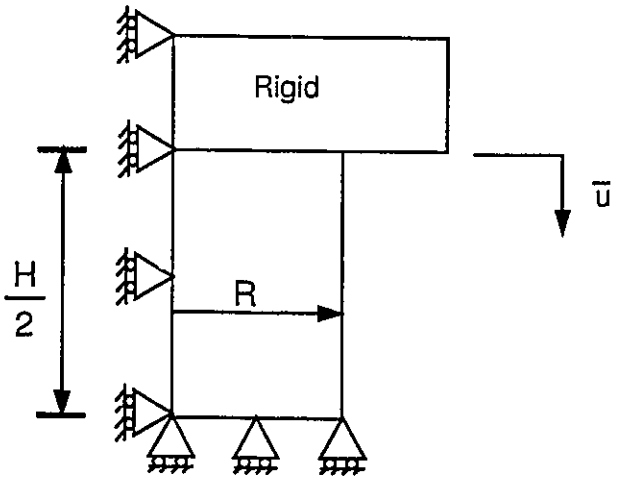

Figure 3.17b: Mathematical Model for Example 2.

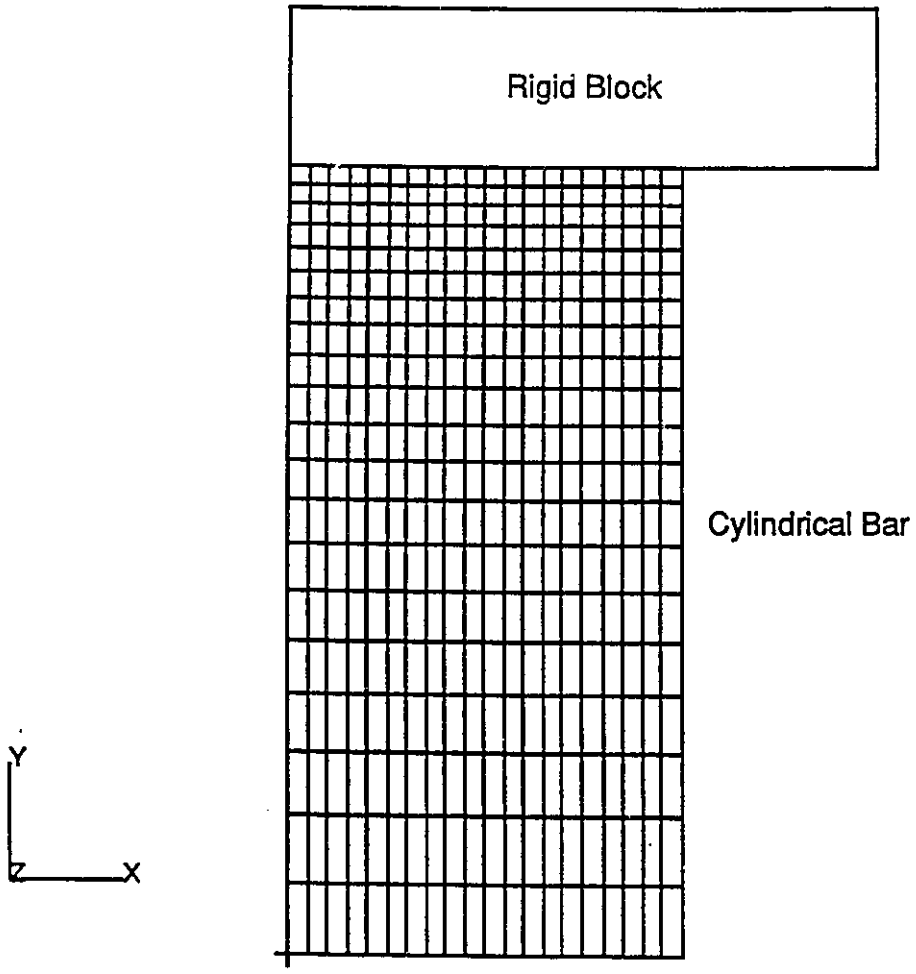

Figure 3.18: Finite Element Mesh for the Cylinder and Rigid Block

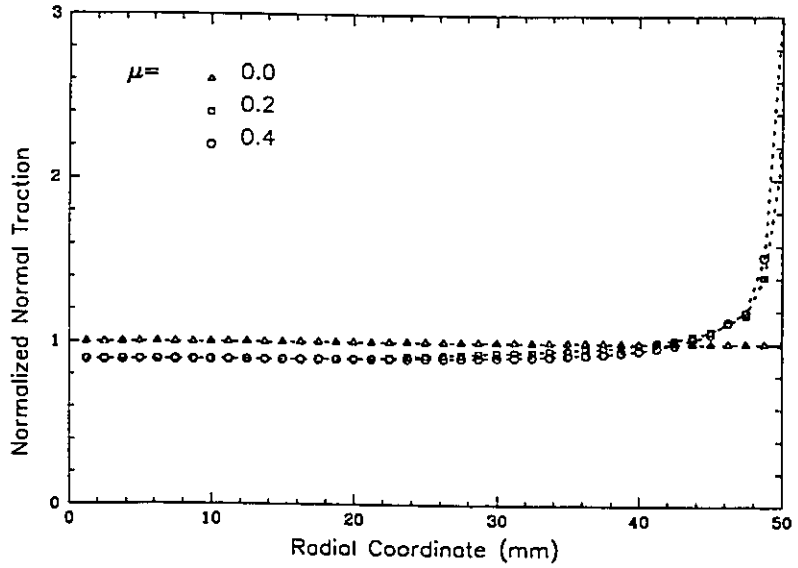

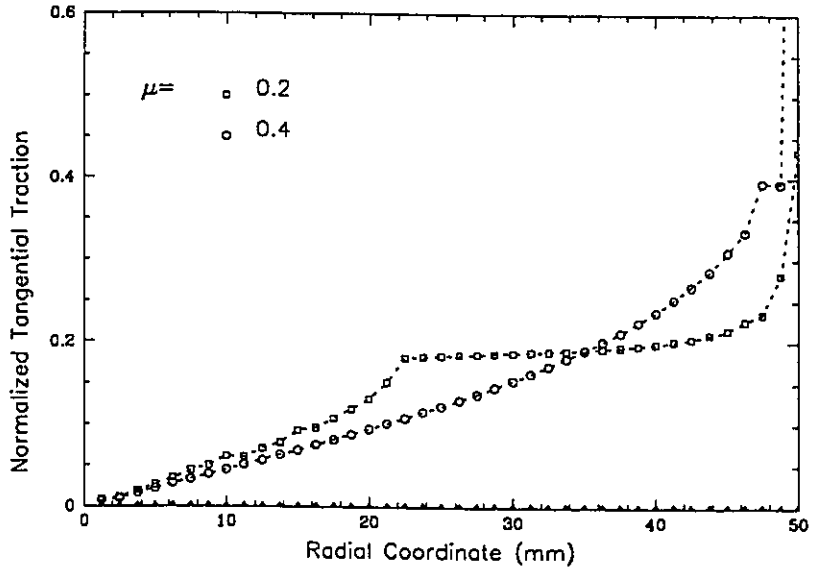

Figure 3.19: Normal & Tangential Contact Traction for the Block and Cylinder Example

$E_f = 10^{12}$

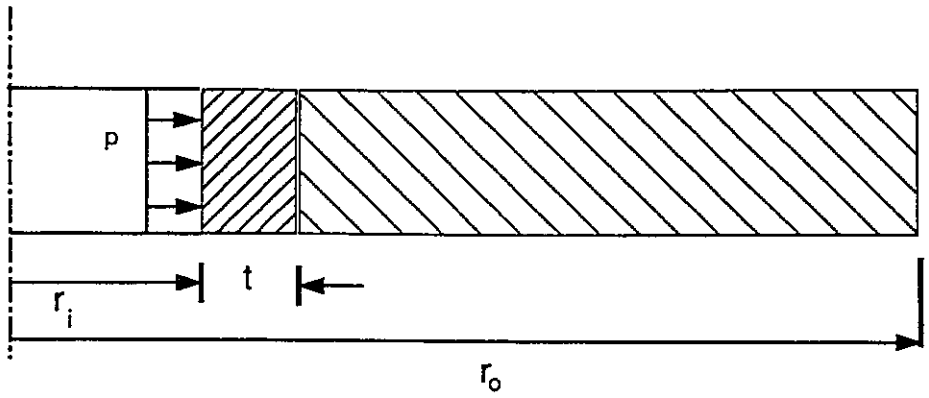

Figure 3.20a: Mathematical Model for A Composite Cylinder

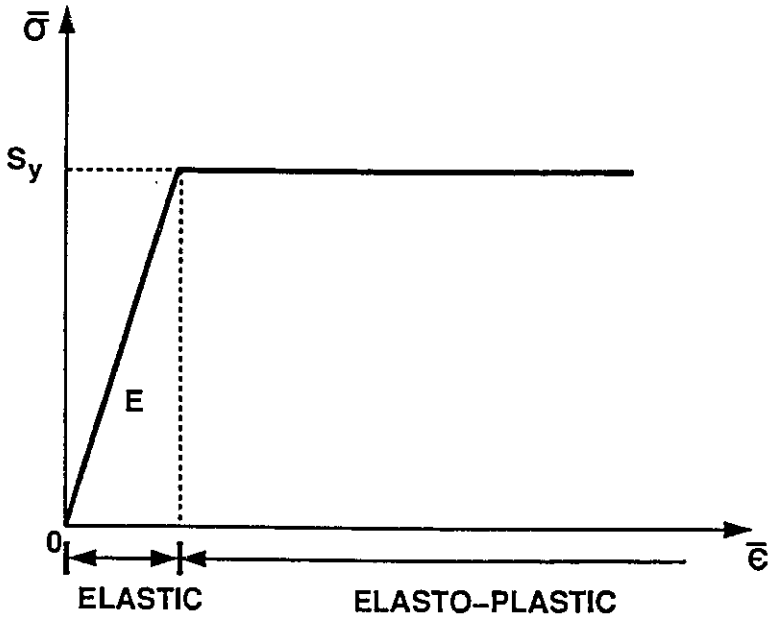

Figure 3.20b: Elasto–Perfectly Plastic Bi–Linear Material Model

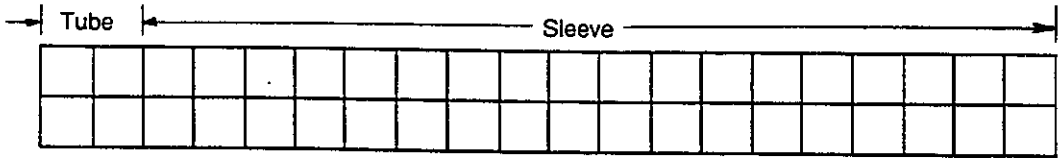

Figure 3.21: Finite Element Mesh for Example 3

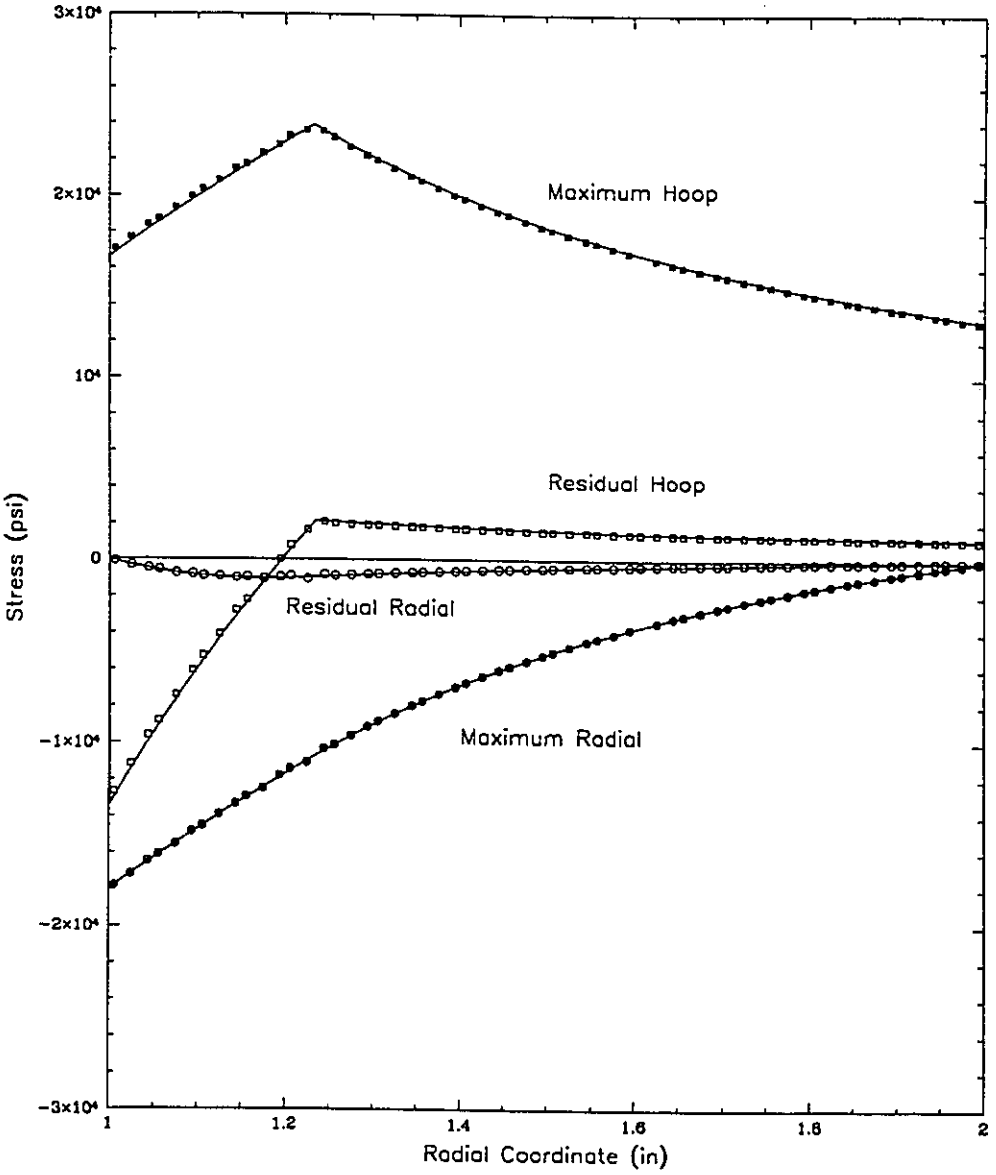

Figure 3.22: Radial and Hoop Stress Distributions for the Axisymmetric Thick Cylinder

(Solid Lines represent the Closed-Form Solution)

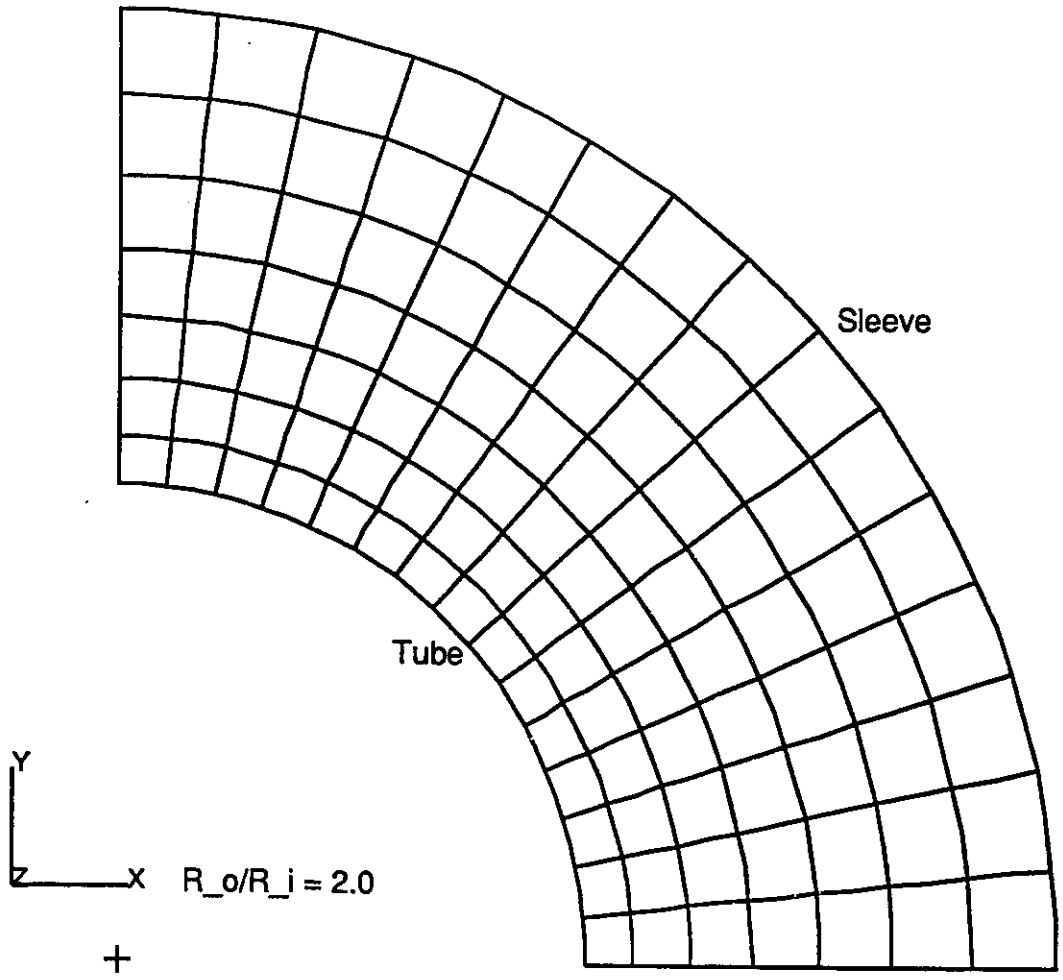

Figure 3.23: Finite Element Mesh for Plain Strain Thick Cylinder

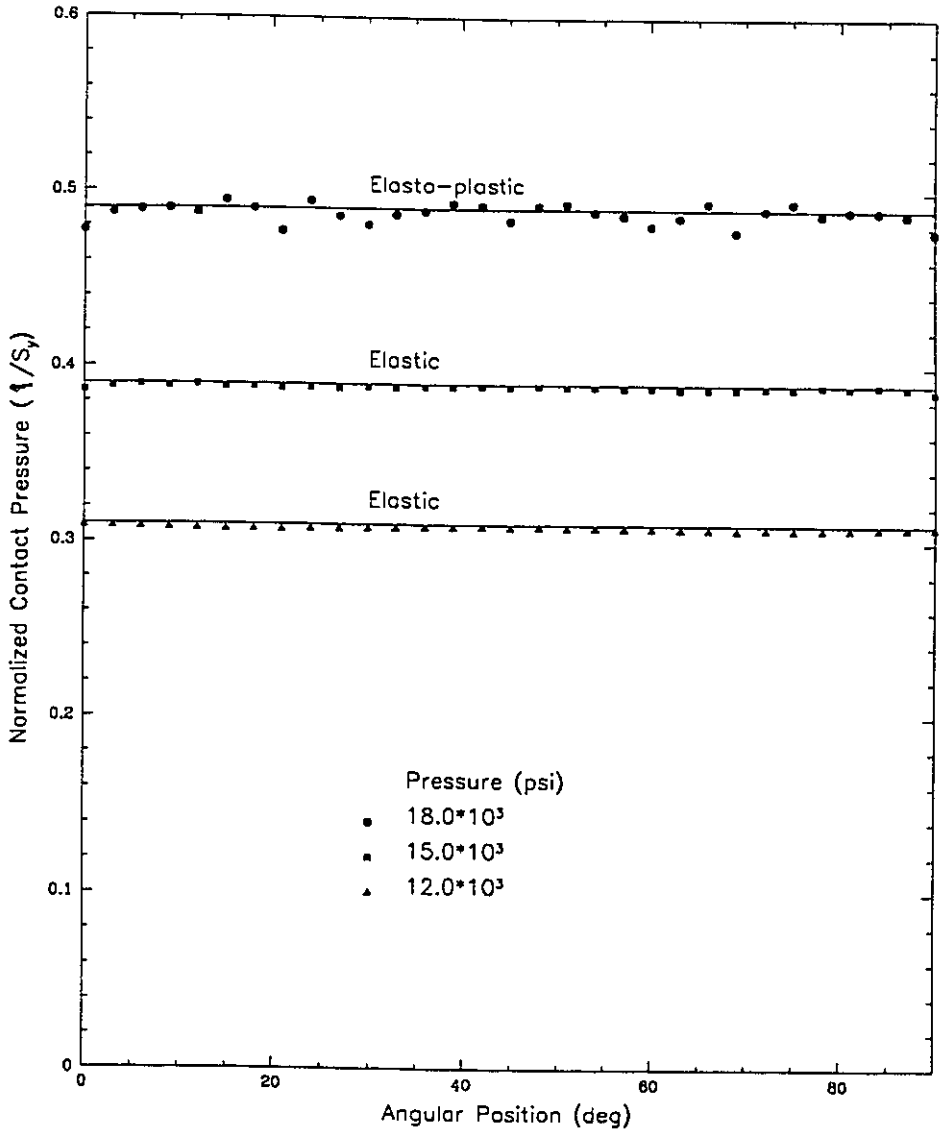

Figure 3.24: Distribution of the Normal Contact Traction for the Composite Cylinder Example
(Solid Lines represent Closed Form Solution)

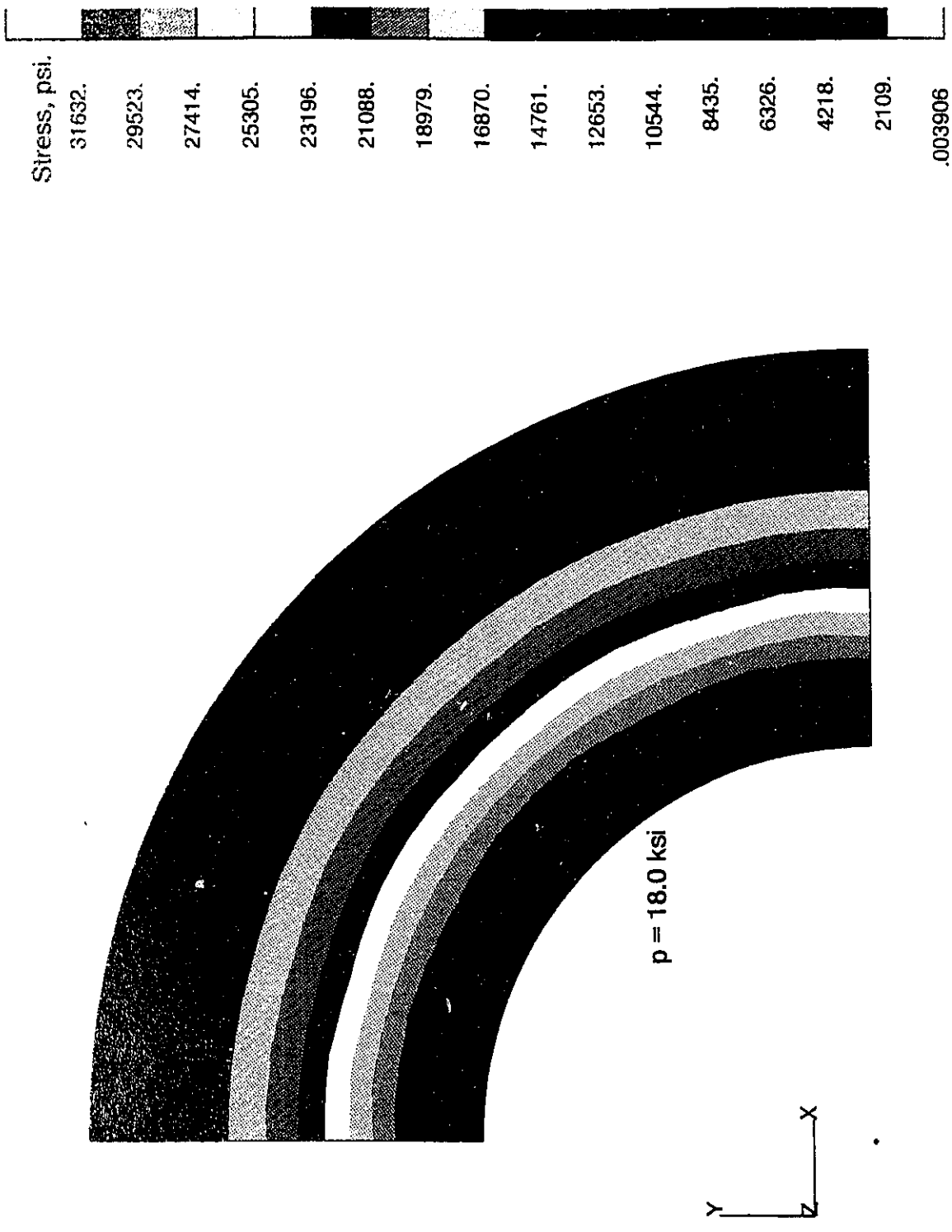

Figure 3.25: Effective Stress for the Plane Strain Thick Cylinder Example

CHAPTER 4

HYDRAULIC EXPANSION OF TUBE JOINTS

4.1 Introduction

The hydraulic expansion of tubes into tubesheets or end-fittings is a highly nonlinear problem. Three sources of the non-linear behaviour are present, namely, the material, the geometric and the contact non-linearities. In this chapter, two single-tube finite element models for the numerical simulation of the hydraulic expansion of tube joints are presented where the three types of nonlinearities are considered.

It should be noted that the single-tube model does not include the effects of the adjacent tube holes in the tubesheet. However, in experimental analyses, a tube is hydraulically expanded in a cylindrical sleeve with an estimated equivalent outer diameter. As such, the finite element analysis with the single tube model presented in this study is meant to correspond to the mock-ups used in the experimental analyses. Moreover, the expansion of the pressure tubes into the end-fittings in the CANDU reactor may be modelled by the single tube model when the expansion process is performed using a hydraulic expander.

A two-dimensional plane stress model is adopted to explore the effects of the material

mechanical properties on the joint strength represented by the residual contact pressure. The mechanical properties considered include the yield strength, the elastic modulus, the tangent modulus and the Poisson's ratio for both the tube and sleeve materials. In the plane stress model it is assumed that the axial stresses are negligible and the transition zone is not present at all. These assumptions limit the use of the plane stress model since the distributions along the tube surfaces cannot be obtained.

Because of the limited scope of the plane stress model, a two dimensional axisymmetric model is adopted. The single-tube hydraulic expansion is represented by a 2-D axisymmetric model since the geometry, loading and boundary conditions are all symmetric with respect to the tube axis in an idealized sense. The axisymmetric model is used to explore the distribution of the residual contact pressure along the tube outer surface and the distribution of the residual stresses along the tube inner and outer surfaces. In the finite element modelling, the significance of using a nonlinear kinematic formulation is checked out and the significance of ignoring the frictional contact interaction on the analysis is investigated.

A 2^3 full factorial experiment is performed to study the main and interaction effects of the expansion pressure, initial radial clearance and the coefficient of friction on the residual contact pressure and the maximum residual tensile stress along the tube walls. The effect of the frictional contact is investigated with the expansion pressure level. The effects of the expansion pressure and the initial radial clearance are further investigated with regard to the residual contact pressure, the maximum tensile stress, the axial extrusion, the increase in the inner and outer tube radii and the percentage

wall-thickness reduction.

Finally, this chapter concludes with an investigation of the effect of including the initial residual stresses and the cold-work layer along the as-received tube outer surface on the maximum residual tensile stresses.

In all the finite element analyses to follow, the materials are modelled by a bi-linear elasto-plastic stress-strain relation. Von Mises yield criterion is used to mark the onset of plastic deformation. An associated flow rule with isotropic work hardening is used to estimate the increments of the plastic strains. The geometric nonlinearity is dealt with by the use of the Updated Lagrangian formulation. The pressure load is applied incrementally and the modified Newton-Raphson iteration technique is used with a selective iterative procedure. The contact interaction is dealt with using the algorithm developed and verified in chapter 3.

4.2 2-D Plane Stress FE Model

The 2-D plane stress model only addresses the expanded tube zone and assumes that no axial stresses are present. Consequently, it has a limited scope since it does not address the question of the residual contact pressure distribution nor the residual stresses along the tube surface in the transition zone. However, this model can be used for studying the effect of the material mechanical properties on the residual contact pressure in a qualitative sense. The mechanical properties considered include the yield strength, S_y, Young's modulus, E, the tangent modulus, E_T, and Poisson's ratio, ν, for both the tube and the sleeve materials.

Geometry & Finite Element Mesh:

Due to the symmetry of the two dimensional disk representing the tube and the sleeve, the mathematical model may be taken as axisymmtric with the appropriate boundary conditions. The model consists of a tube with 0.45 and 0.05 in inside radius and thickness, respectively. The sleeve fits exactly without a clearance surrounding the tube and having 1.0 in outside diameter. A total of four and thirty six 2-D isoparametric quadrilateral axisymmetric finite elements are used to discretize the mathematical model for the tube and sleeve, respectively. The entire model contains 210 node with two degrees of freedom per node.

Mechanical Properties:

A bi-linear elasto-plastic material model is adopted for modelling the material behaviour

during the expansion process. In order to study the effect of changing the mechanical properties on the residual contact pressure, the one-factor-at-a-time approach is adopted. This approach may lead to a loss of the interaction effects between the different parameters. However, it serves our purpose at this stage to shed some light on the behaviour of the joint in a restrictive qualitative sense.

Boundary Conditions:

A uniform expansion pressure is applied along the inner surface of the tube to a maximum value of 21.0 ksi then complete unloading takes place. The contact interaction between the tube outer surface and the sleeve inner surface is considered frictionless since no relative tangential displacements are expected.

Results & Discussion:

In order to explain the effects of the different material parameters on the residual contact pressure it would be instructive if the expansion process is understood properly. The basic idea of the expansion joint is to obtain a permanent radial plastic deformation in the tube while minimizing or even eliminating that of the sleeve. As such, upon removing the expansion pressure the sleeve springs back elastically more than the tube resulting in a residual contact pressure. This residual pressure may be increased by increasing the elastic recovery of the sleeve, decreasing the elastic recovery of the tube or by decreasing the axial flow of the tube.

Figure 4.1 demonstrates the effects of the elastic constants of the tube and sleeve on the residual contact pressure. Furthermore, Figure 4.2 presents the effects of the tube

and sleeve plastic constants.

Figure 4.1.a shows that the increase in the tube elastic modulus, E_{tube}, keeping the sleeve elastic modulus, E_{sleeve}, constant, increases the residual contact pressure. This increase is attributed to the decrease in the spring back of the tube and this continues until the tube becomes very rigid and the elastic spring back stabilizes and the residual contact pressure approaches a constant value. On the other hand, the increase in E_{sleeve} decreases the residual contact pressure because of the same reason; that is the decrease in the elastic recovery.

The increase in the tube Poisson's ratio, ν_{tube}, increases the axial deformation of the tube on the expense of the radial deformation which results in a slight decrease in the residual contact pressure as shown in Figure 4.1.b for different values of the sleeve Poisson's ratio. In contrast, the increase in the sleeve Poisson's ratio, ν_{sleeve}, increases the residual contact pressure since it decreases the radial growth of the sleeve.

As the yield strength of the tube, S_{ytube}, increases, the residual contact pressure decreases. This behaviour, shown in Figure 4.2.a, is due to the decrease in the permanent radial growth of the tube in addition to the increase in its elastic recovery. Nevertheless, as the sleeve yield strength, $S_{ysleeve}$, increases, the residual contact pressure increases until it reaches a constant value corresponding to an entirely elastic sleeve.

In Figure 4.2.b, at the same sleeve tangent modulus, $E_{Tsleeve}$, the increase in the tube

tangent modulus, $E_{T_{tube}}$, slightly decreases the residual contact pressure. This is because the increase in the tube tangent modulus means increasing potential for elastic recovery in addition to the decrease in the radial growth. It may be observed also that the sleeve tangent modulus does not have an appreciable effect on the residual contact pressure.

As such, one may conclude that a stronger joint would be *generally* obtained by:

1. Increasing the tube elastic modulus.
2. Decreasing the sleeve elastic modulus.
3. Decreasing the tube yield strength.
4. Increasing the sleeve yield strength.

4.3 2-D Axisymmetric FE Model

The 2-D axisymmetric mathematical model for the expansion of a single tube into an equivalent sleeve consists of a tube placed freely inside a sleeve with a clearance as shown in Figure 4.3. The expansion pressure is applied along the tube inner surface within the sleeve. The tube and sleeve are both constrained axially at one end with no restriction in the radial direction. A cartesian coordinate system is set up having its origin in the middle of the tube and extends along the tube centre line. As such, the tube and sleeve extend along the domains [-1, + 1] and [-1, 0], respectively.

Geometry:

The same geometry used for the plane stress model is used here where a tube having 0.45in inner radius, r_i, and 0.05in thickness, t, is expanded inside a sleeve having a 0.5 and 1.0 in inner, R_i, and outer, R_o, radii, respectively. The lengths of the tube and sleeve are taken as 2.0 and 1.0 in, respectively. These lengths ensure that any displacement or stress gradient would die out far away from the boundaries.

Finite Element Mesh:

The mathematical model in Figure 4.3 is discretized using a total of 560 2-D axisymmetric 9-node isoparametric quadrilateral finite elements with a total of 1988 node with two degrees of freedom per node. The original finite element mesh is shown in Figure 4.4 where a fine mesh is utilized along the transition zone to account for the high stress gradients expected.

Boundary Conditions:

All nodes along the surface, Y = -1 are fixed against motion in the axial direction. This boundary condition applies on both the tube and the sleeve. The rest of the nodes in the entire model are left free to move in the X-Y plane.

In addition to the geometric boundary condition already mentioned above, there is a load boundary condition represented by a uniform pressure distribution along the tube inner surface. The continuous pressure distribution is replaced by the consistent nodal equivalent which is done automatically within INDAP. The expansion pressure is applied through a bi-linear time function. First, the pressure is increased from zero to a maximum value of $0.9S_y$ then unloading to zero pressure takes place.

Moreover, the contact boundary condition is considered using the developed contact algorithm. In this model, the problem is considered frictional and the coefficient of friction and the friction modulus are taken to be 0.3 and 10^5, respectively.

Material Model:

A bi-linear elasto-plastic material model is adopted to simulate the material mechanical behaviour of both the tube and the sleeve. The bi-linear elasto-plastic model is fully characterized by four numerical values for the mechanical properties as follows:

Elastic Modulus,	E	$= 30.0*10^3$ ksi
Poison's Ratio,	ν	= 0.3
Yield Strength,	S_y	= 30.0 ksi
Tangent Modulus,	E_T	= 2.0% E

Kinematic Formulation:

The linear theory of deformation is an acceptable approximation for problems where both the displacements and strains are small. However, the nonlinear theory using the Updated Lagrange formulation extends the linear theory a step further to account for both large displacements and strains. Throughout this study, the Updated Lagrange formulation is adopted to account for the geometric nonlinearity which may exist because of large clearance values and the feasibility of ignoring the geometric nonlinearity is checked out with the largest clearance value.

Results & Discussion:

The results that can be obtained from the finite element analysis include the displacement, strain or stress values everywhere in the model. However, in the analysis of the expanded tube joints, the distributions along the inner and outer surfaces of the tube are of prime importance. As such, in the following presentations only those distributions are considered.

Figure 4.5 shows the maximum and residual radial displacement distributions along the inner and outer surfaces of the tube. As can be seen, the tube is divided into three distinctive zones where the expanded zone extends over the domain [-1.0,-0.05], the transition zone [-0.05,0.5] and the un-expanded zone [0.5,1.0] in the Y-space. The inner surface grows radially more than the outer which leads to a reduction in the tube wall thickness after the complete expansion. The expanded zone is defined by the area where contact with the sleeve is preserved. Along the outer surface of this zone the residual contact traction is distributed.

Figure 4.6 shows the distribution of the residual contact normal and tangential traction. The residual normal traction is uniformly distributed with an average value of 8.6% of the tube yield strength. On the other hand, the tangential traction increases from zero up to the frictional capacity along the domain [-1.0,-0.3]. The frictional traction is equal to the frictional capacity along the domain [-0.3, -0.1]. The distribution of the tangential traction is positive which means that this residual traction would assist pulling the tube out of the sleeve and resist in pushing it in.

Figure 4.7 shows the distributions of the axial and hoop stresses along the tube outer and inner surfaces at maximum loading and after complete unloading. The residual axial stress along the outer surface of the tube transition zone is compressive while the hoop stress shows a little peak tensile stress of about 8.7% of the tube yield strength. Tensile axial and hoop stress peaks of 44.6 $\%S_y$ and 45.9 $\%S_y$ are observed along the transition zone. These tensile peaks are dependent, among other factors, on the initial radial clearance and the expansion pressure.

4.3.1 Linear vs. Nonlinear Analyses

With regard to the expanded tube joint, the most important results are the residual contact pressure and the maximum residual tensile stress along the tube inner and outer surfaces. As such, the feasibility of ignoring the nonlinear kinematic formulation is investigated counting on these two results. Table 4.1 demonstrates a comparison between a linear and a nonlinear solutions for an initial radial clearance of 0.005in which represents the maximum clearance value adopted in this study. An expansion

pressure of 0.9 S_y is applied and the problem is considered frictionless.

The average contact normal pressure, P_{avg} in Table 4.1, is estimated from:

$$\%P_{avg} = \frac{\int_{A_c} t_N \, dA}{S_y * A} * 100$$

where

t_N is the normal traction

A_c is the contact area

A is the total potential contact area

Table 4.1: Comparison between Linear and Nonlinear Analyses

Response (Units)	$\%P_{avg}$ ($\%S_y$)	$\sigma_{max.}$ (Inner) (S_y)		$\sigma_{max.}$ (Outer) (S_y)		Run Time (hr:min:sec)
		Axial	Hoop	Axial	Hoop	
Nonlinear	6.073	0.749	0.599	0.063	0.007	05:10:45
Linear	6.041	0.750	0.590	0.076	0.007	04:33:37

It is evident from Table 4.1 that a considerable time saving (~12%) is obtained by performing a geometrically linear analysis. This time saving is obtained with a minor change in the residual contact pressure which in this case amounts to -0.5%. Considering the residual tensile stresses, the maximum values are located along the tube inner surface and do not change if a linear kinematic formulation is adopted. As such, it can be concluded that a nonlinear analysis would be redundant in the finite element modelling of the expanded tube joint if the contact pressure and the maximum tensile stresses are the aim of the study.

4.3.2 Frictionless vs. Frictional Contact

The expanded joint is a friction joint in the first place. As such, the frictional contact interaction is investigated. In this section, frictional results are compared with results obtained from a frictionless analysis where both the coefficient of friction and the friction modulus being taken as zeros and the comparison is shown in Table 4.2. The expansion pressure is taken as 0.9 S_y and the coefficient of friction as 0.3.

Table 4.2: Comparison between Frictional and Frictionless Analyses

Response (Units)	P_{avg} (%S_y)	$\sigma_{max.}$ (Inner) (S_y)		$\sigma_{max.}$ (Outer) (S_y)		Run Time (hr:min:sec)
		Axial	Hoop	Axial	Hoop	
Frictional	7.983	0.739	0.583	0.0	0.0	17:49:43
Frictionless	6.073	0.749	0.599	0.063	0.007	05:10:45

It may be observed that the friction interaction plays an important role regarding the residual contact pressure and the maximum tensile axial stress along the tube outer surface. Ignoring the frictional interaction, drastically reduces the run time from 17:49:43 to 05:10:45 (hr:min:sec) which represents a 71% reduction. Unfortunately, this time saving comes at a cost, the average contact pressure,P_{avg} is 13% lower and the axial maximum residual tensile stress along the outer tube surface is overestimated when the friction is ignored.

4.4 A Parametric Study

The design parameters that influence the integrity and quality of the expanded tube joints are divided into three groups, namely, the manufacturing, the geometrical and the material parameters. However, in this study, it is assumed that the joint design is completed with regard to the selection of the materials involved and the dimensional details which in most cases are dependent on the thermal design of the heat exchanger. The only parameters to be considered in this section are the expansion pressure, the initial radial clearance and the coefficient of friction.

In order to investigate the main and interaction effects of the three parameters considered, a 2^3 complete factorial experiment is adopted where three factors (at two levels each) are considered. The full factorial experiment ensures that all main effects and two factor interactions are clear from any aliases.

Table 4.3 shows the design matrix for the full 2^3 factorial experiment in the coded variable values where a minus sign indicates the minimum value for a design factor and the plus sign indicates the maximum.

Table 4.4 represents the run matrix where the residual contact force, the maximum residual tensile stresses and the solution time are reported as the responses. Table 4.4 also shows the un-coded values of the considered design parameters at the low and high levels.

Table 4.3: 2^3 Full Factorial Design Matrix

Design Order	Design Parameters A	B	C	Interactions AB	BC	CA
1	- 1	- 1	- 1	+1	+1	+1
2	+1	- 1	- 1	- 1	+1	- 1
3	- 1	+1	- 1	- 1	- 1	+1
4	+1	+1	- 1	+1	- 1	- 1
5	- 1	- 1	+1	+1	- 1	- 1
6	+1	- 1	+1	- 1	- 1	+1
7	- 1	+1	+1	- 1	+1	- 1
8	+1	+1	+1	+1	+1	+1

Table 4.4: 2^3 Full Factorial Response Matrix

Design Order	P_{exp} S_y	c in	μ ---	P_{avg} $\%S_y$	$\sigma_{max.}$ Inner S_y	$\sigma_{max.}$ Outer S_y	Run Time hr:min:sec
1	0.6	0.000	0.0	1.97	0.052 (a) 0.042 (h)	0.020 (a) 0.030 (h)	01:22:09
2	1.1	0.000	0.0	7.88	0.805 (a) 0.652 (h)	0.092 (a) 0.008 (h)	06:22:09
3	0.6	0.005	0.0	0.65	0.734 (a) 0.603 (h)	0.052 (a) 0.080 (h)	03:19:28
4	1.1	0.005	0.0	6.00	0.834 (a) 0.644 (h)	0.139 (a) 0.008 (h)	08:55:29
5	0.6	0.000	0.3	2.35	0.045 (a) 0.031 (h)	0.087 (a) 0.020 (h)	05:47:29
6	1.1	0.000	0.3	7.00	0.808 (a) 0.658 (h)	0.196 (a) 0.008 (h)	15:11:40
7	0.6	0.005	0.3	2.36	0.726 (a) 0.592 (h)	0.139 (a) 0.068 (h)	09:51:34
8	1.1	0.005	0.3	4.46	0.822 (a) 0.645 (h)	0.186 (a) 0.008 (h)	30:29:44

In Table 4.4, the (a) and (h) stands for axial and hoop components, respectively. From the recorded responses, the effect plots shown in Figure 4.8 are obtained for the average contact pressure and the maximum residual tensile stress. Each effect plot represents the interaction effect of two of the design parameters. The response values on the effect plots for any two design parameters are the average value of the responses obtained at the minimum and maximum levels of the third design parameter. The dotted lines, in the effect plots, represent linear interpolations. In each effect plot, a horizontal line means no effect and the effect increases as the slope increases. On the other hand, parallel lines indicate no interaction and the interaction appears as the relative slope increased. However, It should be mentioned that the interpretation of the data obtained by the factorial experiment is of limited value. In subsequent runs, it is determined that the relationships between the factors and the observations are non-linear. Appendix C gives the estimated main and interaction effects on both the residual contact pressure and the maximum tensile stress along the tube inner surface.

In Figure 4.8.a, as the expansion pressure increases from its lower level to its upper level, the average residual contact pressure increases and the increase seems to be slightly affected by the low and high levels of the initial radial clearance. As such, it may be concluded that there is a slight interaction effect between the expansion pressure and the initial radial clearance on the residual contact pressure. On the other hand, there is a strong interaction between the expansion pressure and the initial radial clearance with respect to the maximum residual tensile stress as shown in Figure 4.8.d where the increase in the maximum tensile stress is higher at lower clearances.

In Figure 4.8.b, the increase in the residual contact pressure with the increase in the expansion pressure seems to be affected by the coefficient of friction. The increase at no friction is more than that with the friction included i.e. there is an interaction between the expansion pressure and the coefficient of friction. However, with regard to the maximum residual tensile stress, Figure 4.8.e shows that there is no main or interaction effect of the coefficient of friction. The increase in the expansion pressure lead to an increase in the residual tensile stress along the tube inner surface.

In Figure 4.8.c it can be seen that there is a very slight interaction between the initial radial clearance and the coefficient of friction and no main or interaction effect at all with respect to the residual tensile stress as shown in Figure 4.8.f.

Since the 2^3 factorial experiment results in linear relationships as shown in the effect plots in Figure 4.8, centre points were examined and it is found that the relations between the design parameters and the performance measures are strongly nonlinear. The factorial experiment shows that the friction coefficient only interacts with the expansion pressure with regard to the residual contact pressure. Therefore, the friction effect is considered briefly for the sake of time saving. In Figure 4.9.a, the residual average contact pressure is plotted against the coefficient of friction. The increase in the coefficient of friction increases the residual contact pressure. This increase continues until a condition of complete adhesion is reached and the contact pressure approaches a constant value. The increase in the residual contact pressure is due to the increase in the radial growth of the tube since friction resists the axial deformation. In Figure 4.9.b, it can also be observed that the coefficient of friction shifts the

residual contact pressure peak towards lower values of the expansion pressure.

Having the frictional effects being understood, it is decided to examine several case studies within the ranges considered for both the expansion pressure and the initial radial clearance considering frictionless contact interaction. A two dimensional array of case studies, spanning over the expansion pressure and the initial radial clearance, is executed. The expansion pressure runs from $0.6S_y$ to $1.15S_y$ in increments of $0.05S_y$ while the initial radial clearance runs between 0.0 and 0.005 in increments of 0.00125 in. In each of these case studies, five responses are recorded, namely, the residual average contact pressure, p_{avg}, the maximum tensile residual stress in the transition zone, σ_{max}, the axial extrusion, e, the increase in the tube outer radius, δr_o and the increase in the tube inner radius, δr_i. Moreover, the percentage wall thickness reduction ratio is calculated using the following formula:

$$\%wtr = \frac{t_o - t_f}{t_o} * 100$$

where

wtr stands for wall thickness reduction

t_o is the original tube thickness.

t_f is the deformed tube thickness.

In Figure 4.10.a, the residual contact pressure is plotted against the expansion pressure for three values of the initial radial clearance. As can be seen in the figure, the residual contact force increases as the expansion pressure increases until it reaches a peak value beyond which it begins to decrease. This behaviour was reported

experimentally as discussed in the introduction. It was attributed to the smoothing of the contact surfaces which results from the relative axial sliding of the contacting surfaces. Since no attempt has been made throughout this study to model the smoothing action, it has been concluded that the phenomenon of peak-strength would have another explanation relating to the parameters included in the finite element modelling.

The analysis started with both the tube and sleeve materials having exactly the same mechanical properties including the yield strength. As the expansion pressure increases, both the tube and tubesheet materials starts to deform. The tube material deforms plastically before the sleeve material does. This means that the tube outer diameter grows in size while the sleeve still elastic and this is exactly what the expansion process is all about; an over-sized tube in a sleeve hole. As the expansion pressure increases further, the plastic zone within the sleeve spreads more leading to a permanent growth in the hole size which starts to defy the increase in the tube outer diameter leading to a decrease in the residual contact pressure.

Considering the initial radial clearance, Figure 4.10.b shows the residual contact pressure against the initial radial clearance at different values of the expansion pressure. As would be expected, increasing the initial clearance decreases, significantly, the residual contact pressure since large clearances would enhance the hardening action of the tube material before even touching the sleeve. The strain hardening of the tube material increases its potential spring-back upon unloading.

The second response to be considered is the maximum residual tensile stress which is found to occur along the tube inner surface in the axial direction in all the cases considered. Figure 4.11 gives its value against the expansion pressure and the initial radial clearance. In Figure 4.11.a, as the expansion pressure increases, the residual stress increases with an interaction effect with the initial radial clearance. A similar interaction phenomenon is shown in Figure 4.11.b where the interaction effect is evident at low initial radial clearance values roughly below 0.001 in.

The tube axial extrusion is plotted in Figure 4.12.a against the expansion pressure at different levels of the initial radial clearance. As the expansion pressure increases, the axial extrusion increases since at higher pressures the radial and axial strains increase. On the other hand, Figure 4.12.b gives the axial extrusion plotted against the initial radial clearance at different levels of the expansion pressure. A straight line relation is shown and the decrease in the axial extrusion is due to the increase in the radial strain on the expense of the axial strain.

The increase in the tube inner and outer tube radii is given in Figures 4.13.a and 4.14.a as a function of the expansion pressure at different levels of the initial radial clearance and in Figure 4.13.b and 4.14.b as a function of the initial radial clearance at different levels of the expansion pressure. Similar relations are observed. As the expansion pressure increases below the peak pressure, the inner and outer radii grow at a slower rate than that at pressures beyond the peak value where the sleeve has gone completely plastic.

The percentage wall-thickness-reduction ratio is given in Figure 4.15.a as a function of the expansion pressure at different levels of the initial radial clearance and in Figure 4.15.b as a function of the initial radial clearance at different levels of the expansion pressure. The behaviour of the %wtr ratio is similar to that of the inner and outer radii and that is expected since it is linearly related to both of them.

In Figure 4.16.a, the residual normal contact traction distributed along the tube outer surface is compared for two clearance values. While in Figure 4.16.b the residual contact traction is plotted for two different expansion pressure values. It can be seen that the increase in the expansion pressure increases the residual contact traction. On the other hand, the increase in the initial radial clearance decreases the contact traction and divides its uniform pattern into two regions. A uniform region extends along the expanded tube followed be a region with a pressure gradient at the end of contact adjacent to the transition zone.

If the sleeve in Figure 4.4 is fixed axially and the tube free end is subjected to an axial force which tends to pull the tube away from the sleeve, the force is called pull-out force. On the other hand if the force is pushing the tube into the sleeve, it is called push-in force. In Figures 4.17.a and 4.17.b, the displacement of the tube outer surface after complete unloading is compared for different expansion pressure loadings and different clearance values, respectively. As can be seen, the increase in the expansion pressure increases the slope of the tube outer surface in a direction which results in an increase in the joint push-in strength. On the other hand, the increase in the initial radial clearance does not seem to have such an effect.

4.4 Initial Stresses & Cold Work along the Outer Surface Layer

Current nuclear steam generator designs for new facilities and replacement projects enhance corrosion resistance through the use of advanced tubing materials and improved joint design and fabrication techniques. Alloy 690TT tubing has demonstrated outstanding laboratory performance in accelerated primary water chemistries. However, the potential for susceptibility to secondary water stress corrosion cracking has not been eliminated for this material. Initial measurements to characterize the un-expanded tube reveal compressive stresses associated with a thin work-hardened layer on the outer surface of the tube. The levels and character of the residual stresses following hydraulic expansion are primarily dependent on the work-hardened surface layer and initial stress state. Low levels of residual tensile stresses in the transition zone would offer an excellent resistance to the stress corrosion cracking initiation. Propagation of any possible cracking would be deterred by the compressive stress field that surrounds the narrow circumferential band of tensile stresses.

In this section the effect of the initial residual stresses and the work-hardened layer along the as-fabricated tube outer surface, on the residual tensile peak stress, are investigated. The joint geometry, mechanical properties and loading are typical values used in the experimental qualification program at Babcock Wilcox International (B.W.I.). Three matrices that cover the variables of interest to the experimental program at B.W.I. were considered. Essentially, three tube-to-tubesheet joint design geometries

are represented (with equivalent sleeve diameters and expansion pressures varying according to these geometric differences) with some variation in the hole diameter and expansion pressure within each of the three design scenarios. Since no conceptual differences have been observed, only one design scenario is considered in this section.

A special 2-D axisymmetric finite element model is constructed for the given geometry and material mechanical properties. The tube outer diameter and thickness are 0.686 and 0.04 in, respectively. The sleeve inner and outer diameters are 0.6955 and 1.294 in, respectively, which results in an initial radial clearance of 0.00475 in. The mechanical properties of both the tube and sleeve materials are given in Table 4.5.

Table 4.5: Mechanical Properties for the Tube and Sleeve Materials

MECHANICAL PROPERTIES	TUBE	SLEEVE	UNITS
Young's Modulus, E	$30.6*10^3$	$29.2*10^3$	ksi
Poisson's Ratio, ν	0.289	0.3	.....
Yield Strength, S_y	43.0	67.0	ksi
Tangent Modulus, E_T	1.0% E	1.0% E	ksi

The finite element mesh is refined about 1/8 of an inch to the sleeve secondary side in order to resemble the length of crevice that usually exists in the fabricated joint. The finite element mesh consists of 380 isoparametric 9-node quadrilateral elements having a total of 1700 nodes as shown in Figure 4.18.

The residual stresses in the as-fabricated tube were measured using X-ray diffraction and are provided by B.W.I. including the surface values in the axial and hoop directions of -12.0 ksi each. Knowing that the as-fabricated tube is in an equilibrium state, the distribution of the radial component of the residual stress in the as-fabricated joint had to be supplied. In order to get around this missing data problem, the residual stresses in the as-fabricated tube is introduced to the analysis thermally. A temperature gradient is imposed across the tube thickness which resulted in the required surface stresses.

Moreover, the effect of the cold-work layer along the tube outer surface is investigated where the tube mesh is refined towards the outer surface to reveal an outer 0.001 in surface layer of elements. These elements are given a higher yield strength corresponding to the cold-work represented by the %strain. Three values for the %strain are considered; 2, 4 and 6 % strain which correspond to surface yield strengths of 55, 70 and 78 ksi, respectively.

In Figure 4.19, the deformed configuration of the tube and the sleeve are shown and Figure 4.20 shows a comparison between the finite element solution and an experimental profile provided by B.W.I for a clearance value of 0.005 and expansion pressure of 33.2 ksi. The close agreement is evident and the model is used for the intended investigation.

Table 4.6 shows the numerical values for the maximum residual tensile stress along the tube inner and outer surfaces for different values of the percentage cold work. It is obvious that the %strain has a profound effect on the residual tensile peak stresses

along the outer surface of the tube at the transition zone. Figure 4.21 shows the axial and hoop stress distributions along the tube outer surface for different values of the percentage surface strain.

Table 4.6: Effect of Cold Work Outer Surface Layer on the Residual Tensile Peak Stresses

% Strain	Max. Stress (Inner), ksi		Max. Stress (Outer), ksi	
	Axial	Hoop	Axial	Hoop
0.0	32.065	26.87	8.85	2.92
2.0	31.952	27.014	18.69	12.74
4.0	31.913	27.174	31.566	25.726
6.0	31.914	27.237	38.268	33.364

On the other hand, Table 4.7 shows the effect of the value of the initial stresses along the outer surface of the as-fabricated tube. It can be observed that there is a slight effect with regard to the axial stresses and a bigger effect for the hoop stresses.

Table 4.7: Effect of Initial Residual Stresses

Initial Stress(ksi)	Max. Stress (Inner), ksi		Max. Stress (Outer), ksi	
	Axial	Hoop	Axial	Hoop
0.0	32.065	26.870	8.85	2.92
-12.0	32.093	26.847	7.137	0.968
-24.0	32.120	26.822	6.25	0.0

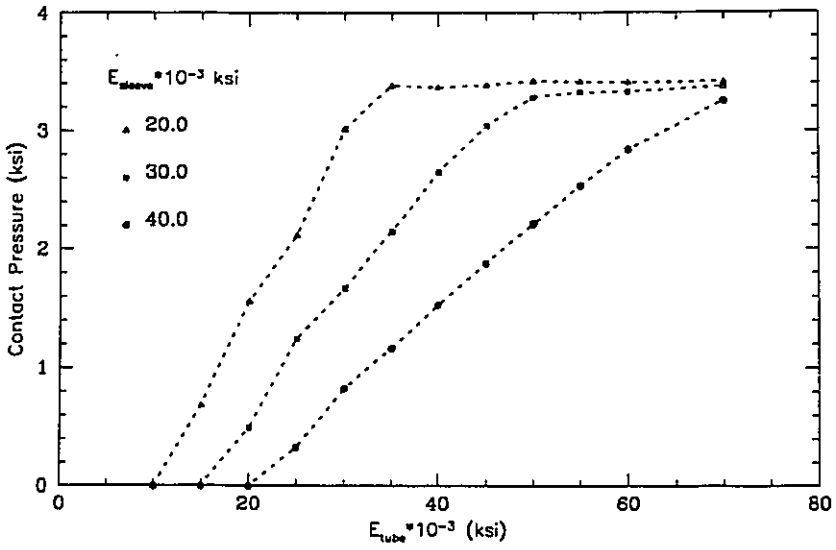

Figure 4.1.a: Effects of Tube and Sleeve Elastic Modulii

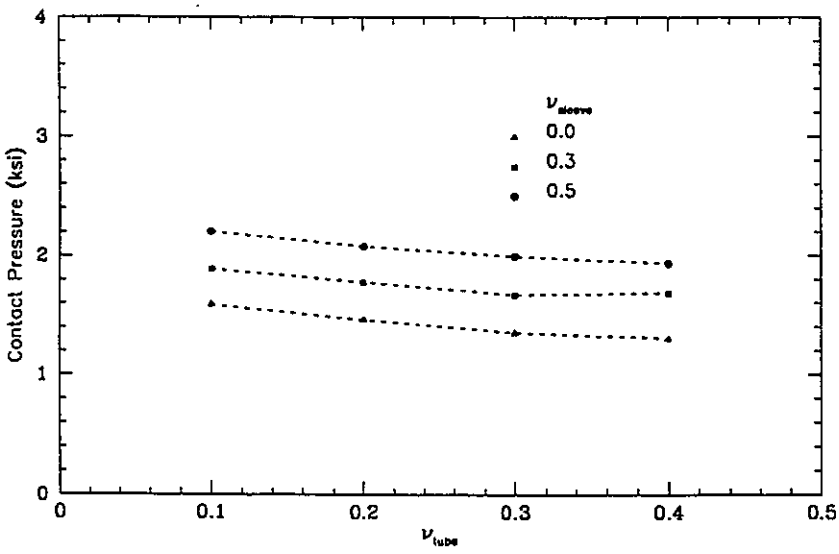

Figure 4.1.b: Effects of Tube and Sleeve Poisson's Ratio

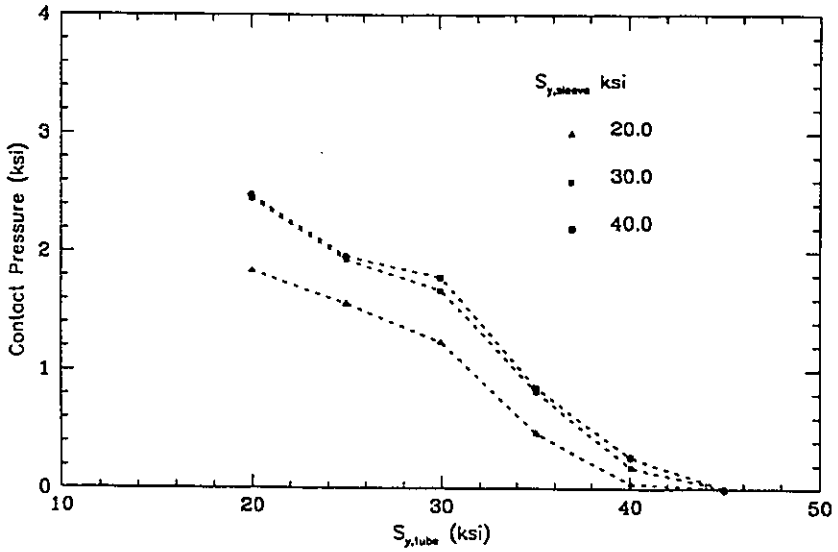

Figure 4.2.a: Effects of Tube and Sleeve Yield Strength

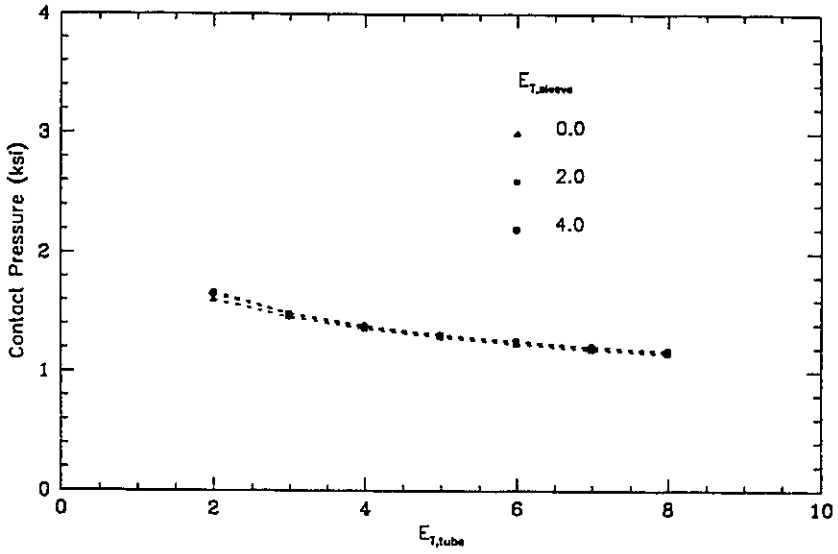

Figure 4.2.b: Effects of Tube and Sleeve Tangent Modulii

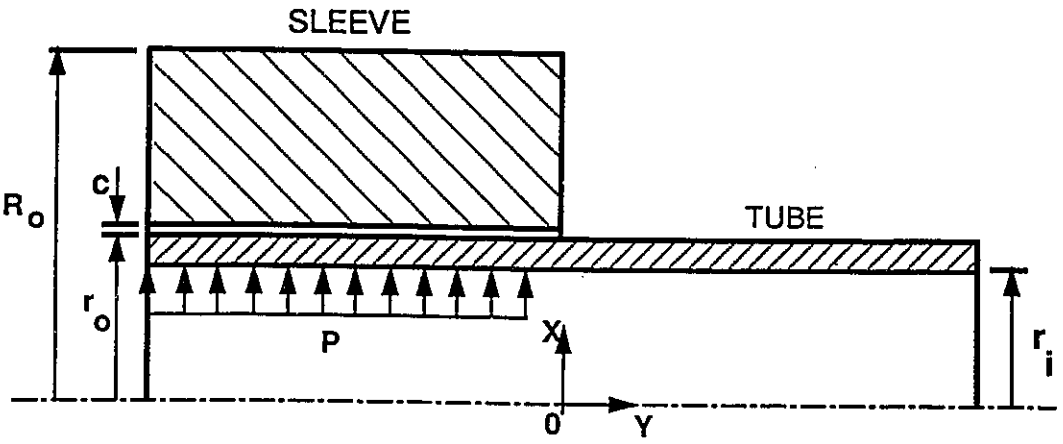

Figure 4.3: Mathematical Model for Tube–to–tubesheet Joint

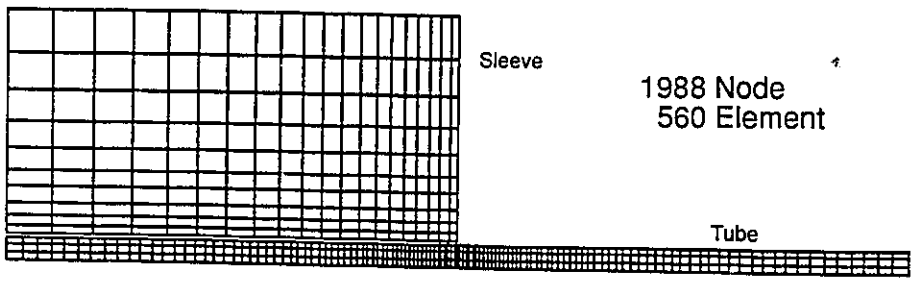

Figure 4.4: 2–D Finite Element Mesh for the Axisymmetric Model

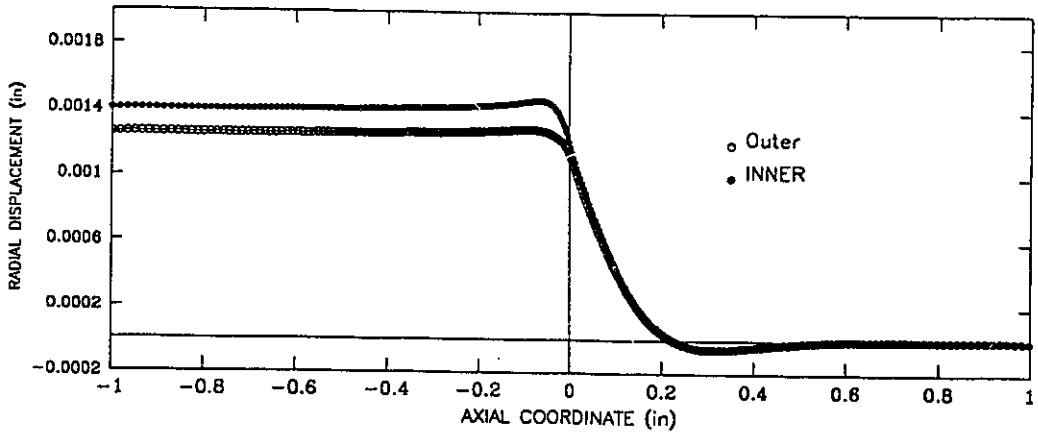

(a) Maximum Displacements

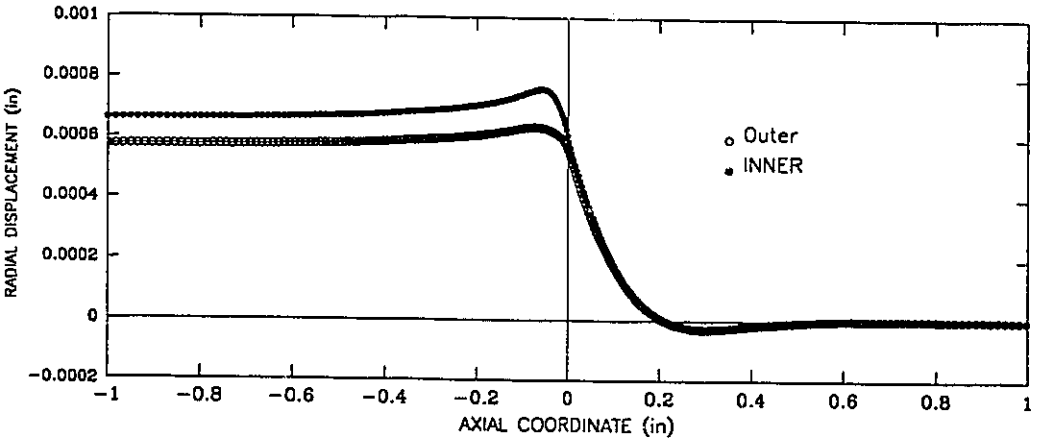

(b) Residual Displacements

Figure 4.5: Radial Displacements along Tube Inner & Outer Surfaces at Maximum Loading and after Complete Unloading

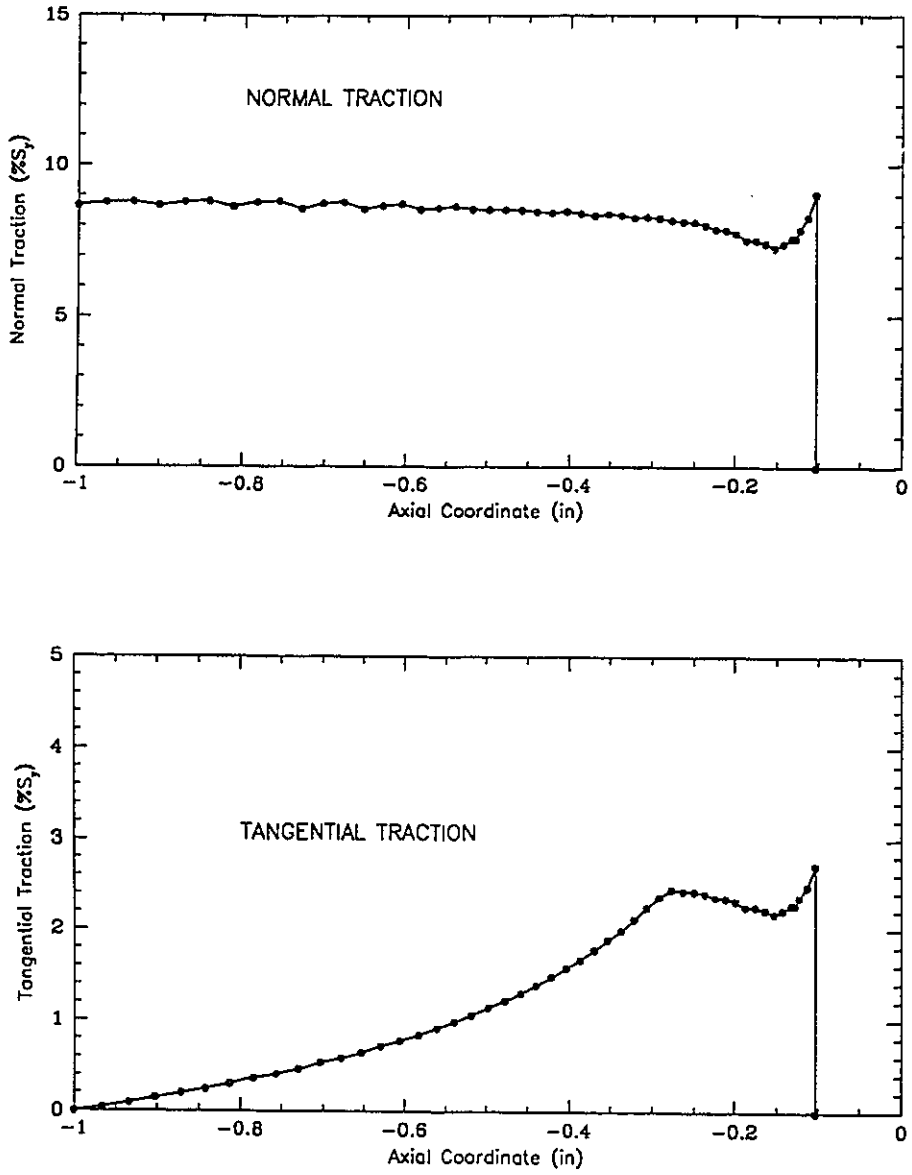

Figure 4.6: Distribution of the Residual Contact Traction
$p=0.9S_y$, $c=0.0$, $\mu=0.3$, $E_f=10^5$

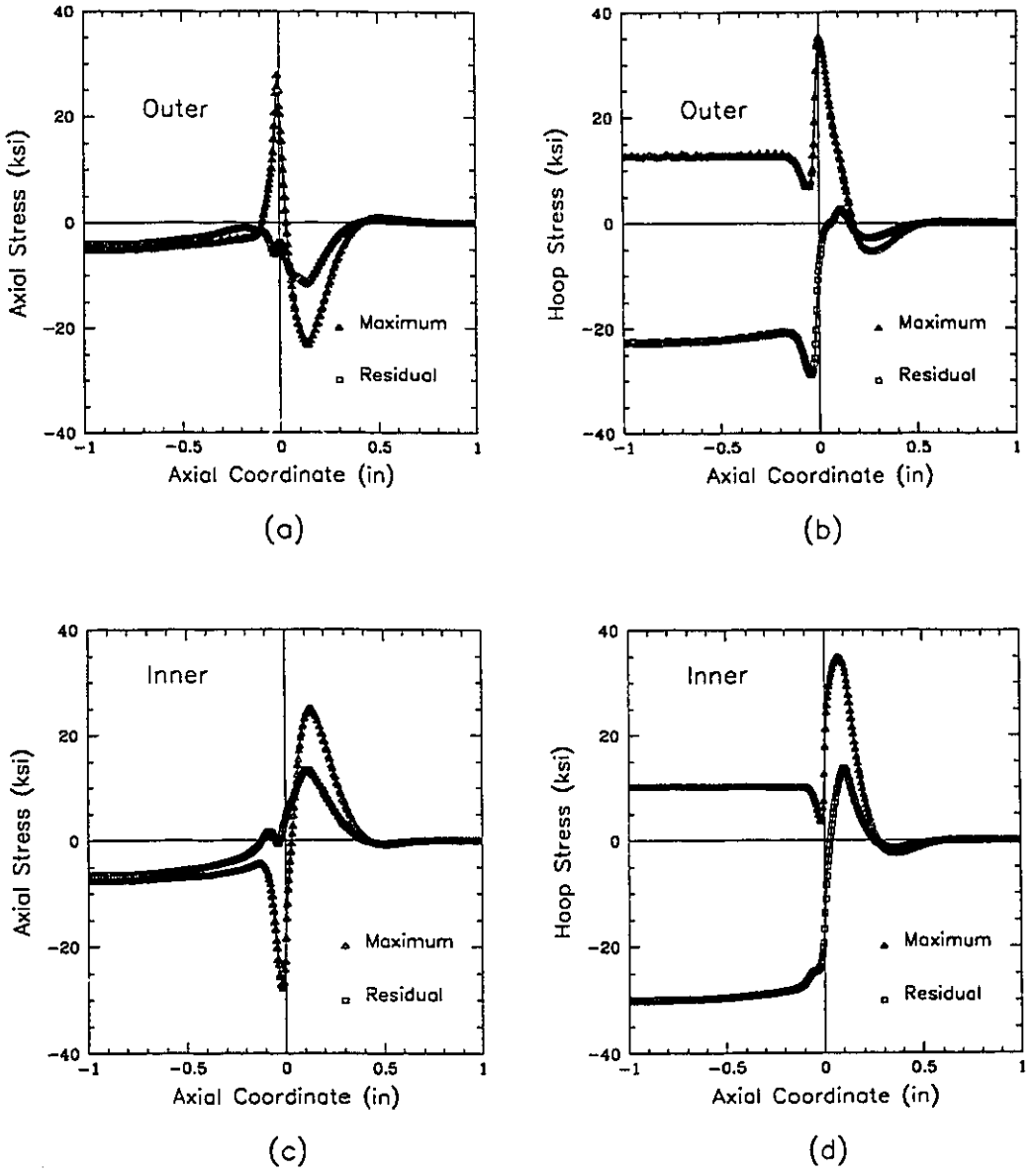

Figure 4.7: Hoop & Axial Maximum/Residual Stresses
along Tube Inner & Outer Surfaces
$p=0.9S_y$, $c=0.0$, $\mu=0.3$, $E_f=10^5$

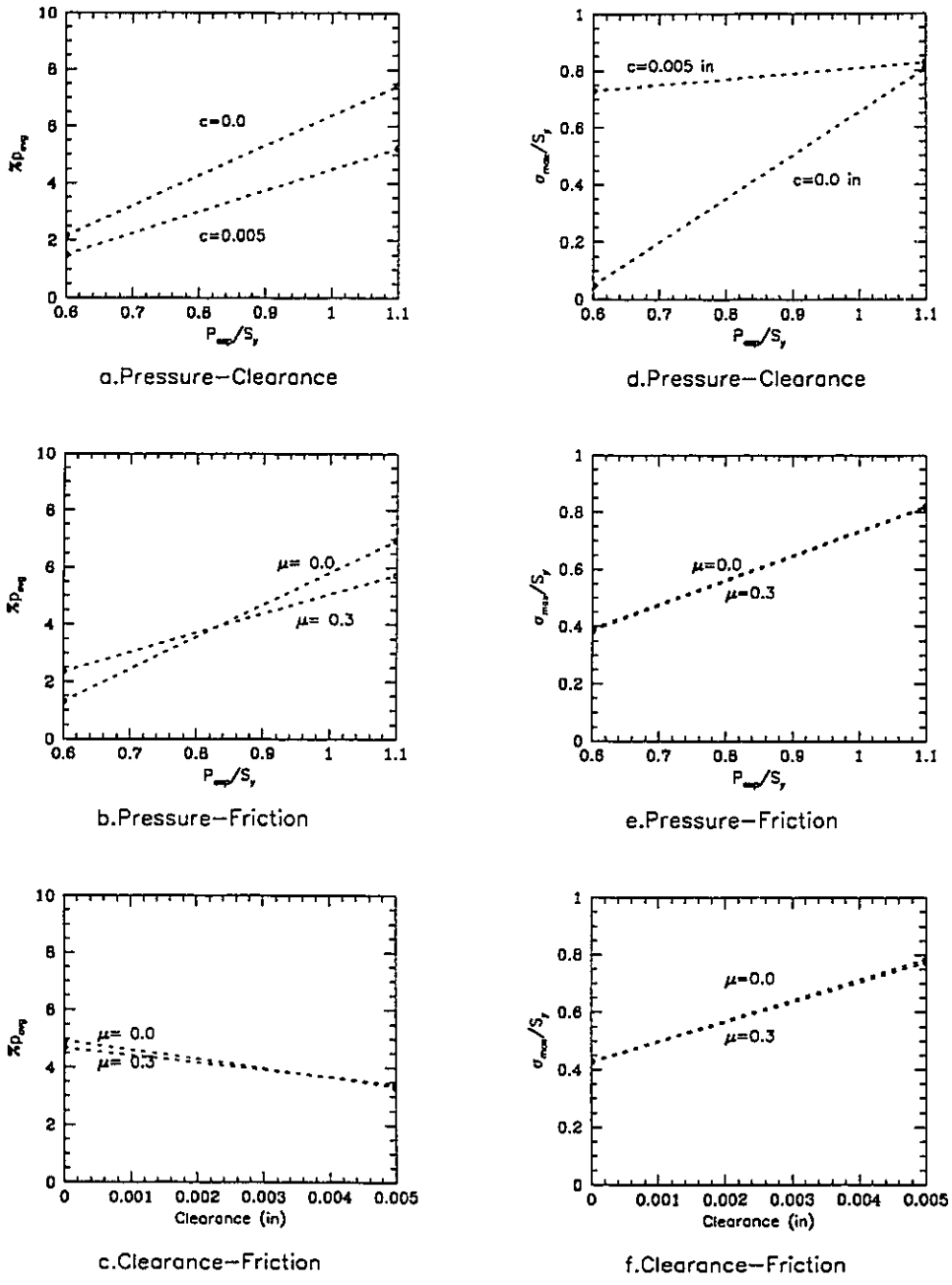

Figure 4.8: Effect Plots for the 2^3 Factorial Experiment

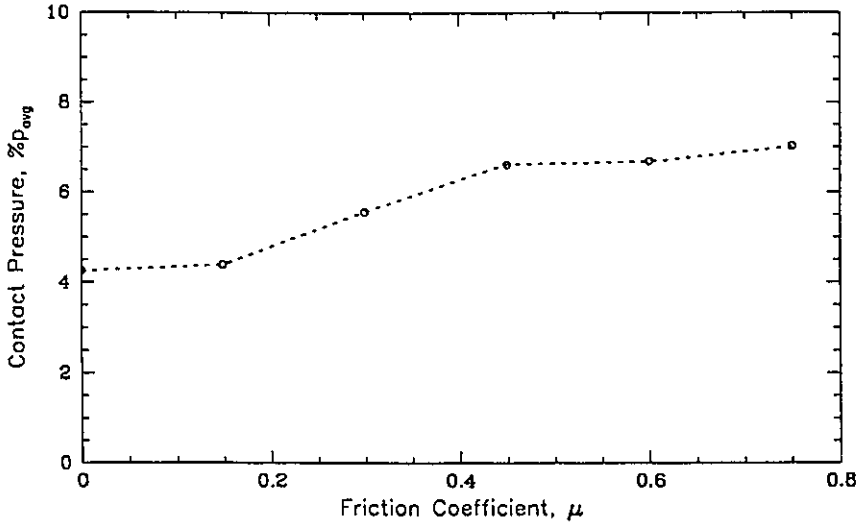

Figure 4.9.a: Effect of Friction on the Contact Pressure

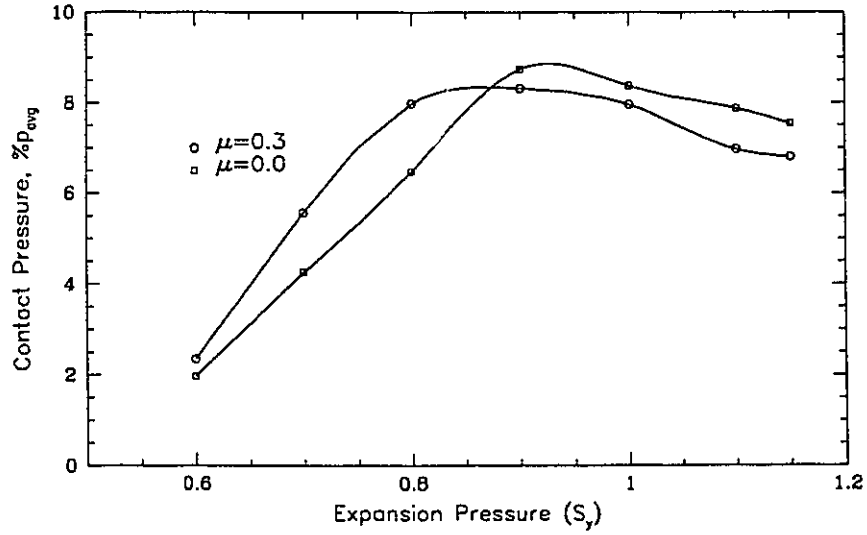

Figure 4.9.b: Frictional vs. Frictionless Contacts

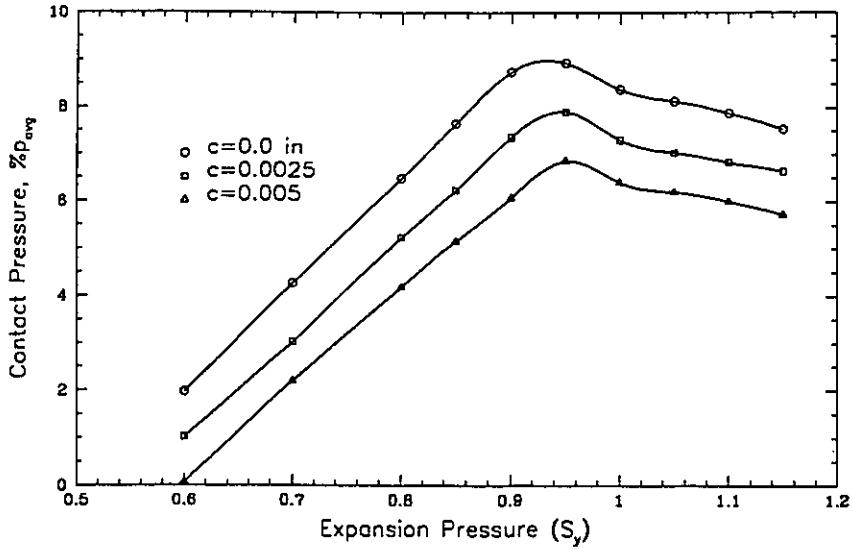

a.Variation for different Clearances

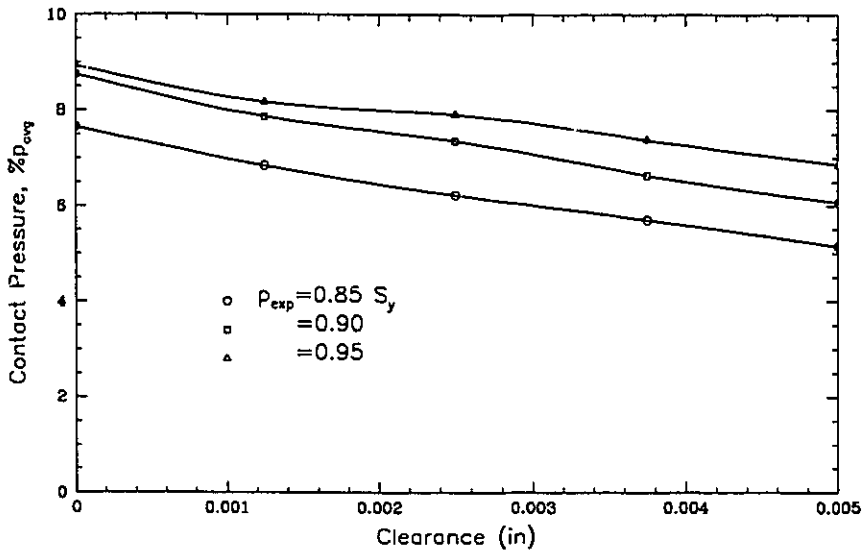

b.Variation for different Pressures

Figure 4.10: Residual Contact Pressure Variation

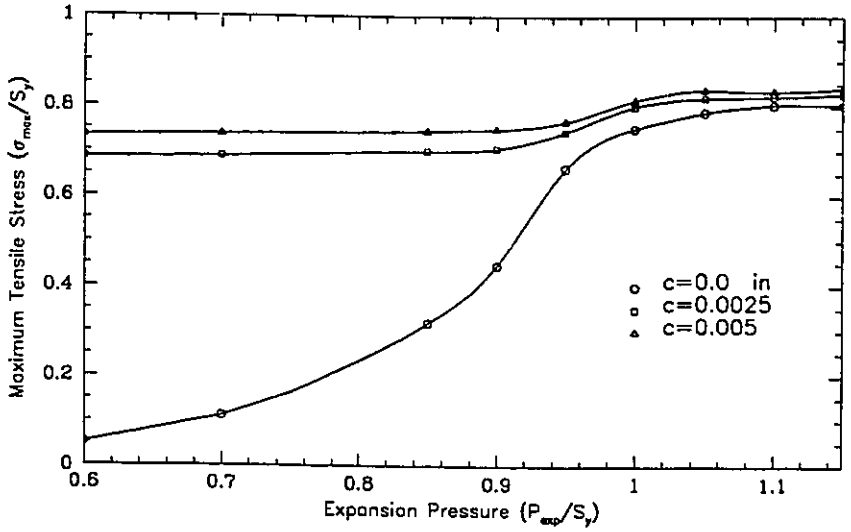

a.Variation for different Clearances

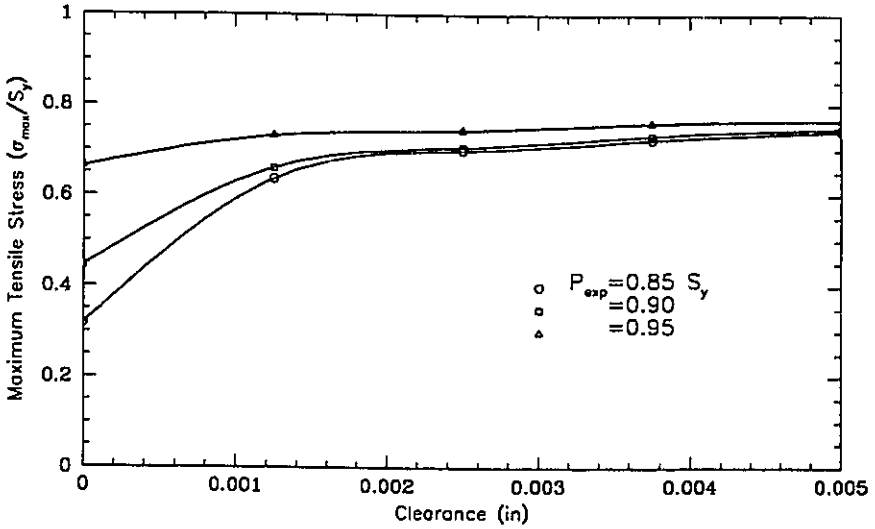

b.Variation for different Pressures

Figure 4.11: Maximum Residual Tensile Stress Variation

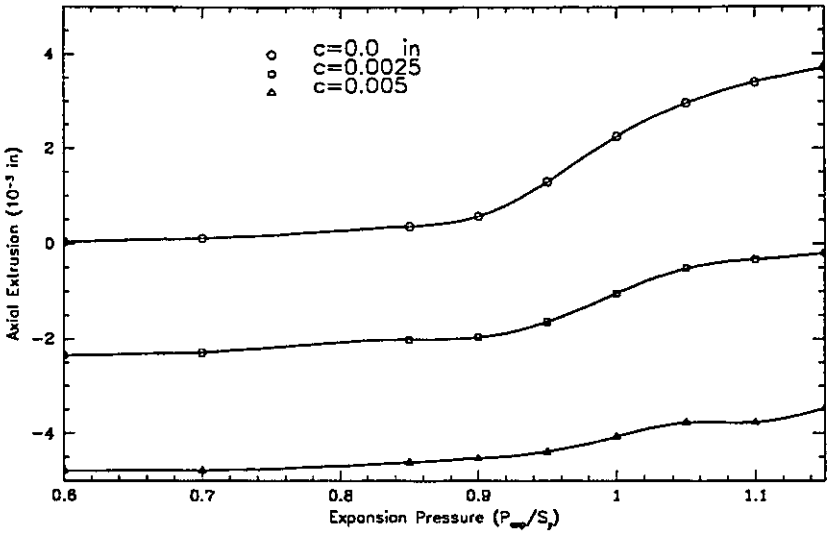

a.Variation for different Clearances

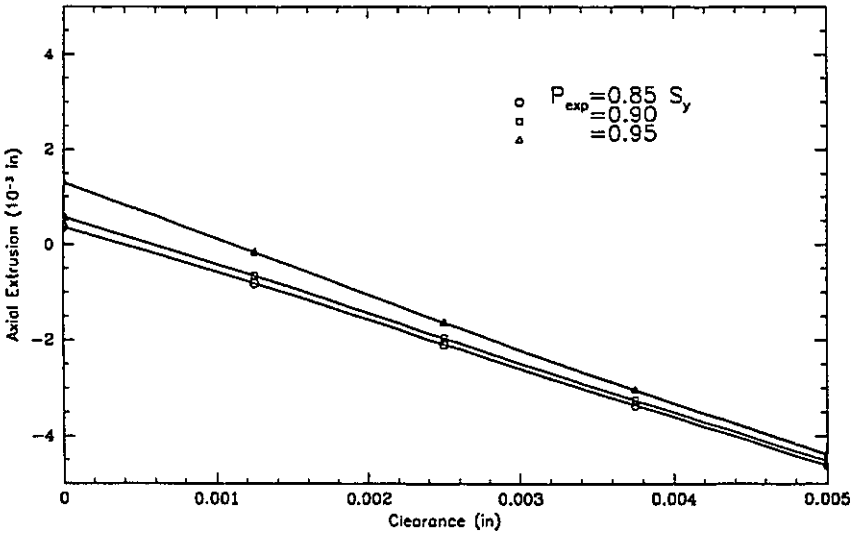

b.Variation for different Pressures

Figure 4.12: Axial Extrusion of the Tube Free End

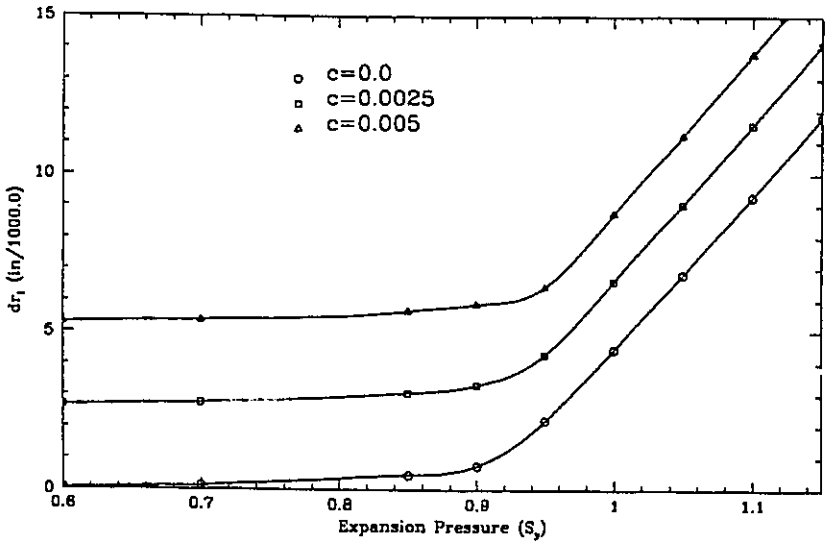

a.Variation for different Clearances

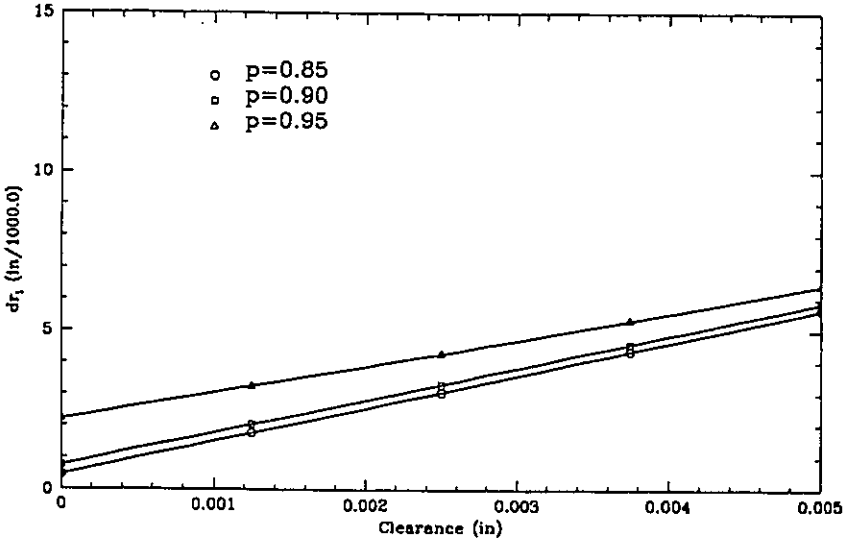

b.Variation for different Pressures

Figure 4.13: Increase in the Tube Inner Radius

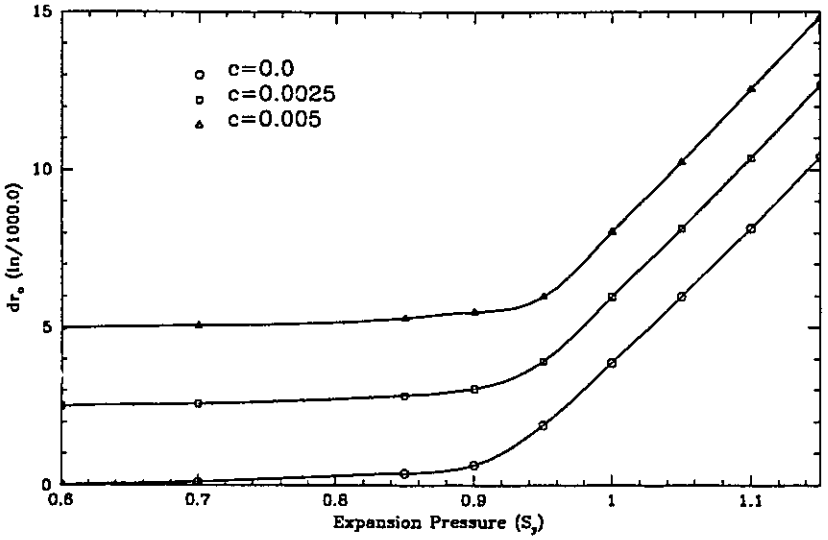

a.Variation for different Clearances

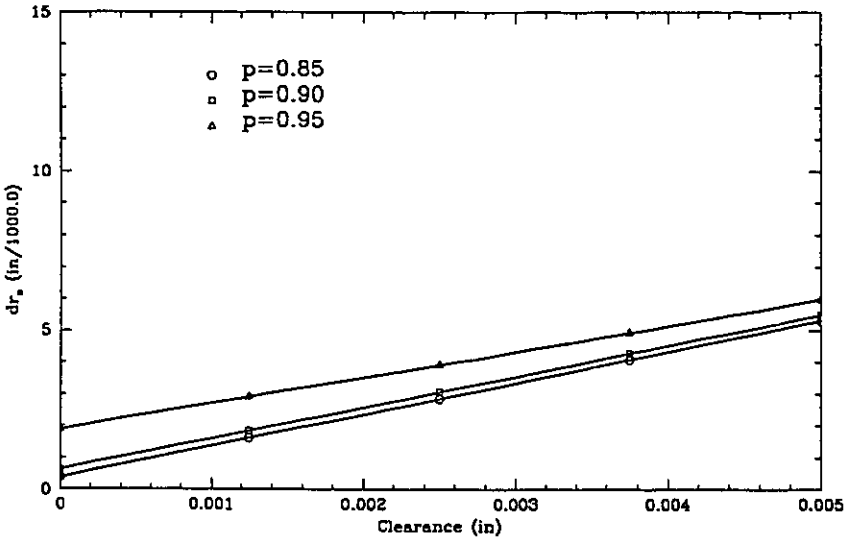

b.Variation for different Pressures

Figure 4.14: Increase in the Tube Outer Radius

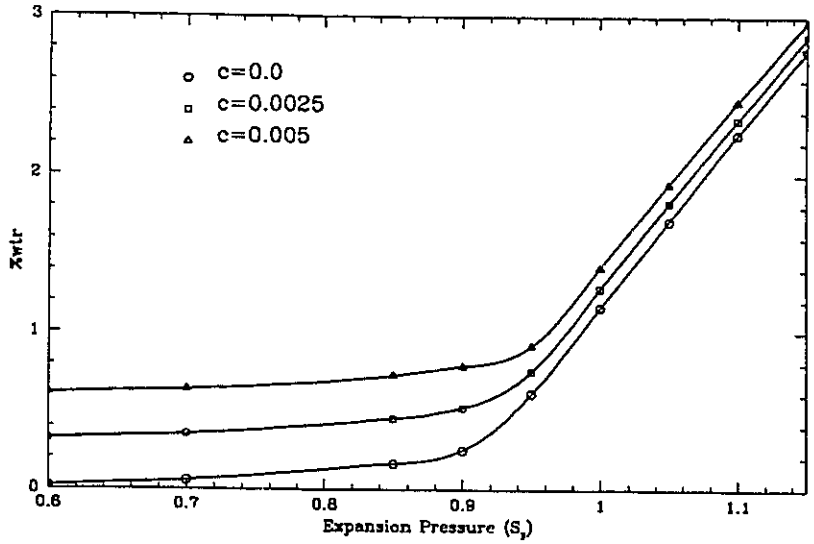

a.Variation for different Clearances

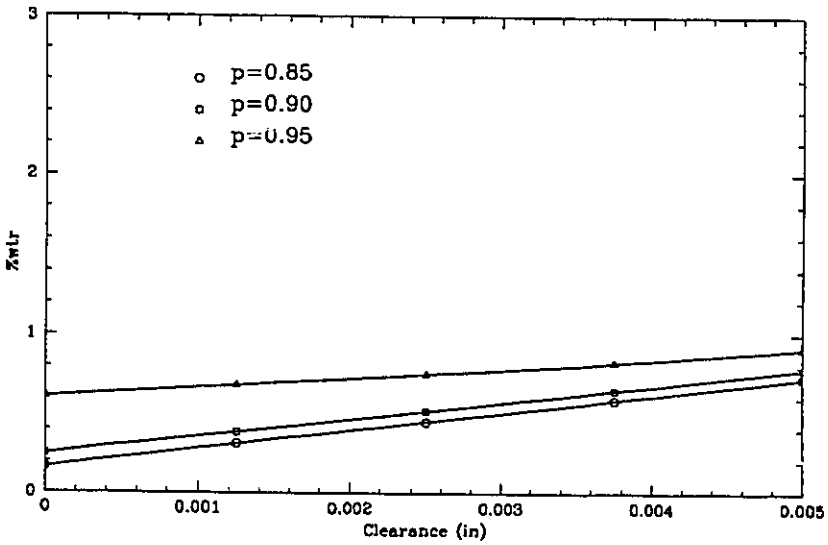

b.Variation for different Pressures

Figure 4.15: Variation in %wtr Ratio

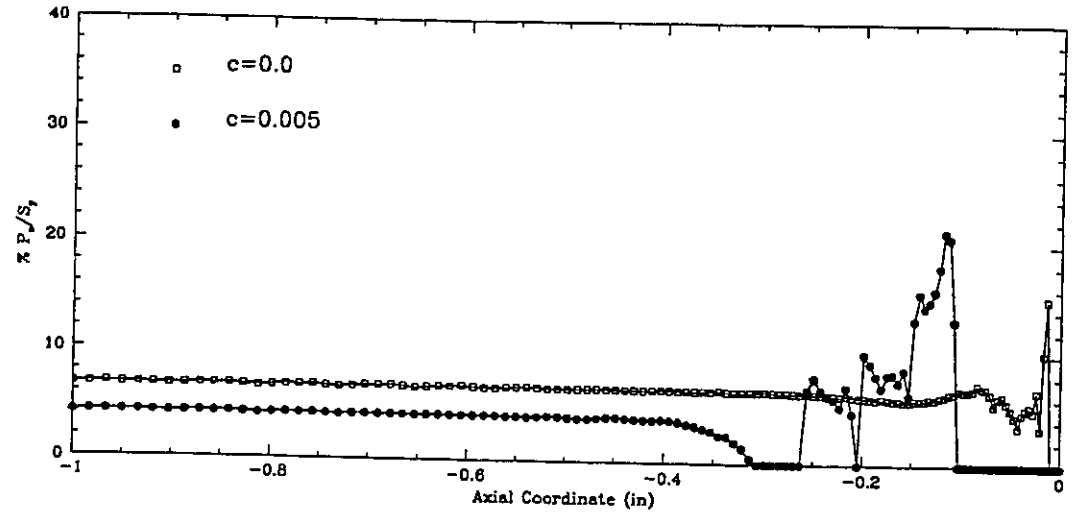

a. Different Clearance Values

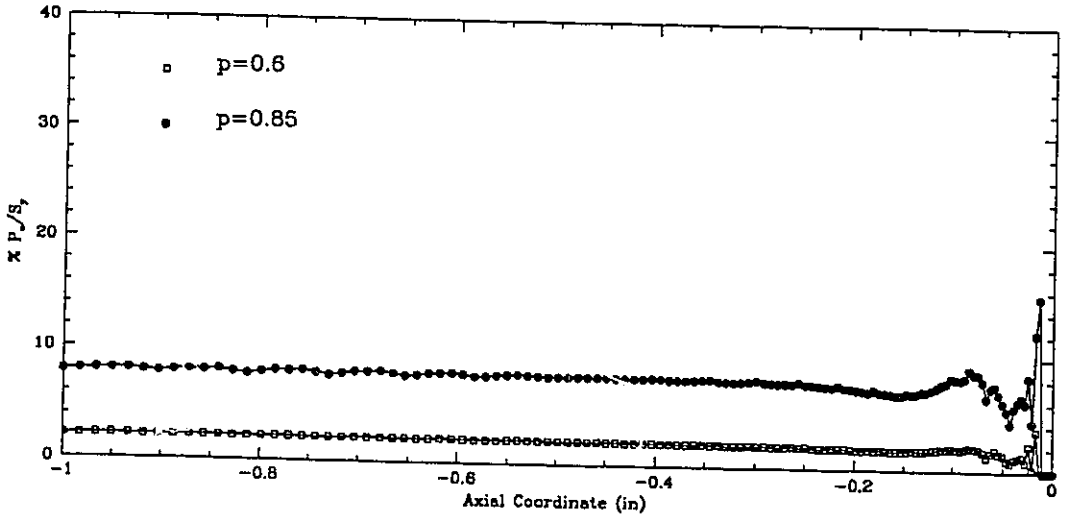

b. Different Pressure Values

Figure 4.16: Residual Contact Normal Traction

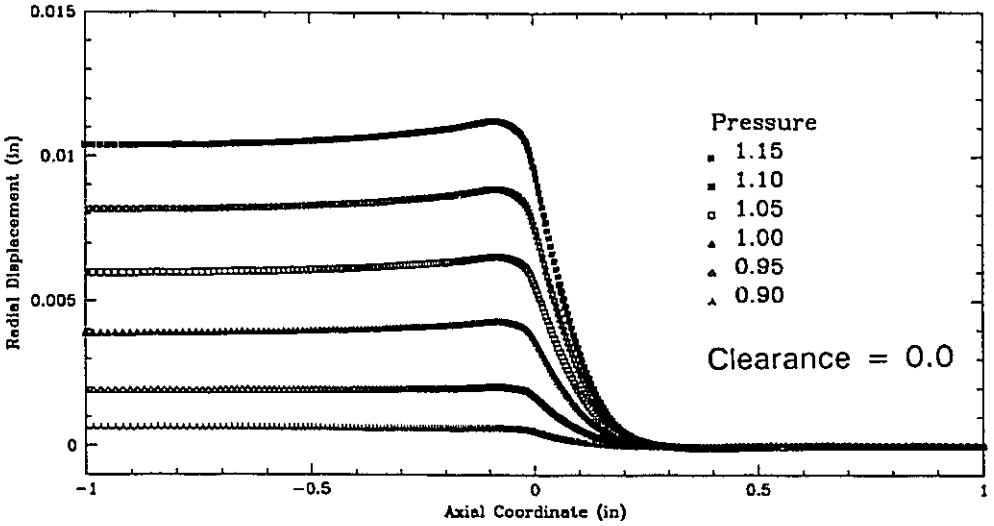

a. Different Pressure Values

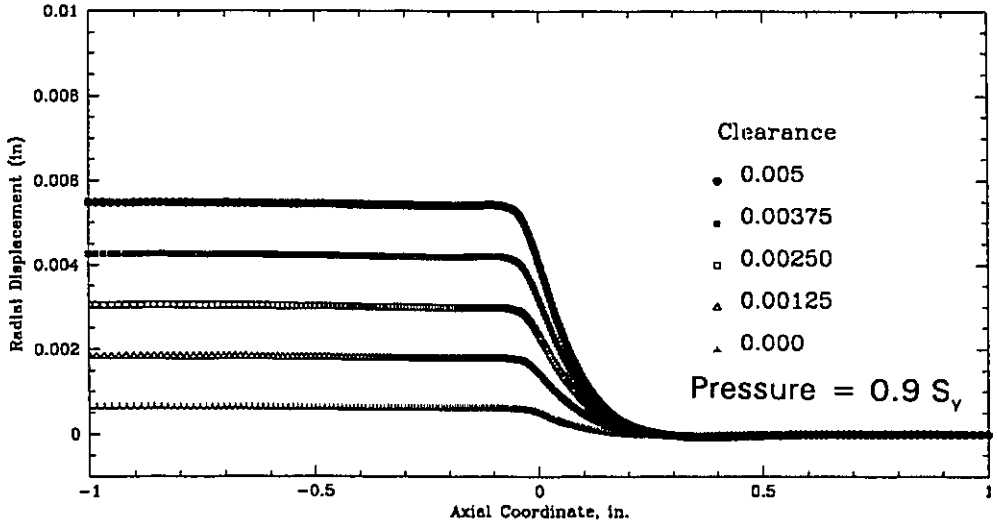

b. Different Clearance Values

Figure 4.17: Residual Radial Displacement of the Tube Outer Surface

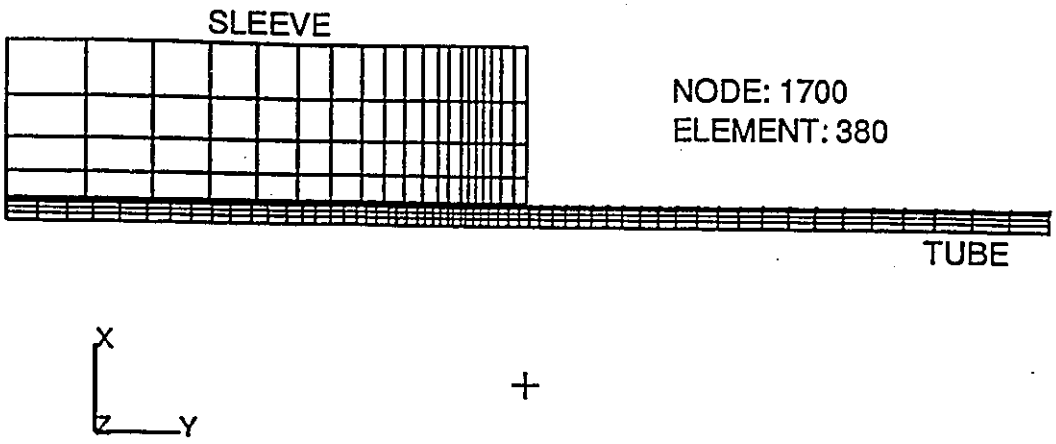

Figure 4.18: Finite Element Mesh for the 2-D Axissymmetric Model

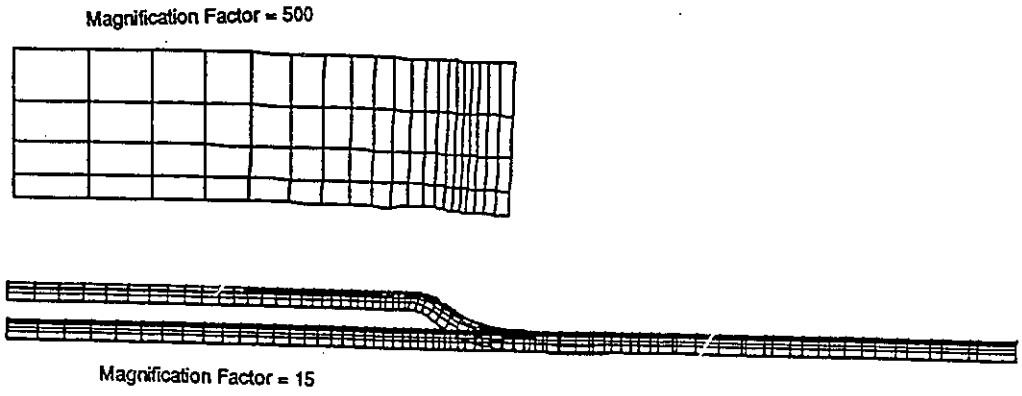

Figure 4.19: Deformed Configuration of the Joint

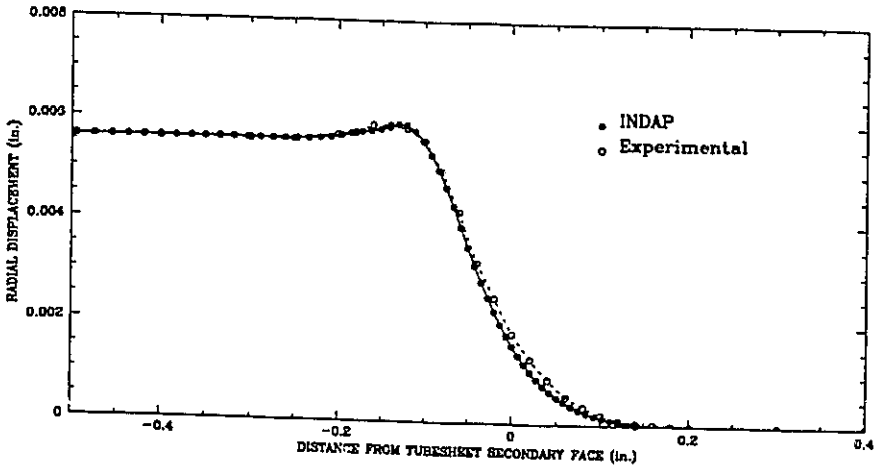

Figure 4.20: Finite Element vs. Experimental Profile

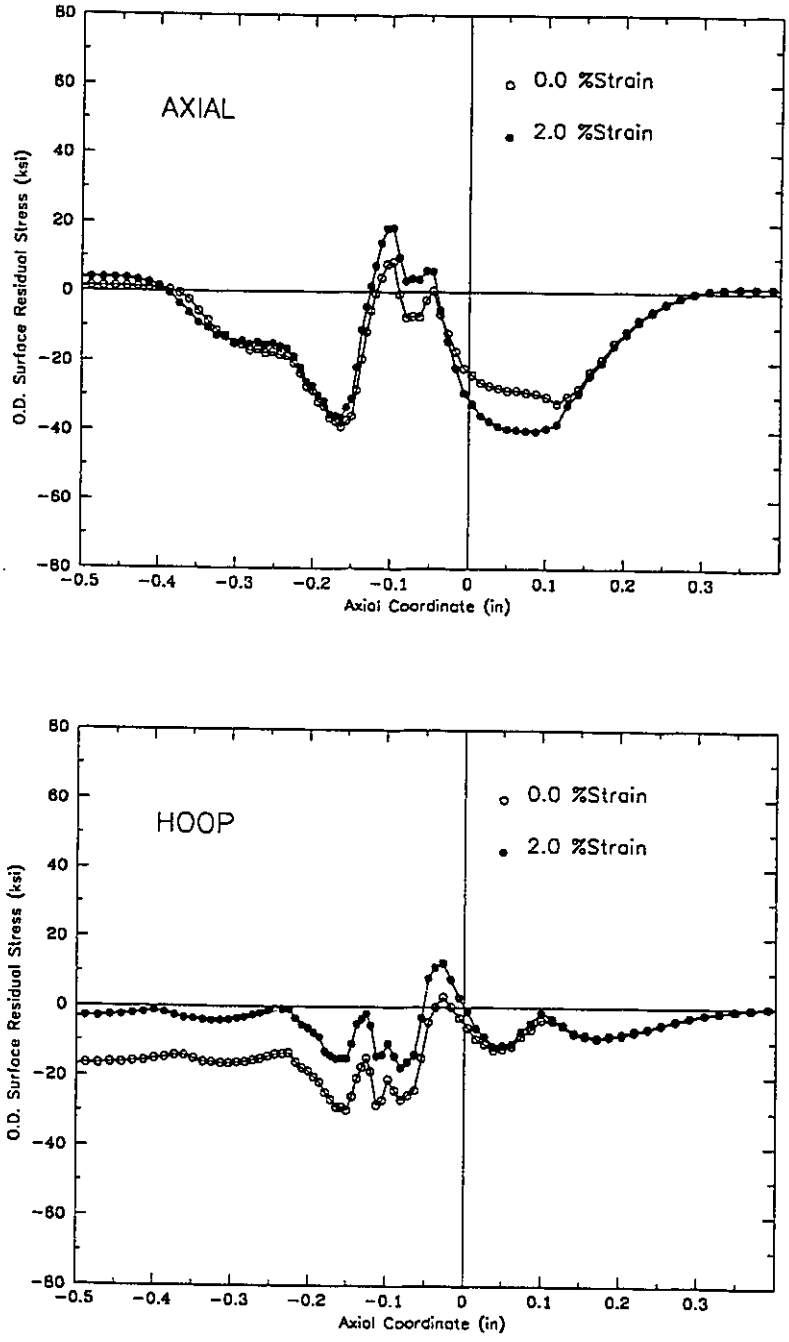

Figure 4.21: Residual Axial & Hoop Stresses along Tube Outer Surface for Different %Strain

CHAPTER 5

CONCLUSIONS & RECOMMENDATIONS

5.1 Conclusions Related to the Contact Algorithm

A finite element contact algorithm is developed and implemented in the general purpose incremental nonlinear finite element program, INDAP. The developed algorithm is made capable of handling nonlinear continuum finite elements in problems with geometric and/or material nonlinearities. No assumptions are made regarding the geometry of the contacting bodies, the location and extent of contact and the nature of the external loading.

A non-classical bi-linear friction model is implemented which may be reduced to the classical Coulomb's law of friction through an adjustable friction modulus. The bi-linear friction model allows for micro and macro relative sliding motions.

The contact problem is solved for the nodal contact forces that remove the overlaps and satisfy the friction law in normal and tangential iteration loops. These nodal contact forces are distributed over the contact surface using linear shape functions for interpolating the contact traction and parabolic shape functions for interpolating the displacement field. As such, the choice of the interpolating functions for the contact

traction only affects the interpretation of the resulting force field. Moreover, this treatment is consistent with the finite element method in dealing with nodal values.

The developed contact algorithm is verified quantitatively in elastic non-conformal frictionless unilateral contact problems represented by the Hertz example of a sphere pressed between two rigid blocks. A very good agreement with the Hertzian contact closed-form solution is obtained. The inclusion of frictional effects is also considered.

Moreover, an excellent behaviour is demonstrated in dealing with elasto-plastic conformal contact problems represented by the thick-cylinder theory applied to a composite cylinder. The close agreement between the finite element method and the closed-form solution is demonstrated for loading and unloading scenarios.

5.2 Conclusions Related to the Expanded Joint

The developed contact algorithm is adopted to model the hydraulic expansion of tube joints. Some modelling aspects are investigated to explore its importance in the overall solution. On one hand, it is found that a nonlinear kinematic formulation would be redundant even for initial clearance values up to 0.005 in as considered in this study. On the other hand, the negligence of the friction interaction would lead to under-estimated joint strength.

A 2-D plane stress model is adopted to explore the effects of the elastic and plastic material parameters on the residual contact pressure. This model is limited in scope since it does not address the stress distributions along the tube inner or outer surfaces.

A 2-D axisymmetric finite element model is adopted in order to investigate the distribution of the residual contact pressure and the residual axial and hoop stresses along the tube inner and outer surfaces. A 2^3 full factorial experiment is performed to investigate the main and interaction effects of the expansion pressure, the initial radial clearance and the friction coefficient on the integrity and quality of the joint. It is found that the coefficient of friction only affects the residual contact pressure with an interaction effect with the expansion pressure. The increase in the friction coefficient moves the peak strength value towards lower expansion pressures.

The effects of the expansion pressure and the initial radial clearance are further

investigated in more detail to reveal their main and interaction effects on the residual contact pressure, the maximum residual tensile stress, the axial extrusion, the tube inner radius, the tube outer radius and the percentage wall thickness reduction ratio.

The effects of the initial stresses and the cold-work layer along the as-received tube outer surface on the maximum residual tensile stresses are investigated. It is found that the cold work layer along the tube outer surface has a profound effect in increasing the residual tensile stress peaks along the tube outer surface. On the other hand, the initial stresses has a minimal effect in reducing the tensile surface stress peaks.

5.3 Recommendations for Future Work

With regard to the finite element solution to the general contact problem, it is felt throughout the course of this study that friction modelling has to be investigated further by introducing different friction models. More importantly, the results obtained from using these models has to be tested against reliable experimental data.

The study of the hydraulic expansion of tube joints needs to be extended further to account for the different design parameters involved to reveal their main and interaction effects. A study of the differences between one-step expansion and multi-step expansions would be of great help for industrial applications where multi-step expansions are necessary.

The differences between the hydraulic expansion and the roller expansion has to be explored. A possible start would be a two dimensional plane stress model. The ultimate goal of such a study is to come up with a criterion to compare both methods of manufacturing the tube joint.

REFERENCES

Abdelsalam, U.A. and Dokainish, M.A. [1995], "Finite element prediction of the residual Contact pressure in Hydraulically Expanded Tube Joints", Computational Mechanics and Experimental Measurements VII, CMEM 95, pp.561-568.

Abdelsalam, U.A. and Dokainish, M.A. [1993[a]], "Tube-to-tubesheet Joints; A Review and Finite Element Analysis", Proceedings of the International Conference on Expanded and Rolled Joint Technology, Toronto, Sept. 13-14, pp.C72-96.

Abdelsalam, U.A. and Dokainish, M.A. [1993[b]], "Hydraulic Expansion of Tube-to-tubesheet Joints; A Finite Element Analysis", Proceedings of the International Conference on the Expanded and Rolled Joint Technology, Toronto, Sept. 13-14, pp.D41-52.

Alexander, J.M. and Ford, M. [1956], "Experimental Investigation of the Process of Expanding Boiler Tubes", Proc. Inst. Mech. Eng., Vol. 171, pp.351-367.

Aufaure, M., Boudot, R. and Zacharie, G. [1987], "Analysis of Residual Stresses due to Roll-Expansion Process : Finite Element Computation and Validation by Experimental Tests", Trans. Of the SMiRT , pp. 499-503.

Ayari, M.L. and Saouma, V.E. [1991], "Static and Dynamic Contact/Impact Problems Using Fictitious Forces", International Journal for Numerical Methods in Engineering, Vol. 32, pp. 623-643.

Bathe, K.J. [1986], Finite Element Procedures in Engineering Analysis, Prentice-Hall.

Bathe, K. J. and Chaudhary, A. [1985], "A Solution Method for Planar and Axisymmetric Contact Problems", International Journal for Numerical Methods in Engineering, Vol. 21, pp. 65-88.

Bathe, K. J. and Chaudhary, A. [1984], "On Finite Element Analysis of Large Deformation Frictional Contact Problems", Unification of Finite Element Methods, Elsevier Science Publishers B.V.(North-Holland), pp. 123-147.

Bathe, K. J. and Mijailovich, S. [1988], "Finite Element Analysis of Frictional Contact Problems", Journal of Theoretical and applied Mechanics, Special issue, supplement no. 1 to vol. 7, pp. 31-45.

Bazergui, A. and Lemarquis, J-P [1976], "Residual Stress Measurements on Sanicro-30

Tube Samples", Centre De Development Technologique De L'Ecole Polytechnique De Montreal, Report No. 2384.

Berkan, K. [1988], A Solution Method for Nonlinear Contact Problems, Ph.D. Thesis, McMaster University, Hamilton, Ontario.

Bohm, J. [1987], "A Comparison of Different Contact Algorithms with Applications", Computers & Structures, Vol. 26, No. 1/2, pp. 207-221.

Chaaban, A., Morin, E., Ma, H. and Bazergui, A. [1989], "Finite Element Analysis of Hydraulically Expanded Tube-TO-Tubesheet Joints: A Parametric Study", 1989 ASME PVP Conference, pp.19-25.

Chaaban, A., Allam, M., Bazergui, H. and Ma H. [1993], "Hydraulic Expansion of Tube-to-tubesheet Joint", Proceedings of the International Conference on Expanded and Rolled Joint Technology, Toronto, Sept. 13-14, pp.D1-13.

Chandrasekaran, N., Haisler, W. E. and Goforth, R. E. [1987^a], "Finite Element Analysis of Hertz Contact Problem with Friction", Finite Elements in Analysis and Design, 3, pp. 39-56.

Chandrasekaran, N., Haisler, W. E. and Goforth, R. E. [1987^b], "A Finite Element Solution Method for Contact Problems with Friction", International Journal for Numerical Methods in Engineering, Vol. 24, pp. 477-495.

Chaudhary, A. B. and Bathe, Klaus-Jurgen [1986], "A Solution Method for Static and Dynamic Analysis of Three-Dimensional Contact Problems with Friction", Computers & Structures, Vol. 24, No. 6, pp. 855-873.

Desai, C.S et al. [1984], Thin-Layer Element for Interfaces and Joints, International Journal for Numerical and Analytical Methods in Geomechanics, v8, pp19-43.

Dokainish, M.A. and Abdelsalam, U.A. [1995] "Finite Element Analysis of the Hydraulic Expansion of Tube-to-tubesheet Joints", Final report submitted to Babcock & Wilcox International Division.

Dokainish, M.A. [1988], INDAP Theoretical Manual, Mechanical Engineering Department, McMaster University, Hamilton, Ontario.

Dokainish, M.A. [1988], INDAP User's Manual, Mechanical Engineering Department, McMaster University, Hamilton, Ontario.

Dokainish, M.A. [1988], INDAP Verification Manual, Mechanical Engineering Department, McMaster University, Hamilton, Ontario.

Druez, J. [1983], "Determination Des Contraintes Residuelles Dans Des Tubes D'Echangeurs De Chaleur", Ph.D. Thesis, Univesite De Montreal.

Druez, J., Bazergui, A. and Pettigrew, M.J. [1985], "Residual Stresses in Roller-Expanded Thin Tubes", Experimental Mechanics, pp. 316-324.

Fender, D.A., Williams, G.J. and Dicker, E.P. [1985], "Current Developments in the On-Going Investigation of System Surface Condenser Roller Expanded Tube To Tubesheet Joints", ASME Pap. 85-JPGC-Pwr-16.

Fisher, F.F and Brown, G.J. [1954], "Tube Expanding and Related Subjects", Trans. ASME, Vol. 76, pp.563-584.

Fisher,F.F. and Cope, E.T. [1935], "Rolling-In of Boiler Tubes", Trans. ASME, Vol.57, pp.145-152.

Fisher, F.F. and Cope, E.T. [1943], "Automatic Uniform Rolling-In of Small Tubes", Trans. ASME, Vol. 65, pp.53-60.

Francavilla, A. and Zienkiewicz, O.C. [1975], A Note on Numerical Computatuon of Elastic Contact Problems, Int. J. Num. Meth. Eng., Vol. 9, pp. 913-924.

Gaffoglio, G.J. and Thiele, E.W. [1981], "Tube To Tubesheet Joint Strengths", ASME Pap. 81-JPGC-Pwr-7.

Gallego, F. J. and Anza, J. J. [1989], A Mixed Finite Element Model for the Elastic Contact Problem, Int. J. Num. Meth. Engineering, Vol. 28, pp. 1249-1264.

Goodier, J.N. and Schoessow, G.J. [1943], "The Holding Power and Hydraulic Tightness of Expanded Tube Joints: Analysis of Stress and Deformation", Trans. ASME, Vol. 65, pp.489-496,.

Gracie, B.J., Metcalfe, R., Pietralik, J.M. and Baset, S.B. [1993], "Development of Rolled Joint Numerical Models", Proceedings of the International Conference on Expanded and Rolled Joint Technology, Toronto, Sept. 13-14, pp.C34-71.

Grimison, E.D. and Lee, G.H. [1943], "Experimental Investigation of Tube Expanding", Trans. ASME, Vol. 65, pp.497-505.

Hamerski, B. [1978], "Strain Gauge Residual Stress Measurements on Roll Expanded Incoloy 800 Tubing", Ecole Polytechnique, Report No. 2551.

Haslinger, K.H. and Fisher, F.M. [1985], "Performance of High Strength Corrosion

Resistant Condenser Tubing and Muntz Tubesheet Joints Under Simulated Operational Loadings", ASME Pap. 85-JPGC-Pwr-63.

Herrmann, L. R. [1978], Finite Element Analysis of Contact Problems, Journal of the Engineering Mechanics Division, Vol. 104, pp. 1043-1057.

Huh, G.J. and Kwak, B.M. [1991], "Constrained Variational Approach for Dynamic Analysis of Contact Problems", Finite Elements in Analysis and Design, 10, pp. 125-136.

Hwang, J.Y., Harrod, D.L. and Middlebrooks, W.B. [1993], "Analytical Evaluation of the Hydraulic Expansion of Steam Generator Tubing into Tubesheets", Proceedings of the International Conference on Expanded and Rolled Joint Technology, Toronto, Sept. 13-14, pp.C97-113.

Johnson, K.L. [1985], Contact mechanics, Cambridge University Press, Cambridge.

Katona, M.G. [1983], A Simple Contact-Friction Interface Element with Applications to Buried Culverts, International Journal for Numerical and Analytical Methods in Geomechanics, v7, pp. 371-384.

Klarbring, A., Mikelic, A. and Shillor, A. [1988], "Frictional Contact Problems with Normal Compliance", Int. J. Engng. Sci., Vol. 26, No. 8, pp. 811-832.

Kikuchi, N. and Oden, J.T. [1988], Contact Problems in Elasticity: A study of Variational Inequalities and Finite Element Methods, SIAM Publication, Philadelphia.

Kim, S. and Kim, J. [1993], "Finite Element Analysis of Laminated Composites with Contact Costraint by Extended Interior Penalty Methods", Int. J. Num. Meth. in Engineering, Vol. 36, pp. 3421-3439.

Krips, H. and Podhorsky, M. [1976], "Hydraulic Expansion-A New Method for Anchoring of Tubes", VGB Kraftwerkstechnik, No. 7, pp. 418-426.

Kwak,B.M. [1991] "Complementary Problem Formulation of Three-Dimensional Frictional Contact", Journal of Applied Mechanics, Transactions of the ASME, Vol. 58, pp. 134-140.

Laursen, T. A. and Simo, J. C. [1993], "A Continuum-Based Finite Element Formulation for the Implicit Solution of Multibody, Large Deformation Frictional Contact Problems", Int. J. Num. Meth. Engineering, Vol. 36, pp. 3451-3485.

Lee, S. [1994], "A Computational Method for Frictional Contact problem Using Finite Element Method", International Journal for Numerical Methods in Engineering, Vol. 37, pp. 217-228.

Ma, H., Chaaban, A. and Bazergui, A. [1990], "Tube-TO-Tubesheet Joints Analysis: A proposed Method", 1990 ASME PVP Conference.

Maxwell, C.A. [1943], "Practical Aspects of Making Expanded Joints", Trans. ASME, Vol. 65, pp.507-514.

Mahmoud, F.F., Salamon, N.J. and Marks, W.R. [1982], "A Direct Automated Procedure for Frictionless Contact Problems", Int. J. Num. Meth. in Engineering, Vol. 18, pp. 245-257.

Mottershead, J. E., Pascoe, S. K. and English, R. G. [1992], "A General Finite Element Approach for Contact Stress Analysis", Int. J. Num. Meth. in Engineering, Vol. 33, pp. 765-779.

Nadai, A. [1943], "Theory of the Expanding of Boiler and Condenser Tube Joints Through Rolling", Trans. ASME, Vol.65, pp.865-880.

Nadai, A. [1950], Theory of Flow and Fracture of Solids, Vol. I, Second Edition, McGraw-Hill Book Co.

Oden, J. T. and Martins, J.A.C. [1985], "Models and Computational Methods for Dynamic Friction Phenomena", Computer Methods in Appl. Mech. Engrg., 52, pp. 527-634.

Oden, J.T. and Pires, E.B. [1983[a]], " Nonlocal and Nonlinear Friction Laws and Variational Principles for Contact Problems in Elasticity", J. Appl. Mech., Vol. 50, pp. 67-76.

Oden, J.T. and Pires, E.B. [1983[b]], " Numerical Analysis of Certain Contact Problems in Elasticity with Non-classical Friction Laws", Computers and Structures, Vol. 16, pp. 481-485.

Okamoto, N. and Nakazawa, M. [1979], Finite Element Incremental Contact Analysis with Various Frictional Conditions, Int. J. Num. Meth. Engineering, Vol. 14, pp. 337-357.

Oldenburg, M. [1994], "The Position Code Algorithm for Contact Searching", International Journal tor Numerical Methods in Engineering, Vol. 37, pp. 359-386.

Oppenheimer, P.H. [1927], "Rolling Tubes in Boiler Plates", Power, pp.300-303.

Parisch, H. [1989], "A Consistent Tangent Stiffness Matrix for Three-Dimensional Non-Linear Contact Analysis", International Journal for Numerical Methods in Engineering, Vol. 28, pp. 1803-1812.

Pascoe, S. K. and Mottershead, J.E. [1988], "Linear Elastic Contact Problems Using Curved Elements and Including Dynamic Friction", International Journal for Numerical Methods in Engineering, Vol. 26, pp. 1631-1643.

Pascoe, S. K. and Mottershead, J.E. [1989], "Two New Finite Element Contact Algorithms", Computers & Structures, Vol. 32, No. 1, pp. 137-144.

Podhorsky, M. and Krips, H. [1979], "Hydraulic Expansion of Tubes", VGB KRAFT WERKSTECHNIC, 59, number 1.

Ramu, S.A., Krishnan, A. and Dixit, K.B. [1987], "Finite Element Analysis of Elastic-Plastic Stresses in Channel Rolled Joints", Trans. 9th International Conference on Structural Mechanics in Reactor Technology (SMiRT), Vol. B, Computational Mechanics and Computer-Aided Engineering, pp.359-368.

Sachdeva, T.D., Ramakrishnan, C.V. and Natarajan, R. [1981], "A Finite Element Method for the Elastic Contact Problems", J. Engrg for Industry, Trans. ASME, Vol. 103, pp. 456-461.

Sachdeva, T.D. and Ramakrishnan, C.V. [1981], "A Finite Element Solution for the Two Dimensional Elastic Contact Problems with Friction", Int. J. Num. Meth. in Engrg., Vol. 17, pp. 1257-1271.

Sachs, G. [1947],"Note on the Tightness of Expanded Tube Joints", J. Appl. Mech., A285-286.

Sandeep Vijayakar [1991], "A Combined Surface Integral and Finite Element Solution for A Three-Dimensional Contact Problem", International Journal for Numerical Methods in Engineering, Vol. 31, pp. 525-545.

Saran, M.J. and Wagoner, R.H. [1991], "A Cocsistent Implicit Formulation for Nonlinear Modelling with Contact and Friction: Part I-Theory", Journal of Applied Mechanics, Transactions of the ASME, Vol. 58, pp. 499-506.

Schafer, S. [1975], A Contribution to the Solution of Contact Problems with the Aid of Bond Elements, Computer Methods in Applied Mechanics and Engineering, v6, pp. 335-354.

Scott, D.A., Wolgemuth, G.A. and Aikin, J.A. [1981], "Hydraulically Expanded Tube to Tubesheet Joints", ASME Paper No. 81-PVP-35.

Shyu, S.C., Chang, T.Y. and Salle, F. [1985], Computational Strategies for Nonlinear and Fracture Mechanics Problems, Computers and Structures, Vol. 20, pp. 193-201.

Simo, J. C. and Laursen, T. A. [1992], "An Augmented Lagrangian Treatment of Contact Problems Involving Friction", Computers & Structures, Vol. 42, No. 1, pp. 97-116.

Simo, Juan C., Wriggers, Peter and Taylor, Robert L. [1985], A Perturbed Lagrangian Formulation for the Finite Element Solution of Contact problems, Computer Methods in Applied Mech. Eng., Vol. 50, pp. 163-180.

Singh, K.P. and Soler, A.I. [1984], Mechanical Design of Heat Exchangers and Pressure Vessel Components, Arcturus Publishers.

Soler, A.I. and Hong, Xu [1984], "Analysis of Tube To Tubesheet Joint Loading Including Thermal Loading", J. Appl. Mech., Vol. 51, pp.339-344.

Sun, S. M., Natori, M. C. and Park, K.C. [193], "A Computational Procedure for Flexible Beams with Frictional Contact Constraints", Int. J. Num. Meth. Engineering, Vol. 36, pp. 3781-3800.

Toba, A. [1966], "Residual Stress and Stress Corrosion Cracking in the Vicinity of the Expanded Joint of Aluminum Brass Tube Condensers", J. Japan Petroleum Institute, Vol. 9, No. 5, pp. 30-34.

Underhill, W.R.C [1992], A Virtual Finite Element Method for Contact Problems, Ph.D. Thesis, McMaster University, Hamilton, Ontario, Canada.

Updike, D.P., Kalnins, A. and Caldwell, S.M. [1988], "A Method for Calculating Residual Stresses in Transition Zones of Heat Exchanger Tubes", PVP-139.

Updike, D.P., Kalnins, A. and Caldwell, S.M. [1989], "Residual Stresses in Transition Zones of Heat Exchanger Tubes", PVP-175.

Updike, D.P., Kalnins, A. and Caldwell, S.M. [1990], "Analysis of Tube Tubesheet Joints with Grooves", PVP Vol. 194, pp. 71-76.

Urgami, K., Sugino, M., Urushibata, S., Kodama, T. and Fujiwara, Y. [1982], "Experimental Residual Stress Analysis of Tube To Tubesheet Joints During Expansion", ASME Pap. 82-PVP-61.

Wanxie, Z. and Suming, S. [1988], "A Finite Element Method for Elasto-Plastic Structures and Contact Problems by Parametric Quadratic Programming", Int. J. Num. Meth. in Engrg., Vol. 26, pp. 2723-2738.

Wilson, R.M. [1978], "The Elastic-Plastic Behaviour of Tube During Expansion", ASME Paper No. 78-PVP-112.

Wienstock, S. and Soler, A. [1985], "Tube To Tubesheet Joint Interface Pressure : Part I - Theoretical Analysis with Strain Hardening and Temperature Dependent Properties", PVP, V89-90, pp227-234.

Zhong, W.X. and Sun, S.M. [1989], "A Parametric Quadratic Programming Approach to Elastic Contact Problems with Friction", Computers & Structures, Vol. 32, No. 1, pp. 37-43.

Zhong, Z.H. [1993], Finite Element Procedures for Contact-Impact Problelms, Oxford University Press.

Zhong, Z.H. and Nilsson, L. [1990], "A Contact Searching Algorithm for General 3-D Contact-Impact Problems", Computers & Structures, Vol. 34, No. 2, pp. 327-335.

Zhong, Z.H. and Mackerle, J. [1992], "Static Contact Problems", Engineering Computations, Vol. 9, pp.3-37.

APPENDIX A

CLOSED FORM SOLUTIONS

A.1 Hertz Contact

For two elastic spheres in contact under the concentrated force P the radius of the contact area is given by, Johnson [1984]:

$$a = \left[\frac{3PR}{4E^*}\right]^{\frac{1}{3}}$$

The pressure distribution is given by:

$$p(r) = p_o\left(1 - \frac{r^2}{a^2}\right)^{\frac{1}{2}}$$

The maximum pressure is given by:

$$p_o = \frac{3P}{2\pi a^2} = \left[\frac{6PE^{*2}}{\pi^3 R^2}\right]^{\frac{1}{3}}$$

The vertical approach is given by:

$$\delta = \frac{a^2}{R} = \left[\frac{9}{16}\frac{P^2}{RE^{*2}}\right]^{\frac{1}{3}}$$

where

$$\frac{1}{R} = \frac{1}{R_1} + \frac{1}{R_2}$$

$$\frac{1}{E^*} = \frac{1-\nu_1^2}{E_1} + \frac{1-\nu_2^2}{E_2}$$

A.2 Thick Cylinder Theory

The following closed-form solutions are obtained for an internally pressurized thick-walled cylinder. An internal pressure p is applied on a cylinder with an inner radius a and outer radius b. The extent of the plastic zone is denoted c. The radial and tangential stress distributions along the radial coordinate are given by:

Elastic zone; c<r<b:

$$\sigma_r = \frac{pa^2(r^2 - b^2)}{r^2(b^2 - a^2)}$$

$$\sigma_\theta = \frac{pa^2(r^2 + b^2)}{r^2(b^2 - a^2)}$$

Plastic zone; a<r<c:

$$\sigma_r = \sigma_y \left[\ln\frac{r}{c} - \frac{1}{2}\left[1 - \frac{c^2}{b^2}\right]\right]$$

$$\sigma_\theta = \sigma_y \left[\ln\frac{r}{c} + \frac{1}{2}\left[1 + \frac{c^2}{b^2}\right]\right]$$

where the radius of the plastic zone, c, is given by:

$$p = \frac{\sigma_y}{2}\left[1 - \frac{c^2}{b^2}\right] + \sigma_y \ln\frac{c}{a}$$

APPENDIX B

SAMPLE INPUT TO INDAP

2-D Finite Element Model For the Hertzian Contact Problem
u = 1.28 in
μ = 0.2 $E_f = 10^{12}$

```
! Specify output file name
**FILE OUT=Res.out

! Specify heading for the output file
**TITLE
      FEA of Hertzian Contact Between an Elastic Sphere and a Rigid Block
                        2-D Model (Axisymmetric)

! Specify Solution Parameters
**SOLUTION
 *BLOCK MAXFRON=500
 *SAVE, DISP=1 , PLOT , STRESS=1
 *TIMING START=0.0 , STOP=1.0  , DELTA=1.0
 *PRINT RUN=1 , DISPL=-1 , STR=-1 , STA=1

! Specify Time Function
**TIMEFUNCTION=1
 0.0   0.0
 1.0   1.0

! Specify Coordinate System and Node Files
**NODES , SYSTEM=CARTESIAN
 *COORDINATES , FILE=sphere.nod
 *COORDINATES , FILE=block.nod

! Specify Material Properties for the Sphere
**MATERIAL=MSPHERE
 *LINEAR , E=200.0E+3 , NU=0.3

! Specify Elements for the Sphere
**ELEMSET=SPHERE , MATERIAL=MSPHERE, TYPE=AXISYMMETRIC
 *CONNECTIVITY , FILE=sphere.con
```

```
! Specify Elements for the Block
**ELEMSET=BLOCK , MATERIAL=MSPHERE, TYPE=AXISYMMETRIC
 *CONNECTIVITY, FILE=block.con

! Specify Kinematic Boundary Conditions
**FIXED
!...SPHERE
 *X  1 TO=7 , 414 TO=423
!...BLOCK
 *X,Y  894 TO=897
**PRESCRIBED
 *Y=-1.28  423 T)=893 INC=10 , 407 TO=413

! Specify Contact information
**CONTACT, ITER=20, TOL=1.0E-5
 *SURFACE=1, 1 TO=225 INC=7
 *SURFACE=2, 894,895

 *PAIR , CONTACTOR=1, TARGET=2, FRICTION=0.3 , FRCSTIF=1.0E+12

**END
```

APPENDIX C

ESTIMATED MAIN AND INTERACTION EFFECTS

Effect	on contact pressure (%S_y)	on maximum stress (%S_y)
P_{exp}	4.503	42.80
c	-1.433	35.15
μ	-0.082	-00.60
P_{exp} - c	-0.778	-33.00
P_{exp} - μ	-1.128	00.15
c - μ	0.167	-00.40
P_{exp} - c - μ	-0.498	-00.35